Development of Ni-Modified Alloy Steel for Power Transmission Gear Material and Investigation of Its Fatigue Failure

By:

Hailemariam Nigus Hailu GSR/0209/08

Supervisor: Daniel Tilahun Redda (Ph.D.) (Associate Professor)

A Dissertation Submitted to School of Mechanical and Industrial Engineering Presented in Partial Fulfillment of the Requirements for the Ph.D. Degree in Mechanical Design Engineering

Addis Ababa Institute of Technology (AAiT)

Addis Ababa University

Addis Ababa, Ethiopia

November 2021, Addis Ababa, Ethiopia

ADDIS ABABA UNIVERSITY

Addis Ababa Institute of Technology (AAiT)

School of Mechanical and Industrial Engineering (SMIE)

Mechanical Design Chair

Development of Ni-Modified Alloy Steel for Power Transmission Gear Material and Investigation of Its Fatigue Failure

By

HAILEMARIAM NIGUS HAILU GSR/0209/08

Approved by the board of examiners:

Dr. Yilma Tadesse	_____	_____
Dean, School of Mechanical and Industrial Engineering	Signature	Date
Dr. Daniel Tilahun Redda	_____	_____
Supervisor	Signature	Date
Dr. Dereje Engida Woldemichael	_____	02/12/2
Internal Examiner	Signature	Date
Professor T V V L N Rao	_____	02/12/21
External Examiner	Signature	Date
Dr. Araya Abera	_____	_____
Mechanical Design chair	Signature	Date

DEDICATION

The thesis is dedicated to the Almighty God who owes everlasting knowledge and strength and to St. Merry for her eternal help in my life.

Authors' Declaration

I, hereby declare that this dissertation entitles '**Development of Ni-Modified Alloy Steel for Power Transmission Gear Material and Investigation of Its Fatigue Failure'** was my research work. It has not been submitted in whole or part to another university for a degree award.

_____ June 29, 2021___

Hailemariam Nigus Hailu **Date**

(Ph.D. Candidate)

I, hereby declare that this dissertation entitles **'Development of Ni-Modified Alloy Steel for Power Transmission Gear Material and Investigation of Its Fatigue Failure'** was conducted under my supervision. I have confirmed that it has not been submitted in whole or part to another university for any degree award.

_____ June 29, 2021 .

Dr. Daniel Tilahun Redda (Associate Professor) **Date**

Authors

Hailemariam Nigus Hailu

Ph.D. student at School of Mechanical and Industrial Engineering (SMIE), Addis Ababa institute of Technology (AAiT), Addis Ababa University, Addis Ababa, Ethiopia

Email: hailuqua@gmail.com

Daniel Tilahun Redda (Ph.D.)

Associate Professor at School of Mechanical and Industrial Engineering (SMIE), Addis Ababa institute of Technology (AAiT), Addis Ababa University, Addis Ababa, Ethiopia

Email: tdaniel412@yahoo.com

Acknowledgment

First, I would like to appreciate the continued support and encouragement of my supervisor, Dr. Daniel Tilahun Redda (Associate Professor) during the entire dissertation process. I also acknowledge Dr.Yilam Tadesse, dean of the School of Mechanical and Industrial Engineering, and Mr. Araya Abera chair of the Mechanical Design Engineering stream for their continual support and encouragement during all activities of this work.

Second, I would like to acknowledge the support of the Tianjin University of Technology and Education (TUTE) and the Tianjin Heat Treatment Research Institute, which have graciously prepared specimens, performed heat treatment, and allow me to conduct some experimental studies.

Besides, I would like to express my deep gratitude to three groups of people: firstly, Engineer Carlos Neri and Mr. Michael Reyes, instructors at the Ethiopian technical University (ETU), who participated in the assembly and calibration of the two roller contact test rigs; secondly, I would like to express my special thanks to Dr. Arun Pathiran, assistance professor at school of electrical and computer science, ETU, who directed and helped me during the ANN Matlab script creation. Thirdly, I would like to thank my research fellow group at the ETU namely; Masresha Fikade, Andinet Asnake, Abay Kebede, Adebabay Tesfa, and Nahom Nega for their contribution to the development of the Twin Disc test rig.

Last but not least, I would like to express my thankfulness and my affection to my wife, Lemlem Tadesse, and my son, Isaak Hailemariam, for their constant patience and encouragement when this job leads me to neglect them.

Abstract

Transmission gears have been working under severe working situations of loads and rotations, due to these situations, the properties and qualities of gear materials are greatly influenced. Consequently, contact fatigue failure is instigated. So, improving the mechanical properties of the existing gear material is very vital since these properties have a direct correlation with gear fatigue failure. Investigations were carried out to determine the mechanical properties of Ni-modified alloy steels by adding 1.55%, 1.75%, and 1.95% of the Ni-content to the existing Cr-Mo alloy steel, by ANN modeling that correlates the complex relationship of the input and output parameters and verified by experimental test. The investigation of these material properties with ANN modeling and experimental tests shows that the more Ni-content added to Cr-Mo alloy steel, the higher the ultimate and yield strength achieved. Likewise, fracture toughness, impact toughness, and percent of retained austenite of these materials were also investigated thoroughly. Thus, results showed that 1.55 % Ni- modified Cr-Mo alloy steel has a higher value on both impact toughness and fracture toughness without sacrificing yield strength compared with other Ni-modified counterparts. Therefore, based on both ANN and experimental results, 1.55 % of Ni- modified Cr-Mo alloy steel showed a better fatigue failure resistance. To address the behavior of lower alloying Ni-contents, the study includes 1.15% and 1.35% Ni-contents and explored with the ANN. Then, the results still indicate that a 1.55% Ni-content has better fatigue failure resistance.

After exploring the best Ni-modified Cr-Mo alloy steel (1.55% of Ni-modified Cr-Mo alloy), based on ANN and experimental approaches, design and fatigue analysis of a single-speed transmission gear was carried out for further confirmation. The methods of design and analysis employed were KISSsoft gear simulation software and AGMA standard. Explorations have been done by altering gear parameters like helix angle, face-width, and input torque to get fitting safety factors, fatigue stresses, and smooth operation of the transmission gear pair. Comparing the two materials, Ni-modified Cr-Mo alloy steel has a higher impact load-carrying capacity manifested by bending safety factor compared to existing gear material. However, there are no significant differences in terms of contact load-carrying capacity expressed in contact safety factors between the sample materials.

So, further investigation was needed to identify the difference in surface durability and to verify the mechanical property results.

Then, Rolling contact fatigue (RCF) experimental test was carried out between 1.55% Ni-modified Cr-Mo alloy steel and existing material. In the RCF test of gears, micropitting was found to be the most vital damage property to characterize the rolled surface of disc samples. In this experiment, RCF tests were done on disc samples, two materials of Cr-Mo alloy steel, and 1.55%Ni-modified Cr-Mo alloy steels to evaluate the surface damage and topography of these materials. The methods utilized to determine the existence of micropitting on these materials were done on an adapted twin-disc machine. It is intended through this test to simulate asperities contact on surfaces of mating gear flanks using disc samples. The disc samples used in this experiment were contained low-speed specimens that are cylindrical-shaped discs, and high-speed specimens consist of crowned-shaped discs to attain a minimum effective contact area of 8.5mm. Thereafter, completing the RCF test, surface topographies were examined by employing SEM and OM for each measure of changes in surface topography and morphological alterations. As revealed from the post-processed micrographs, the 1.55% Ni-modified Cr-Mo alloy steel has better contact fatigue failure resistance compared with the Cr-Mo alloy steel in terms of Micropitted area ratio, pitted depth, and the number of pits. As an additional justification, verifying the result with the previous related literature of having a higher Ni-content (2%) was also compared with the 1.55% Ni-modified Cr-Mo alloy steel under the same conditions owes a 5 % micropitting ratio, and this indicates 1.55% Ni-modified has better surface durability. Thus, the 1.55% Ni-modified Cr-Mo alloy steel is recommended to use for transmission gears with high RCF damage suspicious.

Keywords: Ni-modified, contact fatigue failure, rolling contact fatigue, twin-disc test rig, micropitting

Table of Contents page

Acknowledgment vi
Abstract vii
Table of contents ix
List of Figures xi
List of tables xiv
LIST OF ABBREVIATIONS xv
LIST OF SYMBOLS xvii
CHAPTER ONE 1
1. General Introduction 1
1.1. Background and Rationale of the Study 1
1.2. Statement of the Problem 5
1.3. Objectives of the Research 6
1.4. Significance of the Research 7
1.5. Scope and Limitation of the Study 7
1.6. Organization of the Dissertation 7
CHAPTER TWO 9
2. Literature Review 9
2.1. Introduction 9
2.2. Gear Contact Geometry 10
2.3. Gear Surface Contact and Roller Simulation 16
2.4. Gear Materials, Manufacturing, and Heat Treatment Methods 20
2.5. Rolling Contact Fatigue Test Rig 31
2.6. Transmission Gear Fatigue Failure Mode 38
2.7. Summary 42
CHAPTER THREE 43
3. Methodology 43
3.1. Introduction 43
3.2. Materials 46
3.3. Methods 46
3.4. Test Conditions 63

CHAPTER FOUR 69
4. Result and Discussion 69
4.1. Mechanical Property of Ni-modified Alloy Steels 69
4.2. Fatigue Analysis Ni-modified Alloy Steels 78
4.3. Surface Evaluation and Analysis 89
CHAPTER: FIVE 101
5. General Conclusions and Recommendations 101
5.1. General Conclusion 101
5.2. Recommendations 103
Reference 105
Appendix 125

List of Figures page

Figure 1-1: Failure of gears for contact stress and rotational speed [17]..... 4
Figure 2-1 Model of involute (a): spur gear (b): helical gear [31]..... 10
Figure 2-2: Terminologies for helical gears [29, 30]..... 10
Figure 2-3: Plane of action with the line of contact for helical gears..... 11
Figure 2-4: Gear rolling and/or sliding speeds (a): the beginning of engagement (b): termination of engagement [37] 12
Figure 2-5: Engagement of the tooth with helical gear drive [42]..... 13
Figure 2-6: Comparison b/n the spur and helical gear contact, transverse section (upper figure), spur gear (central), and helical gear (lower) [42]. 14
Figure 2-7: Involute gears in contact (a): schematic geometry of pinion (b) [46] [47]... 15
Figure 2-8: Simulation of (a): roller contacts (b): gear surface contact [56] 17
Figure 2-9: Non-conforming contact (a): two elastic overlapping cylinders (b): semi-..... elliptical contact zone distribution pressure (c): ellipsoidal pressure distribution[57, 58]. 17
Figure 2-10: roller specimens used in twin-disc tribometer a) [70] b) [69] c) [71]..... 20
Figure 2-11: Methods of gear teeth manufacturing [115]..... 25
Figure 2-12: Sequence of treatment conducted on AISI 8620 steel [127]..... 27
Figure 2-13: Comparison b/n carburizing and nitriding heat treatment process [136]..... 29
Figure 2-14: Schematic representation of twin-discs test rig [157]..... 33
Figure 2-15: FZG Contact fatigue test ring..... 35
Figure 2-16: Test rig for monitoring helical gear distributed pitting failure [160]..... 35
Figure 2-17: SUROS twin-disc tester [161]..... 36
Figure 2-18: Micro pitting Rig [162]..... 37
Figure 2-19: (a) TE-72 two- roller test rig: (b) Optimal Instruments test rig [163]..... 37
Figure 2-20: Swerea KIMABs twin-disc test rig [163] 38
Figure2-21: Micropitting generated at contact region of gear tooth [172] 40
Figure 2-22: Pitting of helical gear teeth [176]..... 40
Figure 2-23: Fatigue damage on a helical gear (a): Overview of top helical surface failure (b): Magnification of spall failure (c): Cross-section of spall failure [92] 41

Figure 3-1: Methodology Chart 45
Figure 3-2: Schematic representation of ANN modeling of the developed alloy steel 48
Figure 3-3: Architecture ANN Model [187] 49
Figure 3-4: Schematic representation of error-correction learning [188]]..... 50
Figure 3-5: Mean square error versus epoch for the validation check..... 50
Figure 3-6: Regression fit and R values for training testing and validation 51
Figure 3-7: Size of tensile specimen 53
Figure 3-8: (a): universal tensile test machine (b): prepared specimens of the tensile test 53
Figure 3-9: Size of V-notch Impact Specimen 54
Figure 3-10: Schematic representation of Charpy impact test procedure [189] 55
Figure 3-11: (a): Charpy impact tester machine (b): machine specification 55
Figure 3-12:(a): Size of Rockwell hardness test specimen (b): prepared spacemen 56
Figure 3-13: (a): Vickers hardness test machine (b): Rockwell hardness test machine ... 56
Figure 3-14: (a): Mounting Press machine (b): Bakelite powder (c): specimen..... 57
Figure 3-15: (a): polish machine (b): echant..... 57
Figure 3-16: Optical Microscope (OM) on microstructure analysis..... 58
Figure 3-17: Dimension of test discs [192]..... 60
Figure 3-18: Prepared test discs 60
Figure 3-19: EDM finished specimens 61
Figure 3-20: Adapted twin-disc test rig 62
Figure 3-21: Cross-sectional preparation for metallographic analysis [201]..... 66
Figure 3-22:Axial and circumferential cross-sections polished after hot Mount [56]..... 67
Figure 3-23: Surface and section sampling position [205-207]..... 67
Figure 3-24: Scanning electron microscope 68
Figure 3-25: Particle analysis water segmentation 68
Figure 4-1: Influence of Ni-content on the yield strength 70
Figure 4-2: Influence of Ni-content on ultimate tensile strength (UTS) 71
Figure 4-3: Influence of Ni-content on % total elongation..... 71
Figure 4-4: Influence of Ni-content on Charpy impact toughness 73
Figure 4-5: Influence of Ni-content on fracture toughness..... 74

Figure 4-6: Influence of Ni-content on percent retained austenite 75
Figure 4-7: Influence of Ni-content on surface hardness..... 76
Figure 4-8: Vickers hardness of case depth 76
Figure 4-9: OM micrograph of Cr-Mo-Ni alloy steel..... 77
Figure 4-10: OM micrograph of Cr-Mo alloy steel 77
Figure 4-11: Fatigue stress VS helix angle at input torque of (a): 75 Nm (b): 50 Nm... 79
Figure 4-12: Fatigue stress VS face width at input torque of (a): 75 Nm (b): 50 Nm.... 79
Figure 4-13: Fatigue stress versus (a): helix angle (b): face width..... 80
Figure 4-14**:** Simulation of the strength of material and number of Load Cycles by KISSsoft for (a): Cr-Mo-Ni (b): Cr-Mo alloy steels 80
Figure 4-15: Bending safety factor versus helix angle at input torque (a):75 Nm (b):50 Nm 82
Figure 4-16: Contact safety factor versus helix angle at input torque (a):75 Nm (b):50 Nm 83
Figure 4-17: Bending safety factor versus face width at input torque (a):75 Nm (b): 50 Nm 83
Figure 4-18: Contact safety factor versus face width at input torque (a):75 Nm (b): 50 Nm 84
Figure 4-19: Bending safety factor versus (a): face width (b): helix angle 85
Figure 4-20: Service life of Cr-Mo-Ni alloy steel at input torque (a): 75 Nm (b): 50 Nm85
Figure 4-21: Service life of Cr-Mo alloy steel at input torque (a): 75 Nm (b): 50 Nm 86
Figure 4-22: Safety factors of candidate alloy steels with input torque 75 Nm 86
Figure 4-23: Contact ration versus variable design parameters..... 87
Figure 4-24: Center distance versus helix angle..... 88
Figure 4-25: Mass versus parameters 88
Figure 4-26: Surface map of Cr-Mo alloy steel (a): high-speed disc (b): low-speed disc 90
Figure 4-27: Surface map of Ni-modified Cr-Mo alloy steel (a): high-speed disc after ..... (b): low-speed disc 91
Figure 4-28: Wear mass at each load stage..... 92
Figure 4-29: High-speed Cr-Mo alloy steel after RCF test: (a): SEM Micrograph ..... (b): OM Micrograph..... 93

Figure 4-30: Low-speed Cr-Mo alloy steel after RCF test (a): SEM Micrograph (b): OM Micrograph 93
Figure 4-31: High-speed Ni-modified Cr-Mo alloy steel after RCF test (a): SEM ..... Micrograph (b): OM Micrograph 94
Figure 4-32: Low-speed Ni-modified Cr-Mo alloy steel after RCF (a): SEM ..... Micrograph (b): OM Micrograph 94
Figure 4-33: Ni-Modified Cr-Mo alloy steel of low-speed micropits of (a): equivalent ..... diameter (b): depth (c): shape (d): correlation b/n micropits depth and micropits equivalent diameter 96
Figure 4-34: Ni-Modified Cr-Mo alloy steel of high-speed micropits of (a): equivalent .... diameter (b): depth (c): shape (d): correlation b/n micropits depth and micropits equivalent diameter 97
Figure 4-35: Cr-Mo alloy steel of low-speed micropits of (a): equivalent diameter (b): .. depth (c): shape (d): correlation b/n micropits depth and micropits equivalent diameter 98
Figure 4-36: Cr-Mo alloy steel of high-speed micropits of (a): equivalent diameter (b): .... depth (c): shape (d): correlation b/n micropits depth and micro pit equivalent diameter 98
Figure 4-37: Evaluation of Surface damage of Cr-Mo alloy steel of (a): high-speed disc 99
Figure 4-38: Evaluation of Surface damage of Ni-modified Cr-Mo alloy steel (a) high-speed disc (b): low-speed disc 99

List of Tables page

Table 3-1: Ni-Modified Cr-Mo alloy steels input parameter for prediction 46
Table 3-2: Given lubricant property of SAE90 63
.Table 3-3: RCF test and load stages 65
Table 3-4: controlled parameters during the run-in and RCF test 65

LIST of Abbreviations

AC	Alternating Current
AF	Acicular Ferrite
AGMA	American Gear Manufacturing Association
AISI	American Iron and Steel Institute
Al	Aluminum
ANN	Artificial Neural Network
ANSI	American National Standards Institute
AQ	As-Quenched
ASTM	American Society for Testing and Materials
CNC	Computer Numerical Control
CO	Carbon monoxide
CO2	Carbon dioxide
ETU	Ethiopian Technical University
Cr	Chromium
DIN	Deutsches Institut für Normung
EDM	Electron Discharge Machine
EHL	Elasto Hydrodynamic Lubrication
EP	Extreme Pressure
EVs	Electric Vehicles
FEA	Finite Element Analysis
FZG	Forschungsstelle für Zahnräder und Getriebebau
GBF	Grain Boundary Ferrite
GPa	Giga pascal
HC	Hydrocarbons
HPGQ	High-Pressure Gas Quenching
HPSTC	High point of single tooth contact
HRC	Hardness Rockwell C
IDE	Integrated Development Environment
LOA	Line of Action
LPC	Low-Pressure Carburizing

LPSTC	Lowest Point of Single Tooth Contact
MC	Martensite Cooling
MF	Martensite Finish
Mo	Molybdenum
MPa	Mega Pascal
MPR	Micro Pitting Rig
N	Nitrogen
NH3	Ammonia
Ni	Nickel
NOx	Oxides of Nitrogen
NTC	Negative Temperature Coefficient
OM	Optical Microscope
Pa	Pascal
Q	Quenched
RCF	Rolling Contact Fatigue
RMS	Root Mean Square
RPM	Revolution per Minute
SAE	Society of Automotive Engineers
SEM	Scanning Electron Microscope
SRR	Slide to Roll Ratio
SUROS	Sheffield University Rolling Sliding
T	Tempered
THRI	Tianjin Heat Treatment and Research Institute
TUTE	Tianjin University of Technology and Education
USB	Universal Serial Bus
UTS	Ultimate Tensile Strength
YS	Yield Strength

LIST of Symbols

Symbol	Description	Unit
a	Addendum	mm
b	Face width	mm
b	Half-width	mm
C	Center distance	mm
C_ψ	Helical overlap factor	
d	Pitch diameter of pinion	mm
D	Pitch diameter of gear	mm
d_{a1}	Addendum diameter of pinion	mm
D_{a2}	Addendum diameter of gear	mm
d_{b1}	Base diameter of pinion	mm
D_{b2}	Base diameter of gear	mm
E	Young's modulus	GPa
E_G	Young's modulus materials of gear	GPa
E_p	Young's modulus materials of pinion	GPa
F_t	Tangential force	N
F_r	Radial force	N
F_a	Axial force	N
i	First stage gear ratio	
I	Geometry factor for pitting resistance	
i_g	Overall total transmission gear ratio	
J	Bending stress geometry factor	
K_B	Rim thickness factor	
k_f	Force concentration factor at the base of the gear	
K_H	Load distribution factor	
K_o	Load factor	
K_s	Size factor	

K_v	Dynamic factor	
m	Nodule	mm
m_n	Normal module	mm
m_N	Load sharing ratio	
m_t	Transverse module	mm
N_1	Max motor Speed	rpm
P_{max}	Maximum contact pressure	MPa
p_n	Normal circular pitch	mm
p_N	Normal base pitch	mm
p_t	Transverse circular pitch	mm
Q_v	Gear quality	
r_{bG}	Base circle radius gear	mm
r_{bp}	Base circle radius of pinion	mm
r_G	Pitch radius gear	mm
r_p	Pitch radii of pinion	mm
r_t	Wheel radius	mm
S_c	allowable contact stress number	MPa
S_F	bending factor of safety	
S_H	contact factor of safety	
S_t	allowable bending stress number	MPa
T	input torque	Nm
V	pitch line velocity	m/s
V_{max}	Top speed	m/s
Y_N	stress-cycle factor for bending stress	
Y_Z / Y_Z	reliability factor for bending/contact	
Y_θ	Temperature factors	

Z	length of the line of action in the transverse plane	mm
z_1	Number of teeth pinion	
Z2	Number of teeth gear	
Z_E	Elastic coefficient	$(MPa)^{0.5}$
Z_N	Stress-cycle factor for contact stress	
Z_R	Surface condition factor	
Z_W	Hardness ratio factor for pitting resistance	
ϕ	Transverse pressure angle	degree
ϕ_n	Normal pressure angle	degree
ϕ_r	Operating transverse pressure angle	degree
φ	Helix angle	degree
ω_1	Angular speed of pinion	rad/s
ω_2	Angular speed of gear	rad/s
ρ	Density	kg/m^3
σ_{bi}	Bending stress, if, *i =1* for pinion, *i=2* for gears.	MPa
σ_{ci}	Contact stress, if, *i =1* for pinion, *i=2* for gears.	MPa
σ_S	Yield point	MPa
σ_{ut}	Ultimate Tensile strength	MPa
$\tau_{\max}$	Maximum principal shear stress	MPa
υ	Poisonous ratio	
υ_G	The poisonous ratio of materials gear	
υ_p	The poisonous ratio of materials pinion	

CHAPTER ONE

1. General Introduction

1.1. Background and Rationale of the Study

The growing demand for the protection of natural resources and environmental protection has aroused people's attention to the development of compact and light vehicles. These vehicles have many advantages over conventional vehicles. They are quieter, simpler, and ensure a smooth driving experience. Electric vehicles have excellent motor performance, such as high torque at low speed and constant power in a wide speed range, while reducing the weight of vehicle components. In the power transmission system of high-speed electric vehicles, the gearbox is the main component, which suffers fatigue damage. Transmission Gear is the most important and widely used transmission in mechanical transmission, and the gear performance directly affects the performance of the entire transmission system

The term power transmission in the vehicle industry refers to the group of components used to transmit power/torque from the engine/motor to the road surface. It often uses lower or higher engine rotation (RPM) as slower or faster the speed of the wheel, which decreases or increases the torque output as desired by the operator. Manual transmission, automatic transmission, continuously variable transmission, dual-clutch transmission, automatic manual transmission, and electrically variable transmission are some of the types of power transmission systems employed in vehicles [1, 2]. Therefore, regardless of the type of vehicle it may be, a power transmission system contains several parts.

Recently car producers, due to attentive compulsory procedures and strict fuel consumption regulations, are attracted to manufacture Electric Vehicles (EVs). Climate change concerns have raised problems for the automotive industry, as carmakers have to follow strict emission requirements and regulations. Regulations 443/2009 and 510/2011 of the European Commission restrict the average CO2 emissions from new passenger cars to 130 grams/km by 2012, which is a reduction of about 25% from the 2006 directive, as specified in the Directive regulations [3, 4]. The same pattern is also present in other countries such as Brazil, which set new emission limits for CO (carbon monoxide), HC (hydrocarbon), and NOx (oxides of nitrogen) by Regulations 418/2011 and 314/2002 [5, 6].

So far, the development of electric vehicles requires compact transmission system and lightweight design to compensate for the weight of the battery pack. EVs have been used reduction gear either two-stage gear speed or single-speed transmission system. [7, 8]. Transmission gear in EVs, as discussed in [9], is one of the most important components and requires proper design in terms of different variables to perform for its intended purpose. Modern power transmission systems are much lighter, with the demand for energy-efficient vehicles, and improving fatigue resistance is also a key factor in allowing the design of compact components to be used in advanced vehicle transmissions without scarifying fatigue strength to prevent fatigue failure. The choice of material and the heat treatment method used are crucial to improving the resistance of transmission gears to fatigue failure [10].

Without compromising strength, achieving high load-carrying capacity and reduced gear weight, are major research areas of gear material development, fatigue analysis, surface hardening process, and the development of transmission gear laboratory apparatus. A helical gear is the researchers' preference as a power transmission gear type because it has advantages over other types, such as smoother teeth engagement, noiseless operation, and highly efficient operation. It has a drawback, however, because it generates an axial thrust in addition to the radial and tangential load of spur gears. [11]. Thus, either suitable thrust bearings are used to solve this problem or the axial thrust can be neutralized using double helical gears [12]. The researchers used the former remedies to minimize the thrust load developed by the helical gear.

Power transmission gears are under severe load applications which could cause stress concentration on the active flank and root fillet of the gear. Hereafter, proper material development in terms of chemical composition, mechanical property, and heat treatments shall provide sufficient strength and hardness to resist fatigue failure. Generally, gears are mostly designed for a finite life. Hence, material design and development should be a priority area suited for its intended purpose [13]. Low alloy steels are favored among the prevalent types of materials used for transmission gear due to high dimensional stability under extreme contact and bending stresses. Nonetheless, the current alloy steels are not well-matched to what the author expected. So, material development by adding alloy

elements can lead to what the researchers desired. Also, lowering and controlling the morphology and size distribution of non-metallic oxide inclusions requires lowering other residual impurity elements.[14].

The transmission gear surface should be hard with soft and hardcore to provide wear and fatigue failure protection [15]. To meet this requirement, either carburizing or nitriding processes that generate diffused surface layers are implemented in the Case Hardening method of transmission gears. The method of case hardening is accomplished by diffusing carbon in carburizing processes and nitrogen in nitriding processes. In both instances, particles dispersed to deeper depths within the steel substance and the surface hardened due to the diffused atoms and formed thicker depths of the case. By applying the Low-Pressure Carburizing (LPC) and High-Pressure Gas Quenching (HPGQ) technology, the bending strength of the tooth root can be greatly improved compared to conventional atmospheric carburizing and oil quenching heat treatment.

Although gear design currently relies on different standards like AGMA and ISO standards, to estimate the surface and subsurface stresses in the gear teeth. In determining contact stresses on non-conformal surfaces and bending stress on tooth roots through analytical equations and a comparison of these calculated values within permissible stresses, the design approaches used to size gear teeth are envisaged [16]. Recently, to estimate the two stresses of gear teeth (bending and contact stresses), gear design relies on different principles, derived from a combination of theoretical and empirical research. These days, an investigation was carried out on transmission gear shot peening to increase the bending strength of the tooth in gears. However, surface durability in the form of macro and micropitting is now considered the dominant restriction on gear life and performance. Suzuki [17] studied gear surface in the form of macro and micropitting, and the improvements as illustrated in Figure 1-1. This makes the design life of a gear unit primarily dependent on its surface fatigue capacity rather than on bending fatigue.

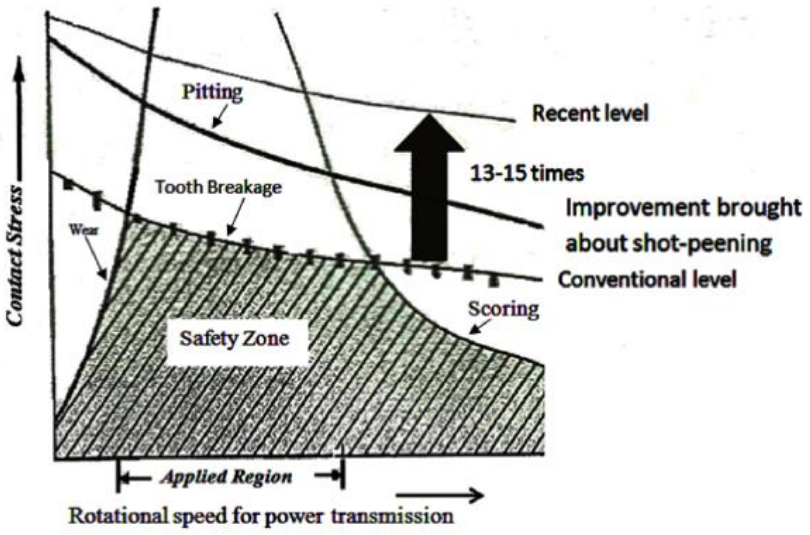

Figure 1-1: Failure of gears for contact stress and rotational speed [17]

During surface modification, a thin but very hard compound layer is formed at the surface of the gear during nitriding procedures. In this process, due to low process temperatures below the transformation temperature, the very hard diffusion layer underneath and a small amount of distortion is created and it takes more time. As a consequence, when contrasted with carburizing processes, it offers the advantage of simpler processes. The method, on the other hand, takes a long time, which is typically at least 80 hours, and the depth of the case obtained after this very long time is very limited. Besides, longer hours are needed during the nitriding process to be able to get the required nitrogen deposition thickness layer on the surface of the gear [18-21].

As a result of fatigue failure on the surface/subsurface of the gear, the transmission gear in vehicles is strongly affected by load variations, driving conditions, and speed. Research studies show that for testing transmission gear fatigue failure, test rigs are required. The performance of the gears depends on parameters such as their geometry, chemical composition of the material, manufacturing process, and work environment [15, 22]. In rolling contacts, such as in gears and rolling element bearings, the typical failure modes are micro pitting, small pitting, pitting, spalling, and scuffing.

1.2. Statement of the Problem

High fuel costs and environmental concerns associated with energy consumption and air pollution have increased the importance of efficient transmission systems. Transmission gears are subjected to cyclic loads as they constantly enter and leave their gear mesh. The successive loading induces cyclic bending stress in the gear root and contact stress on the gear tooth flank surface. The transmission gears have been working under severe operating situations of loads and rotations. This condition leads to gear fatigue failure. Two main factors affect the service life of transmission gears: surface durability (contact strength), and tooth bending strength. As Y.Suzuki,2004 [17] indicated graphically, gear technology has more bending strength than contact fatigue strength as the bending strength was enhanced by applying shoot peening treatment. Similarly, Akyıldız, Kulekci et al.2015 and Soyama, 2019 [23, 24] explicitly show that shoot peening enhances the bending fatigue strength of alloy steel. However, there is a strong demand to improve surface contact fatigue strength as the main factor to enhance service life. In transmission gear, the flanks of the interacting teeth roll and slide simultaneously on each other, except at the pitch diameter, where contact is only obtained by pure rolling. Traction between the tooth flanks is undesirable because it causes an opposing torque, generates heat, and encourages rolling contact fatigue which can lead to surface fatigue failure manifested micropitting. Surface fatigue is a process by which the surface of a material is weakened by cyclic loading, which is a type of general material fatigue.

Thus, all the aforementioned problems need to have a solution accordingly. This study is to resolve the gear contact fatigue failure by improving the existing gear material by adding alloying elements and varying chemical composition. The enhanced surface materials are expressed in micropitted area ratio, micropitted equivalent diameter, and micropitted depth.

1.3. Objectives of the Research

To respond to the key challenges set out in the problem statement, this research entitled "Development of Ni-Modified Alloy Steel for Power Transmission Gear Material and Investigation of Its Fatigue Failure" is conceived and a preliminary concept note is drawn up. The general and specific objectives of the research activities are as stated below. These identified objectives will serve as the basis for the problem-solving effort and will also serve as a guideline and reference for further study in this area.

1.3.1 General Objective

The general objective of this research is to develop power transmission gear for lightweight vehicles and investigate the developed gear materials using an analytical and experimental approach.

1.3.2. Specific Objectives

The specific objectives of the research are to**:**

- Develop contact fatigue-resistant transmission gear material
- Prepare test specimens based on ASTM standards for mechanical properties (tensile, hardness, and impact) and for rolling-sliding contact fatigue RCF test of the developed gear materials
- Carry out fatigue stress analysis and design of transmission gears using KISSsoft gear simulation software and AGMA standard
- manufacture an adapted twin-disc contact fatigue machine
- Investigate the fatigue failure modes and surface topography of the roller specimens using a rolling contact fatigue machine.
- Compare the failure mode of the developed and existing materials.

1.4. Significance of the Research

The importance of this research work is to design and develop power transmission gear for lightweight, and compact vehicles that resist contact fatigue failure. This study concentrates on the investigation of the fatigue failure mode for power transmission gears. This research developed materials by adding a Ni-content to existing gear materials and investigating their mechanical property. In addition, the developed materials examine their fatigue failures using an adapted twin-disc contact fatigue gear test rig. Fundamentally, the twin-disc test rig is used to simulate transmission gear using roller (disc) specimens. It is, therefore, very important to develop the gear test rigs to study the effect of materials, lubricants, and other parameters on the contact fatigue failure mode of transmission gear materials. Lastly, the contribution of the dissertation is to convey the findings to the scientific community and to pave the way for the use of transmission gear technologies on an industrial scale.

1.5.Scope and Limitation of the Study

The main focus of the research was to investigate the mode of fatigue failure of transmission gear materials. To choose suitable materials, the research performs tests such as tensile, hardness, and impact strength tests. However, the fracture toughness test was not carried out because the laboratory apparatus was not available. To compensate for non-available laboratory facilities, the study estimates using an artificial neural network modeling (ANN) model. For validation, a further experimental test has been done using a rolling contact fatigue (RCF) test.

1.6. Organization of the Dissertation

This dissertation consists of seven chapters, and a brief chapter-based overview is given below:

Chapter 1: addresses the general introduction of the study, including the background problem statement, scope, and importance of this study.

Chapter 2 outlines the conceptual structure of this research, beginning with a summary of the study's related literature. Firstly, it presents the mechanics of gear contact and its geometry. The next section describes the machinery and manufacturing processes,

including the heat treatment process and the mechanism of surface hardening. The last section is all about the various modes of failure that have been mentioned.

Chapter 3 discusses the methodology and material design selection of this study, including the presentation of different methods used to develop the material, such as artificial neural networks (ANN) and experimental methods.

Chapter 4: deals with the design and fatigue analysis of the power transmission gear. In this chapter different approaches are implemented to achieve the lightweight and compactness of transmission gear.

Chapter 5: A detailed discussion of the design and development of a Twin-disc contact fatigue machine including accessories and a temperature-controlled lubrication system is presented. This chapter involves designing the machine, manufacturing, assembling parts, and adding some accessory systems as per the design.

Chapter 6: outlines the experimental investigation using a twin-disc contact fatigue test rig into the contact mechanism of test specimens.

Chapter 7: Discussed general conclusions, future study, and recommendations

CHAPTER TWO

2. Literature Review

2.1. Introduction

Gears are mechanical components that are usually used to alter a power source's speed, magnitude, and direction. It is also used based on gear ratios to adjust the output torque as required by the machine operator [25]. Depending on the type of gears they use, vehicle transmission gears may be recommended in different alignments (linear or planetary). As research study shows, spur, helical, ring, and bevel are some of the types based on the gear alignments that can be used for vehicle transmission gears. For gear reduction types, spur and helical gears are usually used. The involute versions of the two most used gears in the vehicle transmission system are shown in Figure 2-1. Both gears have specific advantages and disadvantages, so the spur gears are used where high performance is required and noise levels are of no concern. However, as stated in [26] the helical gears used were quiet in operation and high load-bearing capability are important parameters. Besides, due to the axial tooth overlap, helical gears have a higher overall contact ratio. Consequently, helical gear characteristics enable a considerable increase in the load-carrying ability compared to spur gears. Similarly, the helical gears have a longer life with the same content, efficiency, lubrication, load form, and other factors of spur gear [11, 27]. Overall, the development of spur gears to improve their efficiency resulted in helical gears [28]. Sizing the gear parameters is a key task when designing transmission gears. To do so, the parameters of the helical gear vary from those of the spur gear. Gear parameters such as helix angle are found in helical gear which was not in spur gear. The design parameters and terminologies of the helical gear are shown in Figure 2-2. As can be seen in the figure, it is possible to get different sizes of helical gear by varying these parameters [29, 30].

Helical gears are more advantageous than spur gear of the same size. However, shortcomings of a helical gear are that in addition to the radial and tangential spur gear load [11], it produces an axial thrust force. To overcome such problems either appropriate thrust bearings are used to solve this issue, or the axial thrust can be neutralized with the use of double-helical gears [12].

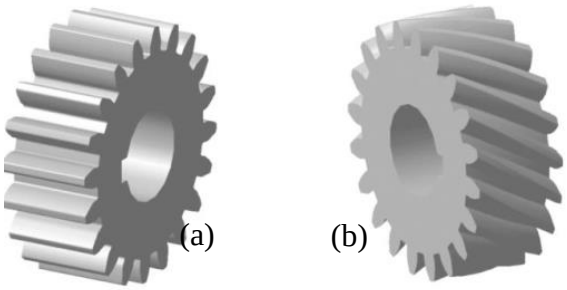

Figure 2-1 Model of involute (a): spur gear (b): helical gear [31]

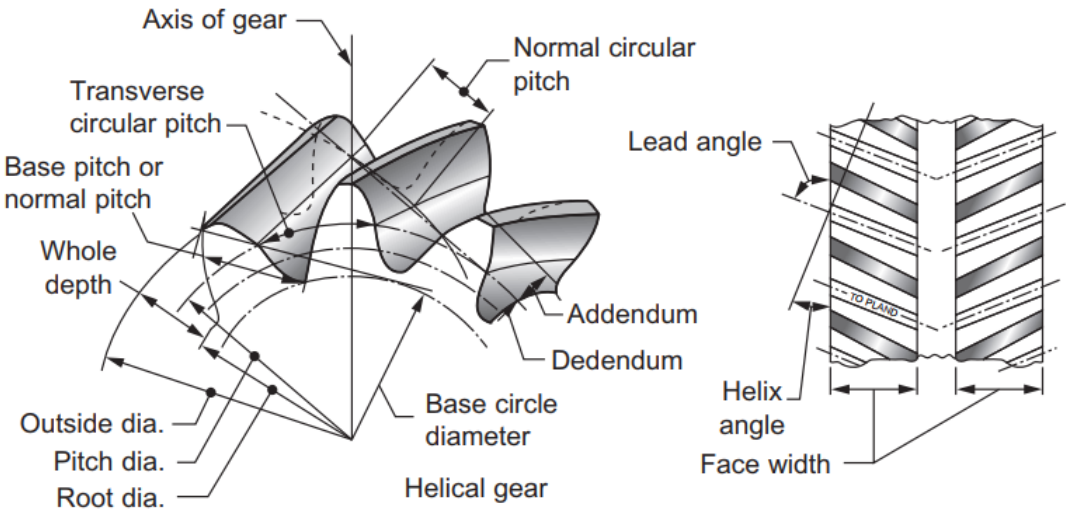

Figure 2-2: Terminologies for helical gears [29, 30]

2.2.Gear Contact Geometry

Designing gears, need to determine variables parameters like a module (m), tooth numbers (z_1, z_2), face width (b), profile shift (x_1, x_2), etc. Besides helix angle and pressure angle also plays a critical role in the gear designing process. Usually, the pressure angle is used at 14° or 20° for both helical and spur gear. These days, it is possible to make gears with different pressure angles due to the advancement of the manufacturing system. During meshing, the contact lines for helical gears are not perpendicular to the moving direction, but instead, have a base helix angle (φ_b) mostly between 0 ° and 45 °. Meanwhile, at an early design stage, the helix angle needs to be chosen. Also, to achieve an effective helix angle, precise measurements of geometrical parameters must be performed as clearly indicated in [32-34]. Other important geometrical parameters in the gear design are the base pitch (P_b) and

the normal pitch (P_N) need also to compute. Concerning the contact between the helical gear pair, the contact line between the two teeth is defined by two points expressed by two parameters, t_1 and t_2, where t_1 expresses the direction of width and t_2 expresses the height. The points are labeled with dots as shown in figures 2-3. The line of contact is the line on the surface of action between the two points expressed in (t_1, t_2). On one side of the gear, t_1 is zero, along with the width of the gear. At the base circle, t_2 is zero, with the radius increasing as noted in [35, 36].

The helical gear teeth pair's preliminary contact area is close to the tip of the driven tooth and near the root of the tooth of the driver as shown in Figures 2-4. As the meshed gears rotate, this contact area shifts from the instant contact. Pure rolling of the contact surfaces was noted only at the pitch point. At the helical gear height increase/decrease, there is a combination of rolling and sliding, above and below this pitch point respectively. When the point of contact shifts away from the pitch line, the sliding speed increases. To elaborate more on this regard, at the beginning and the end of the engagement, see figure 2-4 of meshed teeth, indicating the rolling speed (R) and sliding speed directions (S) respectively. This contact condition always exists for both the driving and the driven gears below and above the pitch diameter as clearly indicated in [37].

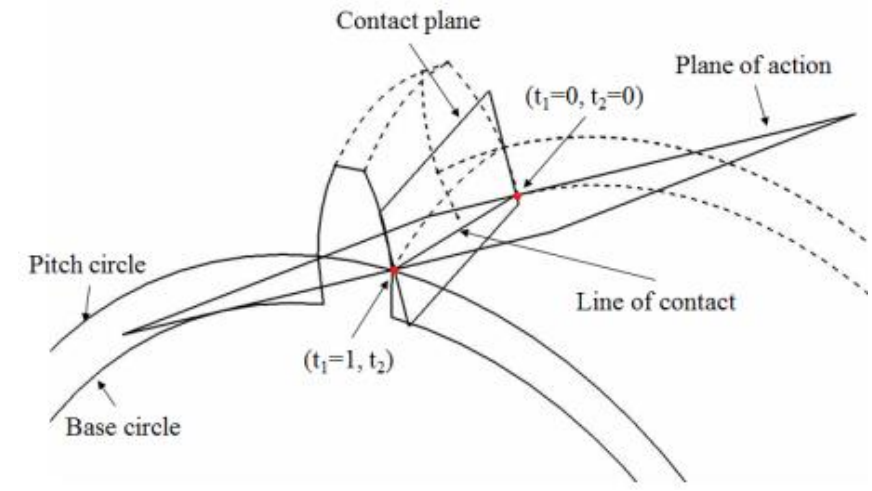

Figure 2-3: Plane of action with the line of contact for helical gears

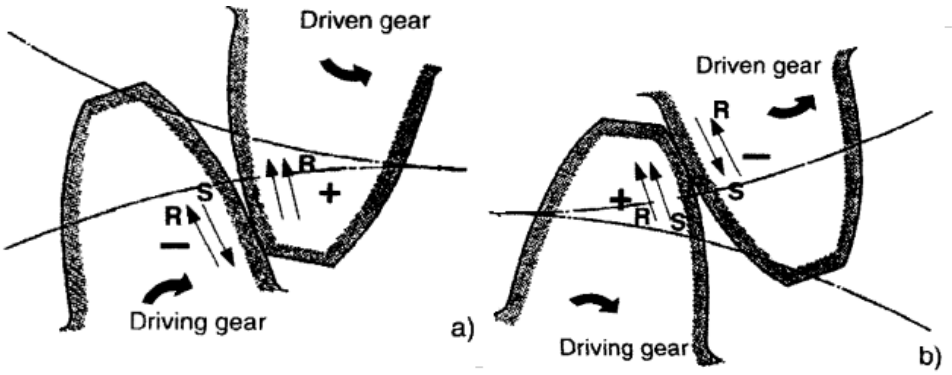

Figure 2-4: Gear rolling and/or sliding speeds (a): the beginning of engagement (b): termination of engagement [37]

The contact properties of helical gear pairs are not the same as those of spur gear pairs. The contact of spur gear pairs takes place lengthwise with a straight line parallel to the gear axis. At the beginning of the tooth meshing cycle, the contact unexpectedly triggered over the full face width and also terminates abruptly at the end, as cited in [38, 39]. The entire load is transmitted by this contacting pair situation which makes load transmission less than completely smooth from one tooth to the next tooth.

Unlike spur gear pair, the helical gear pair contact begins at the first tooth face end as a point and then extends from being a point to a line of gradually increasing length which moves over the tooth flank extending in length until it reaches the second tooth face. An overlap must be achieved from one tooth pair to the next as the contact area shifts across the gear, from one side to the other [40]. Meanwhile, the contact line length subsequently lessens and ends as a point at the second tooth face end. Therefore, between the face ends, the line of contact of helical gear pairs works diagonally. Also, at least a pair of teeth are in contact with helical gears in all conditions, and the total load is divided between these contacting pairs, and only part of the total load is transferred to the next pair. As a result, helical gears have higher load carrying capacity and lower noise, vibration, and harshness (NVH) compared to the counterpart of spur gear. Therefore, the helical gear type is more suitable for transmission systems where noise and vibration were a challenge.

As indicated in figure 2-5, the action of the tooth engaging mechanism of the helical gears and the normal load applied (F_N). At the moment of engagement, the gear contact

mechanism where two pairs of teeth are in contact, such as the tooth (z_1) with the tooth (z'_1) and the tooth (z_2) with the tooth (z'_2) at the same time (see figure 2-5 (a)).The gear contact mechanism at the further position of engagement where the contact tooth (z_1) with the tooth (z'_1) leaves. Meanwhile, the contact line of teeth pair tooth (z_2) with the tooth (z_2') moves away from the lower gear tooth tips shown in figure 2-5 (b). As displayed in Figure 2-6, the contact mechanism comparison between helical and spur gear pair, which shows the directional variations of the line of contact in the two drives as well as the inclination of the line of contact between helical gear teeth relative to the gear axis owing to the helix angle [41-43].

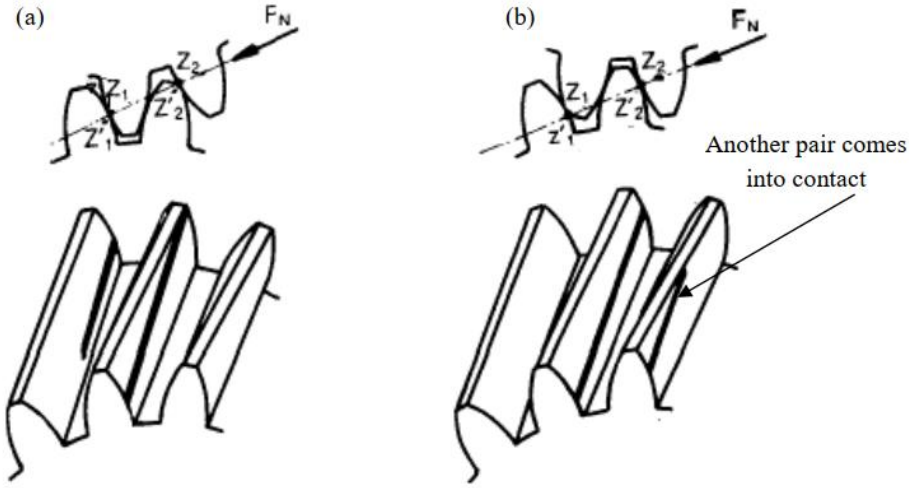

Figure 2-5: Engagement of the tooth with helical gear drive [42]

The schematic representation of involute gear pair in contact (both spur and helical) in the transverse portion (see figure 2-7(a)). As stated in numerous literature, the pair involute teeth engagement generates contact along the action line (AB) that is tangent to both mating gear base circles and is also inclined at the pressure angle (ψ) to the line perpendicular to the gear centerline (O_1O_2) (see figure 2-7 (a)) as indicated in [44, 45]. Likewise, figure 2-7 (b) represents the geometry of driver gear (pinion), and the limits of the path of contact can be determined from the geometry of the triangles outlined in the stated figure 2-7.

As shown in figure 2-7, A and B are the first and last points of contact in the line of action respectively. The position of these points can be determined by the distance as cited in

[43], which is the length from the pitch line to the contact point measured along the line of action. Besides, the average time for a pair of teeth in helical gears to complete their meshing cycle is different from that of the spur gear. If the pitch surfaces of the mating gears are considered, the length of the meshing helices would be the same on both the pinion and the gear. Width is also assumed to be a pure rolling motion in the case of the angular velocity of the contact area around the face, as no actual translation of the metal takes place in this direction. There is, however, a small sliding part that works along with the tooth. The length of the meshing helices will be the same on both the pinion and the gear if the pitch surfaces of the mating gears are considered.

The sliding magnitude will vary with the nature of the tooth. However, the percentage of sliding can vary around the contact area because the sliding velocity depends on the displacement from the pitch surface. The key sliding velocity that happens at the contact of the tooth works up and down the height of the tooth as clearly stated in the paper [40].

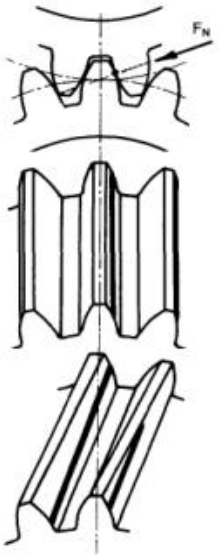

Figure 2-6: Comparison b/n the spur and helical gear contact, transverse section (upper figure), spur gear (central), and helical gear (lower) [42].

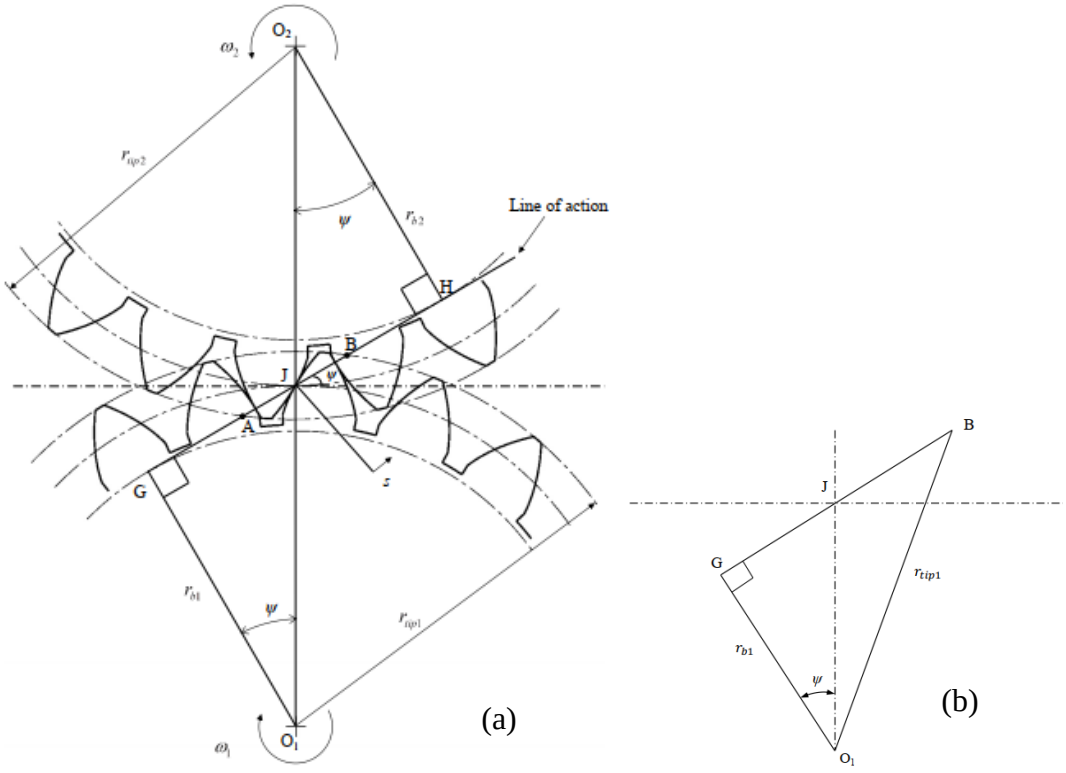

Figure 2-7: Involute gears in contact (a): schematic geometry of pinion (b) [46] [47]

Nowadays, the main issues in gear design have changed over time. Previously, size, interchangeability, strength, and efficiency were major concerns in the gear design process. These days, vibration and noise have become increasingly important considerations in gear design, as quieter gears are considered an indication of product quality [48]. Advances in engineering and increasing the speed of work in today's gear applications have clearly shown that noise and vibration are unwanted side effects associated with the use of gears in the power transmission system. With the market pressures for higher power densities, the development of high-performance, low noise mechanical drives presents a generic problem in the power transmission system, and in particular in the various gearing fields [49].

Therefore, helical gear type for electric vehicles power transmission system was chosen in this study: Electric vehicles equipped with onboard motors that rotate at speeds of more than 10,000 rpm, which is much higher than conventional internal combustion engines (max. 6000 rpm), which creates problems with high centrifugal forces and demanding heat

transfer at the interfaces and generates more noise and vibrations [50]. To alleviate such problems a power transmission system equipped with a two-stage high-speed helical gear transmission system in an electric vehicle speed reducer is taken as the research objective in this study.

2.3. Gear Surface Contact and Roller Simulation

A pair of transmission gear contact surfaces can be categorized as non-conformal contact as a sort of contact presented in figures 2-8. The contact of the gear pair can be simulated by two overlapping cylinder contact as presented in [51]. The shape of the contact areas depends on the curvature of the contacting bodies. Any of the forms of contact are between two balls there are point contacts, between two parallel balls there are line contacts, cylinders, and elliptical contacts occur when two cylinders are crossed, which are most commonly used in many practical engineering applications as shown in figure 2-8 [52, 53]. The interaction between two elastic bodies is represented as simpler contact of two parallel cylinders as indicated in figure 2-9, based on the Hertz principle. For a given geometry, elastic properties, load, and the pressure distribution formed within that contact zone can be determined by the Hertz theory of the elastic contact zone. This theory suggests that contact between two surfaces, involving small strains, is non-conforming and frictionless, and that each body can be considered a semi-infinite elastic solid. The contact, initially started at a point or a line when two convex bodies are pressed together. The contact area will expand as the load increases, forming a shape of a circular or elliptical. A line contact issue in which two identical cylinders are brought into contact is the contact between a pair of involute teeth gear. For two-dimensional line contacts, this type of contact is used to derive contact pressure distribution, stresses, and displacement [43, 54, 55].

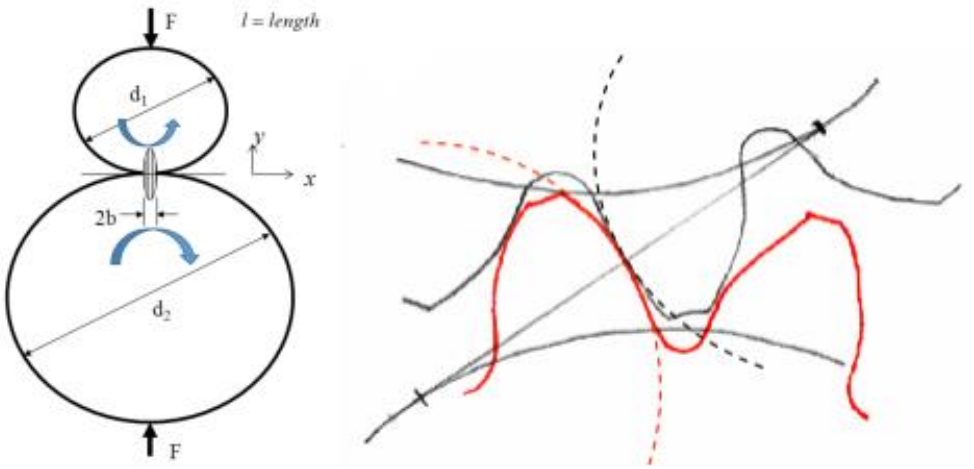

Figure 2-8: Simulation of (a): roller contacts (b): gear surface contact [56]

The non-conformal contact employs Elasto Hydrodynamic Lubrication (EHL) type during high load application. In this regard, over a small contact area generating pressures that are high enough to result in considerable elastic deflection of both surfaces as well as to alter the properties of lubricating oil as it flows through the contact as displayed in figure 2-9. From this point of view, based on the theory of elasticity developed by Hertz, the values of stresses acting in such contact forms can be calculated from the analytical formulas. The distribution of the stress field in the contacting bodies is determined by Hertzian contact theory, depending on the properties of the materials, the roughness of the surfaces, contact geometry, lubrication mechanism, and size of the elastic contact zone [43, 57]. A plot of the pressure distribution in the contact zone is depicted in figure 2-9. The contact pressure (pmáx) is maximum at the center and zero at the edges.

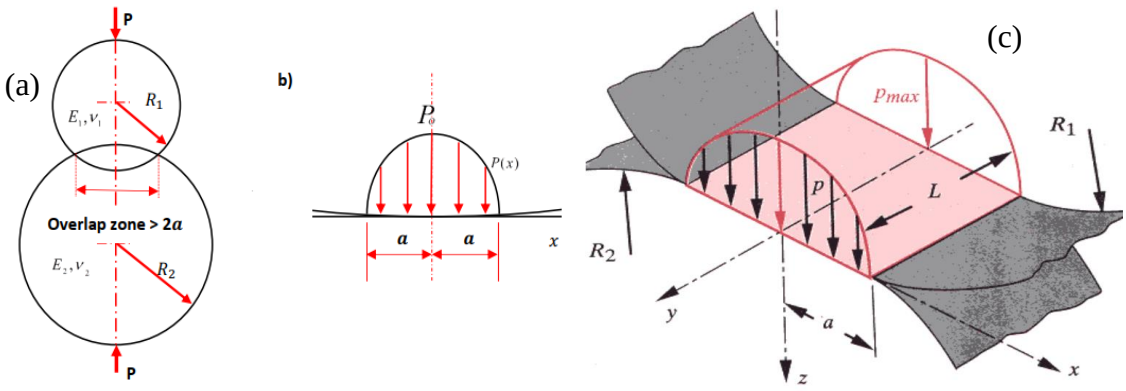

Figure 2-9: Non-conforming contact (a): two elastic overlapping cylinders (b): semi-elliptical contact zone distribution pressure (c): ellipsoidal pressure distribution[57, 58].

The Hertzian contact stress has occurred nearest to the pressure line, and the teeth experience pure rolling contact and zero sliding at the pitch point [59]. Thus, this condition can be modeled as Hertzian contact pressure as indicated in [60]. However, in rolling and sliding situations, the interaction between two bodies causes shear stresses that minimize the component's fatigue lifetime. When a smooth surface is subjected to cycling rolling contact, the maximum shear stress occurs in the subsurface and not at the extreme surface depending on the geometry of the contact (spherical or elliptical) [61-63]. Accordingly, the material encounters a complex stress distribution pattern in an elastic, non-conformal contact.

The shear stress at the surface level would be zero during a pure rolling scenario. However, tangential shear stresses on the surface can occur during sliding contact between the contacting surfaces and the maximum shear stress will move from depth to a level close to the surface [64-66].

During load application, research work reveals how elastic body transforms into plastic bodies. As the elastic and elastic subsurface material comes into contact at lower loads, the surface is elastically deformed with the maximum principal shear stress. The maximum principal shear stress becomes greater than the critical shear stress of the solid when the load rises to some degree [57]. When a small amount of plastic flow occurs within the larger elastic setting, subsurface yielding material will contain. The plastic area grows and the contact pressure rises until the plastic region hits the surface as the load increases rigorously.

To test the gear surface contact behavior, different testing mechanisms were employed. To make it easier to account for gear surface contact analysis, it is useful to replace the complicated contact geometry of the transmission gear pair with an equivalent of two contact rollers or discs to simulate the rolling-sliding surface contact behavior of the power transmission gears. Equivalent rollers or discs have the same radii of curvature as the gear tooth flanks at any point on the line of engagement. This allows the use of Hertz contact theory, where the distribution of contact pressure in the contact area of two cylinders can be simulated. In addition, to simulate the transmission gear, the rollers should have the

same slip-to-roll ratio as gears need to be tested. To simulate the drive gear using roller or disc specimens, tests were performed in a twin-disc tribometer, which simulates sliding-rolling contact fatigue behavior. [67]

Rolling contact fatigue (RCF) of transmission gear test using test facilities where discs are used to resemble gear contact conditions can be traced back to 1935 developed the first twin-disc platform. In fact, in a mesh of gears, the radii of curvature of the teeth, as well as the sliding speed, change continuously with the profile of the involute. In particular, the sliding speed is zero only at the pitch point and increases in the modulus moving towards the tip and the root of the tooth. Conversely, discs allow reproducing only the rolling-sliding conditions at a specific point of the contact path of transmission gears. However, since it is much cheaper to use discs instead of actual gears, and the surface of a disc is easier to inspect and analyze than the recessed surface of a gear. For such conditions, twin-disc test rigs have been used to simulate responsible working conditions of transmission gear [68].

Meneghetti, Terrin, et al. 2016 [68] indicated that to simulate transmission gear, disc or roller samples were used. Typically, samples consist of two discs pressed together to achieve the desired contact pressure. Rolling speeds and diameters can be chosen to generate a relative motion with varying degrees of rolling and sliding between the sample surfaces. The size and shape of the specimens also vary depending on the variations of the type of twin-disc test rig employed. To simulate the power transmission gear of case-hardened alloy steels using a two-roller contact fatigue tester, the size of the test rollers was as shown in figure 2-10 (b). The outside and inside diameters were 70 and 45 mm respectively, and the outside corner of the high-speed roller sample was modified to provide an effective contact width of 7.5 mm as indicated in [69].

Likewise, the fatigue damage of contact railway wheel and rail can simulate using a twin-disc test rig by employing disc samples. The size and dimension of the upper and lower disc samples were 5 and 8 mm respectively in the upper and lower axis (see figure 2-10 (a))[70]. Furthermore, experiments were also carried out on friction and wear testing rigs to simulate the power transmission gear developed by the key mechanical transmission

laboratory of Chongqing University. The sample rollers were used in this experiment (see in figure 2-10 (c)). The diameter of both mating rollers has an equal size of 50 mm and a radius of curvature of 12.5 mm. To reduce the influence of the stress concentration on the edge of the rollers, the widths of the sample rollers were 10and 12 mm respectively. In this study, the outer and inner diameter disc sample sizes were 70 and 45 mm respectively, and 28 mm thick. In this experiment, the geometry of the high-speed disc was modified so that the effective contact area is 8.5 mm.

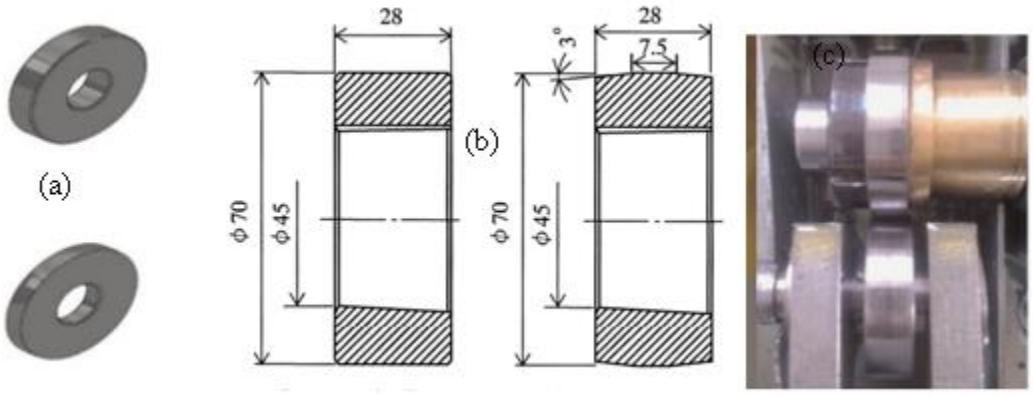

Figure 2-10: roller specimens used in twin-disc tribometer a) [70] b) [69] c) [71]

2.4. Gear Materials, Manufacturing, and Heat Treatment Methods

2.4.1. Gear Materials

Transmission gears are a key machine component between prime movers and driven units and are adopted as power transfer components. Consequently, if gear material is not chosen properly, it could not work well for its intended purpose and cause many complications. The problems encountered with gears are very complex and multitude in nature. Material selection and development for the transmission gears plays an important role in countering the challenges of transmission gear and has become research interest to suit the purpose [58, 72, 73].

Transmission gears are usually subject to extreme load applications that could result in stress concentration on the gear's active flank and root fillet. Subsequently, the proper development of materials in terms of chemical composition, mechanical properties, and heat treatment method must have sufficient strength and hardness to withstand fatigue

failure. So, the design and development of materials should be a focus area suitable for its demanded purpose [13].

The criteria of materials selection for transmission gear includes hard enough to resist tooth root breakages and surface damage. Also, should be tough enough to endure shock loads imposed on the gear pairs. In other words, gear materials need to have a hard case to offer adequate fatigue strength, wear resistance as well as a tough core for preventing brittle failure under high impact loads [74-76]. Thus, to satisfy the transmission gear materials selection criteria, material design and development should due attention to lessen any stress concentration enacted [76, 77].

A wide variety of materials are used to develop gears depending on their applications. Usually, gear materials are steels, cast irons, bronzes, and phenolic resins. Non-metallic materials and non-ferrous alloys are also used for light-duty gears where low torque is needed [78]. Similarly, materials like bronze are used for gears working in a corrosive atmosphere, Polymers employed for gears having a low modulus of elasticity and strength, and steel used for owing higher strength, higher torque, and greater power. Alloy steels are the material of choice for vehicle transmission gears as a result of a wide variety of material strengths that can be achieved [79].

Usually, alloy steels are the most common materials used for the development of gears for machine structural materials [80]. Whereas advanced alloy steels are the most preferred materials to achieve the requirements for high-speed transmission gears [81-84]. Researchers have to choose the best suited or improved existing steels for their function from the vast collection of candidate material choices. Therefore, several advanced material selection techniques are available to select the current steels as an exploit in [85-87] to mention a few decision matrices, pugh method, phase of analytical hierarchy, and Ashby method [88-90]. A crucial research role in promoting the lightweight and compactness of vehicles is the lightweight material design for transmission gears. Like Ashby's method, numerous lightweight material design techniques are indicated in [87, 91]. Material available for vehicle transmission gears is designed either for bending strength requirements or/and for surface strength. During cyclic meshing, gear materials

have to withstand bending and contact stresses and should have high longevity and resist wear.[92].

Case hardened alloy steels have been the material choice for transmission gear for several decades to withstand the stresses developed [83, 93]. Another way to improve the resistance of stresses on gear materials is to modify existing alloy steel by adding alloying components [94, 95]. The influence of the alloying elements such as aluminum (Al) and nitrogen (N) on the microstructure and mechanical properties were investigated experimentally under different conditions was carried out to compare the modified and the existing materials [96, 97]. Likewise, low alloy nickel-chromium-molybdenum steels such as SAE 4320 and SAE 8620 alloys are commonly used and contain about 0.5 to 0.8 percent Cr and 0.2 percent Mo with a nickel content in the former of about 2.9 percent and reduced in the latter alloy to 0.55 percent. Carburizing grades with a simple carbon content of 0.2 percent for both alloy steels. However, modified by the addition of silicon and vanadium, a successful result is shown to achieve greater strength and toughness than the existing material [98-100]. Once commonly used for large case-carburized gears with high nickel content (3.5 percent), EN36 alloy steel has attained a high degree of hardness and difficulty for manufacturers due to resistance to grinding, and SAE 8620 alloy steel, which is hard, can achieve adequate and easy manufacturing for the development of small gears by making lean in nickel material.

Special alloying elements are then applied to the existing alloy steel to achieve high material hardenability, ensure the stability of grain size and fine microstructure, as investigated by [101], and are important for high-performance case hardened steels. To modify the existing gear steels, the four most prevalent alloying elements are used. These include nickel, molybdenum, chromium, and manganese as clearly indicated in [102]. These modified alloy steels have their advantages and disadvantages: chromium alloy steels are used when only low hardenability is needed, manganese-chromium alloy steels often used with medium hardenability are desirable, and medium/high hardenability chromium-molybdenum alloy steels are required, highly hardenable chromium-nickel molybdenum steels for severely loaded components and nickel-chromium steel steels.[103-106].

The Modified alloy steel was formed by adding alloying elements like nickel, chromium, and molybdenum to get a strong and tough part. Noticeably, the composition of modern gear steels is important for these alloying elements [107, 108]. Nevertheless, the developed alloy steels their load-carrying capacity depending on microstructure (inclusion size) and chemical composition. If the amount of alloy content is not precise, the possibility of initiating a crack below the surface can occur. A fundamental way to fix these problems is to change the alloy steel's chemical composition, heat treatment, and case hardening. Studies [109, 110] indicate that remedies can be made in adding alloying elements to modify the chemical composition in case hardened steels are as follows :

- Prevent MnS inclusions and reduce S, limit Mn;
- Prevent TiN inclusions and control Ti/N wt % ratio close to three;
- Improve hardenability and increase Mo;
- Improve toughness *and* increase Ni and Mo;
- To refine and homogenize grain size and balance all Nb, Ti, Al, and N
- Strengthen grain boundaries and reduce P and S, add Mo and Nb [109, 111].

From the discussion on different research studies, the gap analysis on various alloying elements of transmission gear material is as follows; The power transmission gear is the basic component that mostly suffers from fatigue failure through the formation of bending and contact stresses. As cited in Suzuki [17], the bending failure mode was improved by applying shoot peening treatment, but the contact failure mode still needs to be optimized to combat the fatigue failure. As a result, the transmission gear material type plays a key role in withstanding fatigue failure, since different research studies indicate that there is no single type of material that can endure contact fatigue. Besides, by adding alloying elements to the existing gear material, the study strives for better materials to increase contact fatigue strength. Commonly, the high-speed transmission gears used Cr-Mo alloy steel (DIN 1.7243), which is widely applied for highly stressed transmission gears. Even though the contact fatigue strength of this material is also suffering contact fatigue failure to overcome the challenges with existing gear materials, as mentioned in the discussion, the modification of the chemical composition using alloying elements is a key activity. Adding an alloying element to the existing gear material can create different mechanical

and physical properties than before. So far, the alloying elements have their pros and cons over the existing ones. To mention some alloying elements, Manganese is used for less demanding applications due to its comparably low cost. Mn alloying can also generate inclusions by reacting with sulfur and creating MnS [112]. Similarly, Titanium alloying added to the optimum range is difficult by creating grain coarsening. In addition, Ti can produce TiN inclusion if not properly controlled the contents[111]. Another alloying element is carbon content in the cemented layer itself ensures good hardenability. However, it is limited to enable good impact strength [113].

Likewise, other alloying elements can be added for obtaining high core hardness. Nickel alloying provides a moderate increase in hardenability, yet the main reason for its addition is improving toughness. Higher additions of nickel can cause stabilization of retained austenite, especially in the carbon enriched surface-near area, resulting in reduced strength and wear resistance. Moreover, higher manganese and chromium additions have been favored for many gear applications [83]. However, such addition of alloying, although providing good hardenability, has limitations in terms of toughness and tempering resistance. Besides, the prevention of intergranular oxidation requires Mn and Cr levels to be reduced. Adding the amount of alloying element of Si and Ni of carburized alloy steel improves mechanical property and surface durability. Therefore, modifying the existing Cr-Mo alloy steel with Ni can enhance toughness and hardness. Thus, this study seeks to investigate the amount of Ni content added to the commercially available materials to withstand rolling contact fatigue failure.

2.4.2. Manufacturing Method

The gear manufacturing process starts by producing a gear blank once the material is selected, which is completely relieved of stress to reduce distortion that could have occurred during the early stage of the manufacturing process. The gear blank is a gear part that can be shaped simply without any teeth. With the aid of measuring tools, the gear teeth are then patterned to the appropriate shape and size. The processing techniques used for the forming of gear teeth can be different depending on the application of the gears. In line with the literature, three kinds of techniques such as casting, forming, and metal removal

can be used to manufacture gear teeth. Each category can be further divided into many categories as shown in Figure 2-11 as indicated in [79, 114, 115].

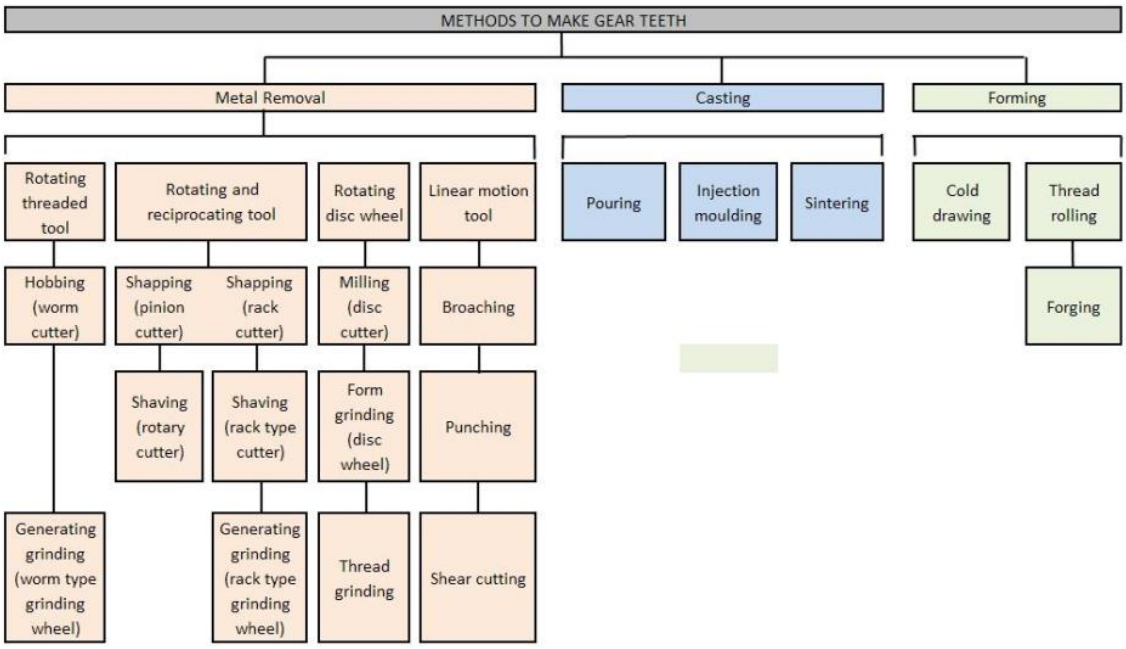

Figure 2-11: Methods of gear teeth manufacturing [115]

Manufacturing transmission gear needs advanced and highly specialized techniques since as the apparent complexity of gear geometry modification increases, to do so, it needs advanced technology. Most gears are performed on specialized machine tools specially built for the development of gears, i.e. many axis CNC machine tools have become available, more gearing can be performed using these tools as long as detailed models can be imported into the machine [116-118]. Thus, the manufacturing process of the gear is usually long and complicated, but it is then important to produce effective and well-performing gear.

The available manufacturing technology and methods employed to produce transmission gears and challenges associated with the conventional processes can be summarized as follows: Machining (material removal) methods such as hobbing, milling, and shaping pose limitations include long setup time, tool wear, creates tool marks on the gear, requires subsequent polishing operation for further quality improvement and consumes large amounts of cutting fluid and energy [119]. However, in recent years, significant progress

is being observed in the development of modern metal forming processes like InvoMilling and five-axis machining have been developed that allow the use of standard multi-tasking machines and standard tools to provide a solution to these gaps. InvoMill utilizes a face cutting tool to interpolate the involute of the gear tooth. Therefore, the major gear parameters like module, pressure angle and helix angle are determined by the tool path. These multi-tasking machines are very flexible utilizes a parametric model to define the form of the gear [120].

Similarly, gear forming processes such as stamping and extrusion also have defects, including finishing requires shaving, extrusion die wear, and limited tooth width and thickness. Another method of gear production, gear additive processes such as die-casting and powder metallurgy have limitations trimming after the gear has been removed from the die, arrangement of fine metal powder of all types is difficult and not suitable for gears other than a spur gear. Introduce alternative and advanced gear manufacturing and processing technologies, such as gear rolling and electric discharge machining (EDM). Macro EDM and micro EDM have been recognized as potentially important alternatives to conventional machining because of their excellent repeatability, geometric accuracy, surface integrity quality, short set-up time, easy-to-cut complex geometries and shapes, and elimination of mechanical stress during machining [121].

Forging has long been used to manufacture gears, especially gear blanks, which are then machined to obtain the final desired shape. Gear blanks are made by open die and closed die forging, and precision forging gears. These gears require little or no post-processing and are now widely used in automobiles, trucks, and off-road industries. And the energy and mining industries. Studies have shown that the impact resistance of forged gears has increased by 30% [122]. Accordingly, this study employed the following manufacturing process of test samples; melting the commercially available material (ingot) in a vacuum or argon atmosphere furnace, adding % Ni-content and hot forging and rolling the forged material into the desired shape, heat treatment, and finally, the surface is refined by EDM.

2.4.3. Heat Treatment Method

Most transmission gears are made of case-hardened alloy steel that withstands high load-carrying capacity, fatigue, and wear. The transmission gear case hardening method is applied by either carburizing or nitriding processes that produce diffused surface layers [123]. The method of case hardening is accomplished by diffusing carbon in carburizing processes and nitrogen in nitriding processes. In both instances, particles dispersed to deeper depths within the steel substance and the surface hardened due to the diffused atoms and formed thicker case depths [80].

In the presence of a carbon-containing gas atmosphere furnace, the gear is heated to a temperature in an austenite temperature range during the carburizing process. Carburization in industrial processes limits temperatures up to 1050 ^{0}C and for 25 hours of treatment time. Under these conditions, carbon diffuses into the near-surface layer during a prolonged holding period. The depth of diffusion increases as the holding time increases. A concentration of elements makes the surface harder at the end of the diffusion period [124]. To achieve a martensitic structure, the gear is normally quenched in different media (water/oil). Carburized gears are usually associated with problems of contact fatigue that lead to extreme tooth deformation and grain coarsening [125, 126]. To make the sequence carburizing process of AISI 8620 steel more elaborate, take a schematic representation as shown in figure 2-12 [127, 128].

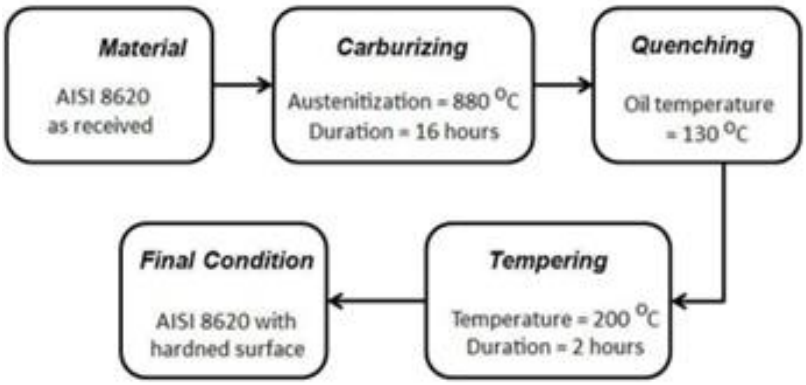

Figure 2-12: Sequence of treatment conducted on AISI 8620 steel [127].

The demand for case-carburized gears has now shown that there are some inadequacies in existing alloy steels that are not case-hardened [129]. Large gears used in high-power windmills, for example, have repeatedly been unexpected and prone to early failure due to gear tooth breakage or pitting damage on gear flanges [130, 131]. This form of fatigue failure involves a complete shift in the gearbox and entails high repair costs. Carburization and quenching are commonly used to reinforce transmission gears, but due to structural phase transformation, they undergo significant distortions. To correct this big distortion, an extra cost is needed [132]. For this reason, at a low cost, both high fatigue strength and low distortion have to be realized. [133].

Nitriding is a method of heat treatment by the injection of ammonia (NH3) gas in a furnace and heating up to 500 to 580 ° C to diffuse nitrogen into alloy steels. Heat treatment of alloy steels at austenitic or higher temperatures, with significant distortion issues. Therefore, modern hardening methods have been produced at a lower temperature as a result of reducing the distortion of the nitriding heat treatment as discussed in [134]. During this process, it was difficult to obtain a fatigue strength equal to or higher than that of carburized and quenched steel and a material hardness adequate for gear machining at the same time [135]. This day, however, obtaining high-strength nitriding steel for gears having a hardness adequate for the machining before the treatment and then the fatigue strength equivalent to that of carburized and quenched steel after treatment as experimentally tested [133].

The main role in the nitriding process is to produce a thin yet very hard compound layer on the gear surface. In this process, due to low process temperatures below the transformation temperature, the very hard diffusion layer underneath and a small amount of distortion is created and it takes more time. As a result, when compared with carburizing processes, it offers the advantage of simpler processes. The merits of the hard compound layer can be completely achieved through the application of nitriding after the grinding process as indicated in Figure 2-13. This method, on the other hand, takes a long time which is typically at least 80 hours, and the depth of the case obtained after this very long time is very limited. Also, longer hours are needed to be able to obtain the necessary

nitrogen deposition thickness layer on the surface of the gear during the nitriding process [18-21].

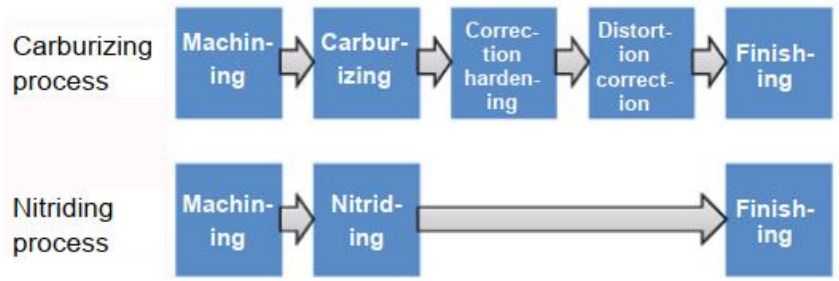

Figure 2-13: Comparison b/n carburizing and nitriding heat treatment process [136]

As the load-carrying capacity of gears has been intensively investigated, nitriding is a necessary heat treatment method for highly loaded components such as high-speed vehicle transmission gears [137]. A high load-carrying capability can be assured as long as the compound layer is intact. It can be concluded that a high nitrided gear load-carrying capacity depends on the sufficient depth of the diffuse layer and the stable layer of the compound. However, the risk of micropitting often increases due to the increased surface roughness following nitriding. Therefore, it may be favorable to grind the gears after nitriding as shown in Figures 2-13. Therefore, as shown in Figures 2-13, the grinding of the gears after nitriding can be favorable. A high load-carrying capacity can also be provided by the ground gears, but it must be taken into account that wear efficiency decreases significantly as it is mainly affected by the compound layer [138]. In general, the realization of an adequate nitriding hardness depth with transmission gear is the focus of the research study to establish a stable compound of the layer.

During the formation of austenite alloy steel, a wide variety of properties can be obtained during quenching at the same time by modifying the carbon content and subsequent tempering treatment, in which hardness can be "traded off" toward toughness to balance mechanical properties with the design requirement. Martensite is formed from the austenite field in low alloy steels following rapid cooling (quenching). In alloy steel, the martensite phase will attain strength and hardness. However, as strength and hardness grow, its ductility is lost.

Tempering is a low alloy steel heat treatment mechanism introduced by heating at intermediate temperatures to recover some ductility and toughness even with a reduction in strength. This temperature is referred to as martensite cooling (Mc) during cooling, the martensite begins to form at a characteristic temperature. As the temperature decreases, the amount of thermal martensite transformed continually increases. When further cooling does not increase the amount of transformed martensite, the martensite finish (Mf) temperature is reached. With martensite, some retained austenite usually occurs even at a temperature below Mf. Mc in low-alloy steels decreases with increasing carbon content and most of the alloying elements that enter the austenite phase into a solid solution [139]. The diffusion of carbon and nitrogen to the retained austenite from transformed regions stabilizes the untransformed austenite (an impediment to further transformation of the martensite) [140].

Thermomechanical treatments such as nitriding and carburizing are often used to improve the surface of transmission gear. An important difference between these treatments is the temperature at which they are performed. Hard and stable nitrides are formed in the diffusion layer, if the base alloy steel contains alloying elements Cr, Mo, and Al. To achieve significant hardening and depth of the diffusion layer, a material containing alloying elements with a high affinity for nitrogen. Thus, aluminum is a strong nitride former however, higher more Al content will cause surface cracks under working conditions. Chromium is a very ideal element because it improves the mechanical properties of alloy steels by improving hardenability and nitrablity. Similarly, Molybdenum also forms stable nitrides at the nitriding temperature. However, Nickel, manganese, and copper do not interact with nitrogen.

Carburizing consists of an accumulation of carbon on the surface, which gradually decreases toward the core. Alloying elements usually used to improve the hardenability of carburized steel are manganese, chromium, molybdenum, and nickel. Chromium and molybdenum are strong carbide former. Manganese is not a potent carbide former as chromium, however, promotes cementite networks. Within the standard range of carburizing steel, nickel and silicon reduce the lattice parameters of iron, making the gap more difficult to dissolve and slowing down carburization.

For this reason, this research has focused on the nitriding case hardened, which is performed at a relatively low temperature with less distortion, and successfully produced a new type of steel for nitriding high-speed transmission gear. Therefore, nitriding is more suitable to transmission gear containing alloying elements as tabulated in table 3-1 because it permits minimum distortions and high dimensional control due to the absence of phase transformation. As a result, this study uses the nitriding method for the surface hardening mechanism.

2.5. Rolling Contact Fatigue Test Rig

Machine components subjected to repeated Hertzian loads often fail due to contact fatigue. Contact fatigue damage manifests as nicks or cavities formed by fatigue cracks that have developed under repeated loads until the material falls off. In rolling contact fatigue, the point of failure is not well defined. Components may run even after a single pitting formation with a slight deterioration in performance. Therefore, the identification of the failure point is still under research. Some researchers consider the formation of a single pit to be a failure, some others consider 5% of the pitted contact area to be a failure, and still, others considerably more. As pitting is the manifestation of rolling contact fatigue failure, to examine rolling contact fatigue of transmission gear, use a set-up of contact fatigue test rig. To experiment, two specimens with the form of discs were rolling in opposition to every other. Each of them was driven through a motor. Rolling contact fatigue test rig used to test gear contact fatigue parameters. Some of the parameters that should be taken into consideration when seeking to simulate situations on gear surface flanks are, material, surface profile, load, lubrication, and size effects.

The development of the railway, transmission gear, and bearing materials with improved rolling contact fatigue and wear resistance is a long and expensive process. This process may involve different types of laboratory experiments at different scales, including, but not limited to, small-scale twin-disk tests and full-scale test bench experiments, as well as track tests. The time required to perform such experiments varies from one hour for twin-disc experiments [141] to several years for track tests[142, 143], full-scale test rig experiments [144, 145], in which a piece of rail, gear, and bearing, usually requiring several days of testing. Relatively short test times and good reproducibility of contact situations related to

the components degradation mechanisms make full-scale test bench experiments of developmental interest to examine the relationship between conditions, load, and damage patterns in a repeatable and systematic manner.

RCF experimental tests are used to simulate small-scale operating conditions, evaluate and characterize new materials, to reduce the cost of railway and transmission gear operations[146]. Twin disc is perhaps the best testing option and has therefore been widely used to test fatigue and wear resistance of railway wheels and rails and transmission gear and bearing [147], as it allows the control and measurement of the variables experimental, is economical and efficient compared to other test options [148] and can reproduce contact pressure and slip conditions[149].

However, the small-scale testing approach can result in the loss of information about the actual behavior of materials, although there are correlations between wear and plastic deformation of the surface between laboratory and full-scale testing [150]. Kráčalík et al. [148] reported that the size of the contact area in twin-disc tests is different from full-scale tests. Therefore, it may be wrong to assume that the material behavior in the twin-disc test can be scaled to actual size because the contact and plastic strain issues are not linear. Lewis et al. [151] explain that the contact geometry in small-scale tests is simplified and that the conditions of the operating environment are difficult to reproduce. In contrast, Buckley-Johnstone et al.[152], performing dry and lubricated tests on a full-scale platform and twin- disc to assess the performance of a friction modifier, concluded that under conditions of dry contact, the wear rates were statistically the same, while in the presence of the friction modifier the change in the traction coefficient was similar in the two tests. Lewis e Olofsson [153], when mapping wear coefficients for railway and transmission gear steels, collected experimental data from field measurements and twin-disc tests and noted that the rate values of wear rates are reasonably consistent. There are still many gaps in the literature regarding the assessment of similarities and differences, as well as the possibility of extending the wear and RCF results found in laboratory tests to full-scale tests and ultimately to machine component conditions real, which makes this type of work essential [151].

Rolling contact fatigue testing is the primary method for studying the rolling contact fatigue performance of materials under simulated working conditions. To ensure that the fatigue test can achieve accurate and reliable test results, the testing machine should accurately simulate the test conditions and has the function of continuously working for a long time and accurately recording the data of functioning [154]. As multiple types of research indicate, there are many types of machines to test rolling contact fatigue for different components.

A Delta Research Corporation developed three-ball RCF test stand was used to assess the longevity of the three alloyed materials under complex RCF conditions by simulating the types of load and fatigue conditions experienced by bearing components in service. A more detailed description of the setup and functionality of this particular RCF tester is provided in [155].

A twin-disc contact fatigue test rig was used to carry out experimental investigations on rolling-sliding contact rollers in various fields of study. The wheel and rail twin-disc test rig has been explicitly designed to examine the specimens of wheel and rail contacts of the railway system [156]. The test specimens were positioned one test disc head over the other disc with horizontal axes as shown in figure 2-14. And concerning load application, as clearly shown in Figures 2-14, the disc samples were hydraulically loaded together and powered independently by two electric motors. To track the compressing force of the two-disc samples, a load cell has also been built into the rig.

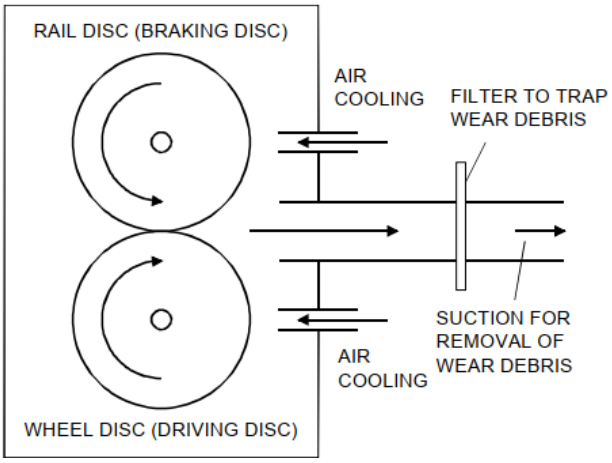

Figure 2-14: Schematic representation of twin-discs test rig [157]

For the contact fatigue tests, the FZG-LASC tribometer was used to test spur gear as shown in Figures 2-15. This tribometer was designed, manufactured, and assembled at the Contact and Surface Laboratory UTFPR (LASCUTFPR). Using the principle of power recirculation, two pairs of gears can be tested at the same time. The load is imposed on the gears by applying a torque to the shaft on which the wheel is mounted (FZG loads k6 and k9). Torsion on the wheel axle is achieved by applying an eccentric load, using a lever and a dead weight. To produce accelerated wear on the side of the gear teeth, it is common to use gears with a modified profile [158]. The gears used as samples were tested in the FZG machine following a similar procedure proposed by the FZG Institute (FZG, 1992) for pitting tests. In this method, in addition to the geometric characteristics of the gears, the shapes of the run-in load and the phases of the pitting test are also presented.

Another type of test rig is a back-to-back power circuit of the Forschungsstelle für Zahnräder und Getriebebau (FZG), which has a drive gearbox and test gearbox engaged by two torque shafts. A clutch is incorporated on the first shaft for the load application mechanism, and the temperature regulated for the test specimen was also employed [159]. For the investigation of load-carrying power, elastohydrodynamic lubrication, tribological contact, performance, dynamic coatings, and fatigue strength, the FZG testing rig provides an efficient setup. The experimental test of the spur gear pair was carried out on the FZG test bench. The test bench for the FZG pitting test is a back-to-back spur gear test bench, can test gears that have a center distance of 91.5 mm with a closed power circuit. A standard lubrication system was also used with the temperature-controlled immersion of the tested gears.

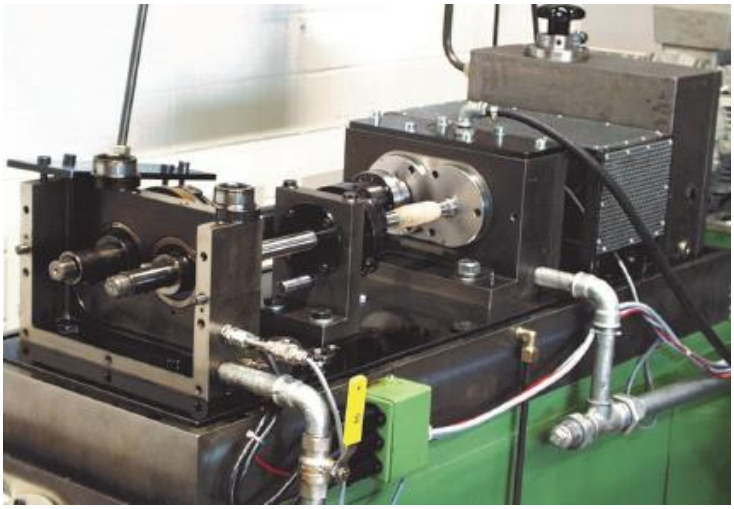

Figure 2-15: FZG Contact fatigue test ring

Among the RCF machine, a distributed pitting failure test rig was employed to monitor distributed pitting failure in helical gears as presented in [160] and shown in figure 2-16. The test machine has a stiffened structure used to mount the driving motor and a two-stage helical gearbox, which has a speed range from 0 to 3000 rpm. The test rig has an accelerometer to detect the vibration signal created by the gears. To carry out the experimental test of the pitting failure of helical gear load (KN) ranges were selected at 16.07, 20.5, and 29.36; rotational speed (rpm) range was 750, 1000, and 1500; Pitch line velocity (m/s) was taken as 3.57, 4.76, and 7.14.

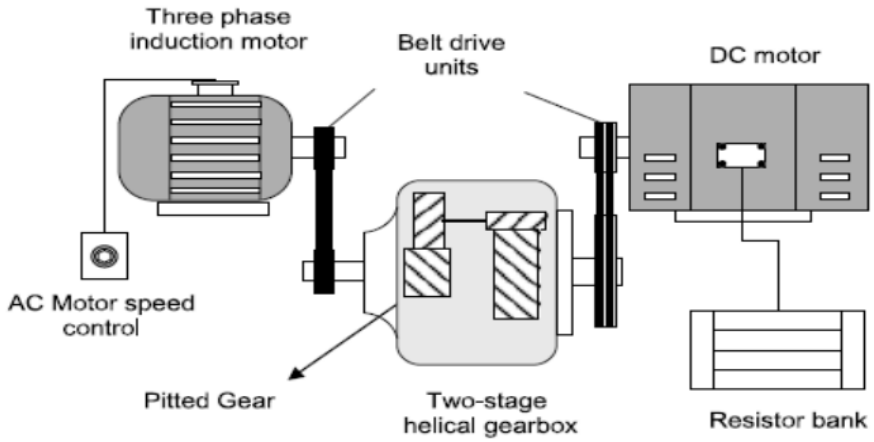

Figure 2-16: Test rig for monitoring helical gear distributed pitting failure [160]

Furthermore, a twin-disc contact fatigue tester has been also developed by Sheffield University Rolling Sliding (SUROS). As shown in figure 2-17, the SUROS was carried out on a Colchester Mascot lathe with an independently operated AC motor at the tailstock end. The SUROS test rig allows rail-wheel and transmission gear interface testing at a small scale. Investigation of rail-wheel and gear rolling contact fatigue (RCF), wear and adhesion, testing of lubricants, traction products, track circuits, and sanding investigations are the main areas of testing for the machine. A torque transducer and a load sensor were incorporated into the test rig. The pair of test discs used for testing on this test rig was machined with a contact width of 10 mm and a diameter of 47 mm. It enables a computer-controlled variable slip (0 to 20%) and load (900-1800MPa contact pressure). Data can be logged for the load, traction, and slip. Water was using a channel, applied to the surface of the test disc at a rate of about 2 drops per second for lubrication purposes in the SUROS machine testing process.[161].

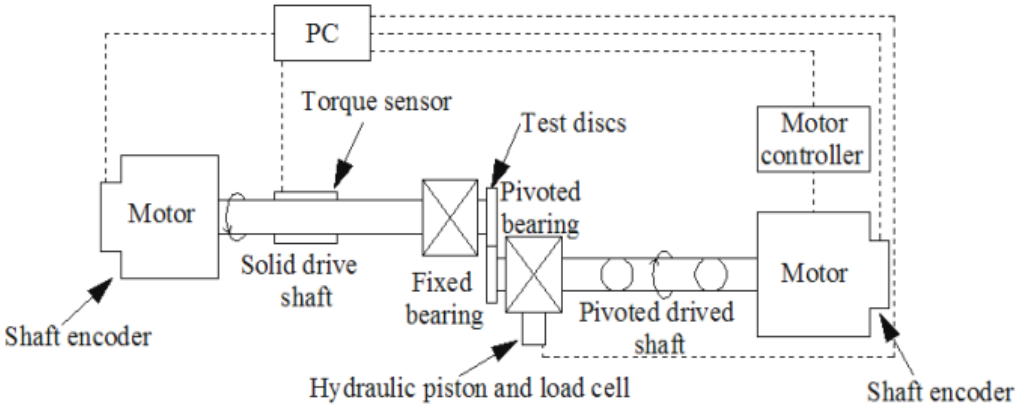

Figure 2-17: SUROS twin-disc tester [161]

Similarly, Micro Pitting Rig (MPR) is also a contact fatigue tester in which three counter-face disc samples are loaded against a central roller sample (see figure 2-18). The test rig consists of three counter face discs and a small roller specimen, each mounted on a separate drive shaft with sample assembly. A ball screw that is operated by a stepper motor is attached to the loading arm. The load is applied to the roller specimen via the top counter face disc and transferred to the lower two discs. The test rig used a temperature-controlled dip lubrication device to lubricate the roller samples, partially submerging the counter-face discs and dragging oil into the contacts during operation.

The roller specimen shaft is fitted with a torque meter which, during the tests, provides a continuous amount of torque. Besides, the MPR rig is fitted with an accelerometer that returns a vibration measurement to the loading arm. The degree of vibration signal is prone to pitting damage on the test sample so that when a malfunction happens, the rig can be immediately stopped [59].

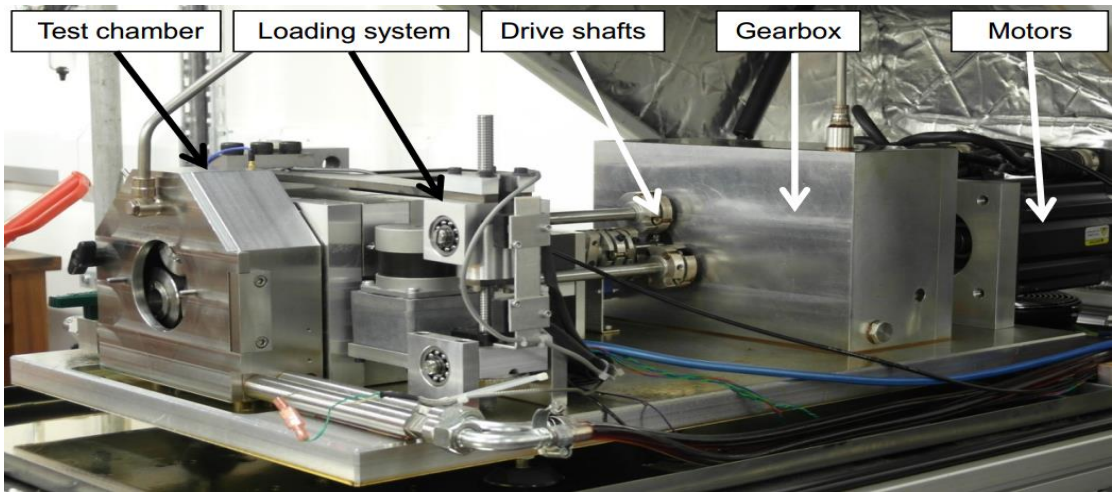

Figure 2-18: Micro pitting Rig [162]

TE-72 Two roller test rig (see figure 2-19 (a)) is a research machine designed to study material wear and rolling contact fatigue under pure rolling and rolling-sliding conditions. There are two motors in the unit, one to supply the input power and the other to absorb the transmitted power. The ideal instrument test rig has a twin-disc test rig that uses two axles placed opposite to each other, which is similar to the TE-72 set-up, but as shown in figure 2-19 (b), it does not have bearings on both sides of the test specimen.

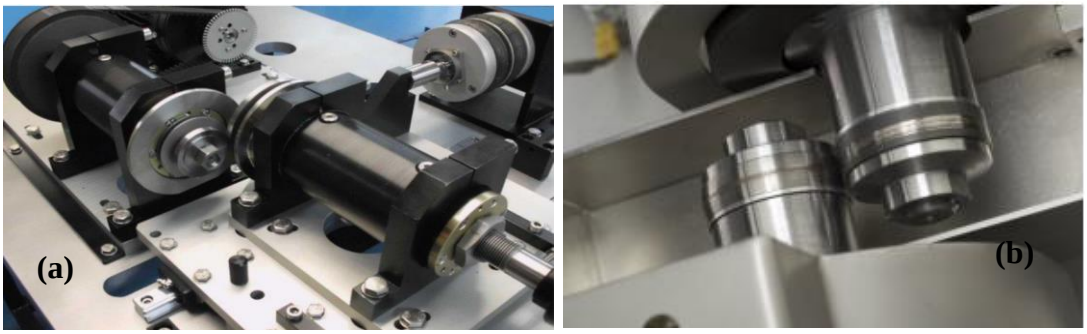

Figure 2-19: (a) TE-72 two- roller test rig: (b) Optimal Instruments test rig [163]

Finally, the Swerea KIMAB test rig was manufactured in the Netherlands by SKF Engineering & Research Centre is used for micro-and macro-pitting processing. This test rig uses two horizontally oriented discs, as can be seen in figures 2-20, where the test specimens were slightly smaller than the loading disc. Under the environmental chamber, the loading mechanism is located and uses a lever arm that is loaded [163].

Figure 2-20: Swerea KIMABs twin-disc test rig [163]

2.6.Transmission gear fatigue failure mode

Transmission gears, like many other machine components, are deemed to have failed when the intended loads are no longer carried out. The surfaces of mating gear teeth are assumed to be separated by a very thin layer of lubricant from a tribological point of view, and the main modes of tooth failure are likely to be identified as micropitting, small pitting, pitting, sapling, and scuffing. Light pitting failure that occurs at the pitch diameter can only be an indicator of surface irregularities in the natural accommodation. The sliding action of the teeth creates a risk for sliding wear on the high spots of asperity in the dedendum and addendum. At the pitch line, where there is zero relative sliding of the teeth and the film of hydrodynamic lubricant tends to break down, attention is focused on this place.

The presence of surface fatigue on the dedendum of driver gear is another option. This is the tooth area that first contacts the driven gear tooth and where the sliding action is opposite to the rolling action, creating higher stresses. This scenario also indicates the gears are overloaded. Note that the pitting is evenly distributed over the tooth length, indicating that alignment was good.

Micropitting is fatigue failure caused by stresses of cyclic surface contact on the gear flank, wherein the addendum and dedendum areas, but not along the pitch circle, rolling, and sliding motion prevails. Micropitted regions, as shown in Figures 2-21, have a dull, evenly grey look [164]. The size of micropitting is much smaller than pitting up to 10 μm dimension [165]. A research study by Oila and Bull [166] checked that the most important factor in instigating micropitting initiation was applied load to the surface of the gear, other factors such as temperature, material, surface finish, lubricant, and slide/roll ratio were less compared to the former. The slide/roll ratio and speed, however, were the factors that caused and had the greatest impact on the spread of micropitting failure.

An essential cause of micropitting formation is plastic deformation at the asperity points of gear contacts. The research studied by [167] determined that the rate of formation of micro pits with time tends to null when pressures on surface asperities are at the elastic level. In the same manner, Ahlroos et al.[168] explored that frictional performance, material properties, surface treatment, surface roughness, and lubricant types influence micropitting. A similar study by Moorthy and Shaw [169] disclosed that rough surfaces showed local valley features that can lead to stress concentrations in the area, resulting in micropitting. Polishing the surfaces was found to reduce the occurrence of micropitting. Further studies have also shown other causes of micropitting such as a paper by [170], which studied the effect of material treatments on micropitting.

A factor in influencing the micropitting event based on Elasto Hydrodynamic Lubrication (EHL) film thickness is also the operating conditions of the transmission gear. Numerical experiments performed by Evans et al. [171] and Sharif et al. reveal that EHL affects the formation of micropitting. Figure 2-21 shows the contact region generated by micro-pitting based on the micro-EHL modeling of the gear tooth contacts. Micropitting tests of gears where the final manufacture of the hardened steel teeth was carried out using various grinding processes were used for the gear tooth contacts used for these studies.

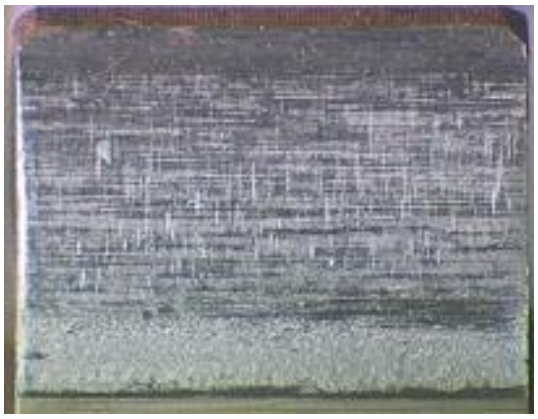

Figure2-21: Micropitting generated at contact region of gear tooth [172]

Pitting is caused by rolling contact or a mixed condition of rolling and sliding contact [172] and can be characterized by small scattered holes, i.e. pits, which occur on the gear surface area. The sizes of the pits rely on the gear material [173]. Large pits of millimeter sizes may occur on a soft gear tooth that is of through-hardened material while surface hardened gears, like carburized or nitrided gears, became smaller pits in micrometer sizes [173]. The material in the fatigue region gets removed and a pit is formed as shown in figure2-22. Pitting sometimes can be seen by the naked eye. Pitting can be categorized as initial and progressive pitting depending on the size [174, 175]. The initial, minor pitting may arrest when the gears operate for a considerable time. Sometimes, however, pitting continues to progress rather than halting due to a high load. This progression leads to pits merging which then results in comparatively larger size pits. The progressive form of pitting is likely to be found on the tooth dedendum but it may spread further to the pitch line area.

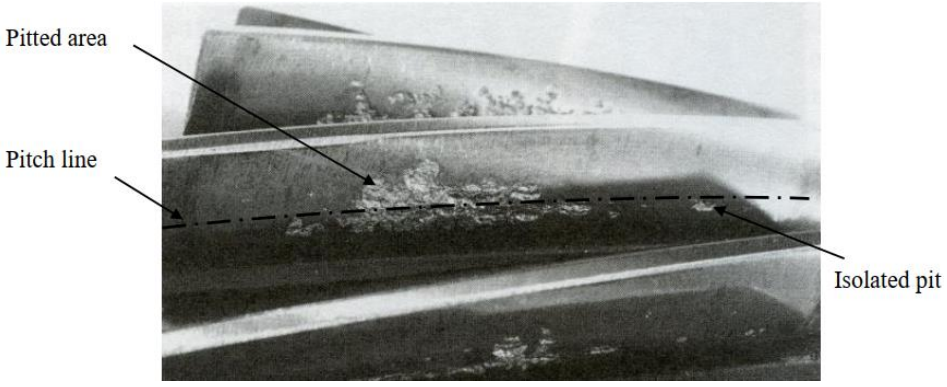

Figure 2-22: Pitting of helical gear teeth [176]

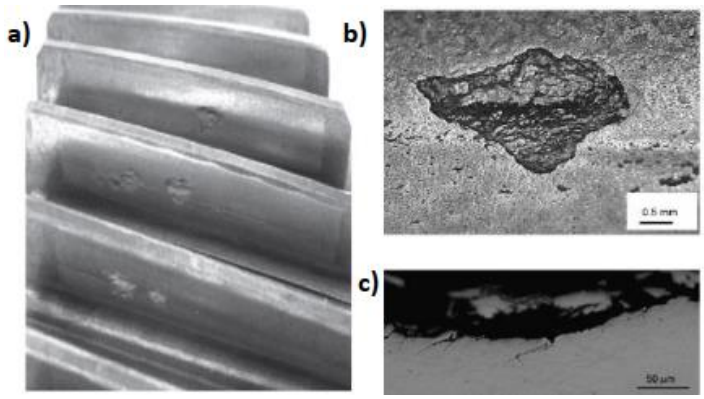

Figure 2-23: Fatigue damage on a helical gear (a): Overview of top helical surface failure (b): Magnification of spall failure (c): Cross-section of spall failure [92]

Spalling is a macro-scale type of Hertzian contact fatigue failure that results in the formation of macroscopic hollows in the contact area. Spalling is the same as subsurface pitting, except when compared to pitting in terms of size, the spalled areas are larger. It is a broad-ranging assumption that when destructive pitting takes place in the dedendum section of gear teeth, spalling occurs due to overload conditions. The ends of pits will disintegrate and then wide asymmetrical shapes that can attach are created. Spalling is called this type of surface impairment which occurs mostly due to high contact stresses. However, in addition to reducing the operating load, it can also be avoided by an improvement in surface hardness [177]. To facilitate spalling several factors can be encountered. A research paper by Hannes and Alfredsson [92] discoursed that the effect of surface roughness that has asperities strongly encourages the initiation of rolling contact fatigue (RCF) crack. The researchers then went on to demonstrate how the asperity point load mechanism could predict the spalling crack path, as shown in figure 2-23.

Until complete hydrodynamic lubrication has been developed, scuffing is most likely to occur during the starting time of gear activity. The scuffing relies heavily on the lubricant properties (minimum film thickness and flash temperature), making it more of a tribological issue. For this purpose, in gear lubrication, extreme pressure (EP) additives are used to avoid damage associated with the startup. Research results suggest that scuffing is caused by factors such as surface stresses, friction, and sliding velocities[178, 179].

2.7. Summary

This review was aimed to summarize gear geometry and contact mechanics, gear materials, and gear manufacturing processes, and the mode of gear failure discussed based on relevant and recent literature. As several papers have noted, altering the chemical composition and surface hardening process plays a key role in improving existing alloy steel materials. The selection of heat treatment and surface hardening generates a high lifelong load-carrying ability to perform its intended purpose. High-speed EV power transmission system like the conventional type, the transmission gear is the basic component that mostly suffers from fatigue failure on the fillet root and flanks through the formation of root bending and contact stresses. As suggested by the literature, the bending failure mode was improved by applying shoot peening treatment, but the contact failure mode still needs to be enhanced to combat the contact fatigue failure. The transmission gear suffers from contact failure due to the constant meshing of a single-speed gearbox type. Consequently, the transmission gear material type should withstand contact fatigue failure. Extensive research studies have also shown that the surfaces of mating gear teeth are assumed to be separated by a very thin layer of lubricant from a tribological point of view, the main modes of tooth failure are likely to be defined as micropitting, pitting, spalling, and scuffing. Several parameters like load, surface roughness, sliding, material hardness, material inclusions, and lubricant type were found to influence tooth failure modes.

CHAPTER THREE

3. Methodology

3.1. Introduction

In this chapter, developing Ni-modified alloy steel for power transmission gear employs various procedures such as investigating mechanical properties of the developed alloy steels using ANN modeling experimental test methods. Hence, the best material from both methods is selected. After this, fatigue stress analysis of the best-selected alloy steel in comparison with the existing material is carried out using AGMA standard and KISSsoft gear simulation software. AGMA standard on gear contact fatigue life calculation based on an empirical model developed from experimental data fitting. The contact fatigue stress and bending fatigue stress equations clarify how to calculate and design the loads and other parameters. The fatigue stress equations of the AGMA standard are mainly based on experience and take abundant factors into account.

Another approach to calculating progressive contact fatigue failure of gear is using KISSsoft simulation software. KISSsoft is a tool for performing sizing calculations for machine elements. Besides different types of gears, it can calculate transmission elements including shafts, bearings, gears, connecting elements, springs, etc. It is possible to compare the results concerning different standards such as ISO, AGMA, and DIN. In addition, the software is also capable of providing different designs and optimization functions. In KISSsoft gear design various options of gear set can be nominated and analyzed. By filling gear parameters such as module, the number of teeth, pressure angle, helix angle, lifetime, etc., the software possibly can calculate the maximum bending stress, maximum contact stresses, and lifetime for the selected type of gears and their safety factors.

KISSsoft gear simulation software has been used to verify the AGMA Matlab script calculations. The AGMA standard Matlab script and KISSsoft gear simulation software exploited different gear combinations with different modules and several pinion teeth that are within the given constraints. The important step in designing transmission gears is also to define the required safety factors particularly the tooth root bending and flank contact

safety factors to sort out the possible solutions. Besides compactness, lightweight, and smooth operation are key parameters that play an important role in this design process. So far, in computing fatigue stresses and various factors for power transmission gear, the design factors rely on different features of geometric design, material, manufacturing processing, and operating conditions.

After conducting fatigue stress analysis, simulating the surface durability of the transmission gear by using a disc sample is very important to verify the best material in combating rolling contact fatigue. To carry out this experiment, the twin-disc test was manufactured locally. The twin-disc contact fatigue testing rig is used to give a duty cycle for test roller specimens to simulate the performance on power transmission gear material by providing the appropriate load that is needed to create the contact fatigue failure. Using gear samples to test the material properties of a newly developed alloy steel gear material requires various test procedures and tracking records, which are time-consuming and expensive. Instead, the contact state of the gears is changed to two test rollers (discs), which are used to simulate the contact between the teeth of the two gear's flanks, which is easier compared to the gear sample preparation and test condition. Therefore, this research employed disc specimens to simulate gear meshing.

As each fore detailed chapter of the thesis does not correspond to each defined objective of the study, a thesis methodology flow chart is suggested in figure 3-1. Recalled and highlighted the addressed objectives, the concerned steps of development of Ni-modified alloy steels, and the employed twin-disc test rig test and sample characterization techniques. As schemed in figure 3-1, the different objectives can hardly be treated independently one after the other since they often interact and increment each other, i.e. development of fatigue failure resistant alloy steel, fatigue analysis of the developed alloy steels, and investigation of fatigue failure mode.

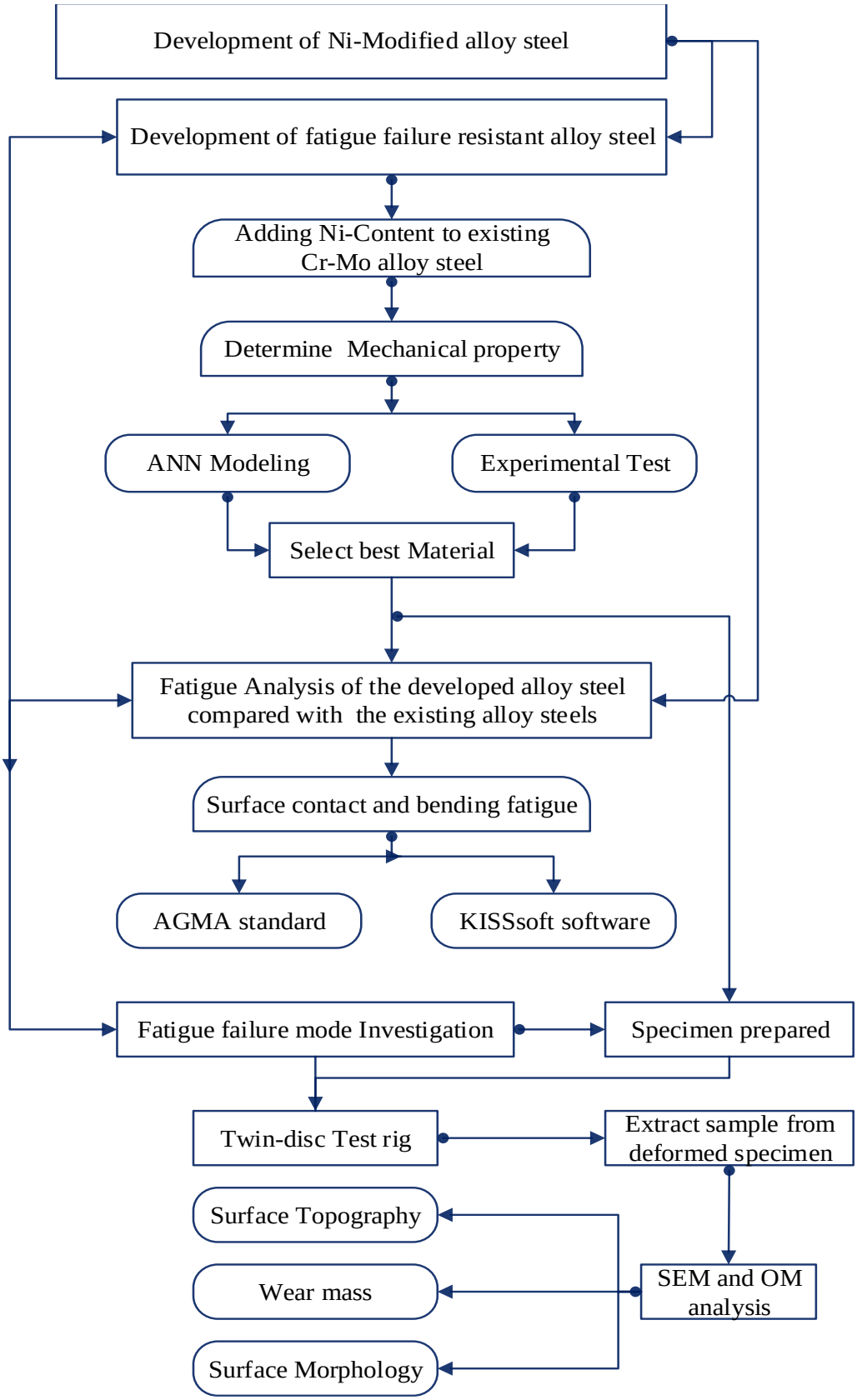

Figure 3-1: Methodology Chart

3.2. Materials

In this study, the materials developed to predict its mechanical properties were prepared by adding Ni-content (mass in percent) to the existing alloy of 1.0 Cr-0.2 Mo-alloy steel. By varying the Ni- content four candidate alloy steels were prepared including the base alloy steel namely 1.0 Cr-0.2 Mo-0.22Ni alloy steel, 1.0 Cr-0.2 Mo-1.55Ni alloy steel, 1.0 Cr-0.2 Mo-1.75Ni alloy steel, and 1.0 Cr-0.2 Mo-1.95 Ni-alloy steel. The chemical composition of the materials is listed in table3-1.

Table 3-1: Ni-Modified Cr-Mo alloy steels input parameter for prediction

Alloy steel	Chemical composition mass (%)									
	C	P	S	Si	Mn	Cr	Ni	Mo	Cu	Bal
Cr-Mo	0.21	0.002	0.003	0.25	0.65	1.15	0.22	0.21	0.18	97.12
Cr-Mo-1.95 Ni	0.17	0.002	0.003	0.23	0.64	1.12	1.95	0.20	0.17	95.51
Cr-Mo-1.75 Ni	0.18	0.002	0.003	0.24	0.64	1.13	1.75	0.20	0.18	95.67
Cr-Mo-1.55 Ni	0.18	0.002	0.003	0.24	0.65	1.13	1.55	0.21	0.18	95.85

3.3. Methods

The typical techniques to investigate the mechanical properties of alloy steels for transmission gear, to select the best material mostly relied on experimental test methodologies which consume time, money, and manpower. However, to overcome the supposed challenges the ANN prediction modeling is a better option to predict the properties of alloy steels to save money, time, and wherever experimental facilities are not available. In this research, the mechanical properties of the Ni-modified alloy steels explore using ANN modeling and experimental test methods then results are compared and scrutinized.

- Artificial Neural Network (ANN) Modeling

There are various modeling types including empirical modeling, computational modeling, finite-element modeling, and ANN modeling. The ANN modeling is an explicitly useful method for addressing issues where solutions are not clearly articulated or where there is no clear formulation of relations between inputs and outputs. The ANN modeling prediction carry out on multiple combinations of alloying conditions, processing routes,

and heat treatment temperatures in the development of new alloy steels. The modeling has been used widely in material science with varying success [180]. It has been demonstrated that it is very effective at predicting mechanical properties such as yield strength, ultimate strength and even crack growth rates with given correct information. To learn the correct data trend the networks involve a large amount of input dataset as addressed in [181].

During the development of the ANN modeling in MATLAB, the following procedures are very vital which comprises data collection from a variety of sources and subsequent filtering of the collected data in conjunction with training, load data source, generate the input and output for the data, transfer the data from excel files to MATLAB files, choose the architecture of ANN, training functions, training algorithms and parameters of the ANN, train the ANN with the processed data, test the trained ANN to evaluate the network performance and use the trained ANN for simulation and prediction.

The dataset used to train, test, and validate the ANN modeling was collected from various experimental test results related to transmission gear materials that were published in [182-185]. The amount of the experimental data collected should be adequate to give an essential amount of input data, and, at the same time, control the amount to avoid overuse of costly experimental resources [186]. The collected data is tabulated in table A1 and table A2 as given in the appendix. Then the collected data divides into three parts: training data, testing data, and validating data. From the collected data, 70% is selected as the training data, and the remaining 30% constitutes the testing data and validating data (15% each). The structure of the dataset for training, testing, and validating has been arranged as input parameters expressed in chemical composition (% C, % P, % S, % Si, % Mn, % Cr, % Ni, % Mo, % Al, % Cu and % Fe (mass %) and heat treatment conditions (tempering and austenite temperatures) in consecutive order. The output parameter of the dataset is also expressed in mechanical properties including ultimate tensile strength (UTS), yield strength, percent of total elongation, surface hardness, fracture toughness, Charpy impact toughness, and percent of retained austenite as indicated in the appendix table A2. The chemical composition of the Ni- modified Cr-Mo alloy steels desired to predict the output parameters are shown in table3-1. The heat treatment conditions such as the tempering

temperature of all the samples are as-quenched (AQ) and tempered conditions from AQ, 200 °C - 500 °C. Similarly, the austenite temperature for all samples is 900 °C.

Training and testing set to the ANN are named epoch. At each epoch the dataset is randomized and the examples in the training set are used to modify the connection weights of the neural network. The neural network architecture refers to the number of nodes in the input layer, the number of hidden layers and the number of neurons in each hidden layer, and many neurons in the output layer. The architecture of the ANN consists of at least three layers, i.e. input, hidden, and output layers as clearly seen in figure 3-3. In this study, a multilayer feed-forward neural network has been employed. In addition, the input layer has three input variables (chemical composition, tempering temperature, and austenizing temperature), and the output layer corresponding to the output variable (ultimate tensile strength, yield strength percent of elongation, retained austenite, impact toughness, and fracture toughness and surface hardness) as figure 3-2 shows a schematic representation of the ANN model of the newly developed alloy steel.

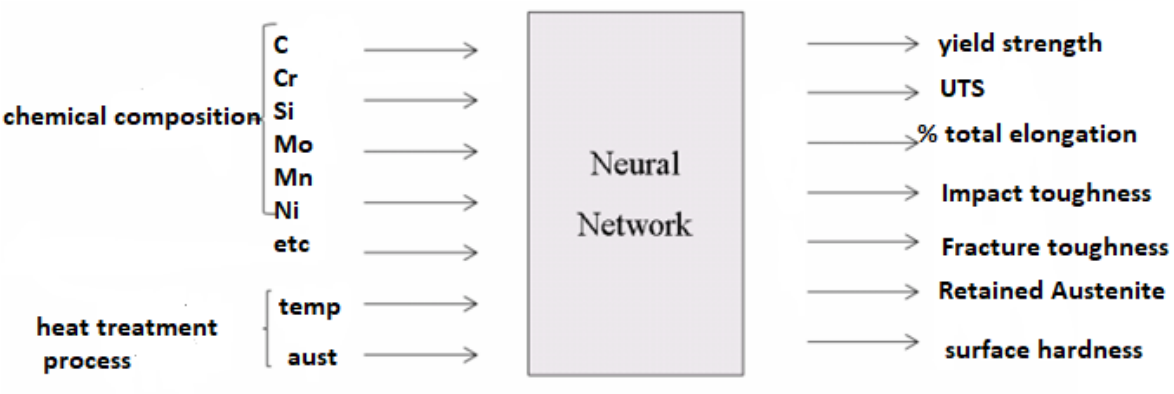

Figure 3-2: Schematic representation of ANN modeling of the newly developed alloy steel

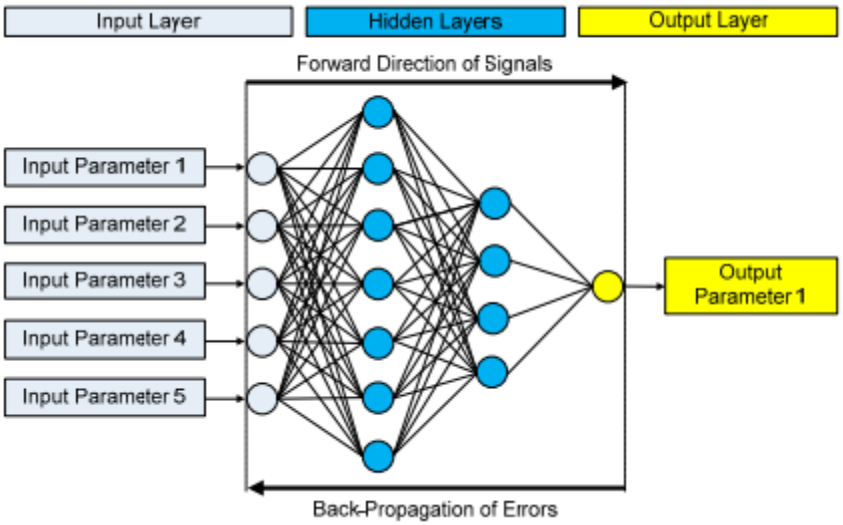

Figure 3-3: Architecture ANN Model [187]

In ANN modeling, Six different training algorithms were used namely Quasi-Newton (trainbfg), Bayesian Regularization (trainbr), Powell-Beale Conjugate Gradient (traincgb), Adapative Learning Rate (traingdx), Levenberg-Marquardt (trainlm), and Scaled Conjugate Gradient (trainscg). For all networks, tan-sigmoid transfer function (tansig) was used in the hidden layers while the linear transfer function (purelin) was used in the output layers. The structure of the network is first defined, activation functions are chosen and weights and biases are initialized. The training algorithm parameters like error goal, the maximum number of epochs (iterations), etc., are defined and then run the training algorithm. Lastly, simulate the output of the neural network with the measured input data and this is compared with the measured outputs. To verify, validation must be carried out with independent data. The training examples are obtained from experimental or simulation data. The network generates an output by processing the input and compares the output with the target. The difference between the target and the output determines the error. Then the synaptic weights of the network are modified by the training algorithm proportional to the error. The goal of the training process is to reduce the error below a predetermined value on an iterative basis. This requires a presentation of many training examples, which constitutes a training set. The presentation of a complete training set is an epoch. This form of supervised learning is error correction learning. Figure 3-4 shows a schematic representation of error-correction learning.

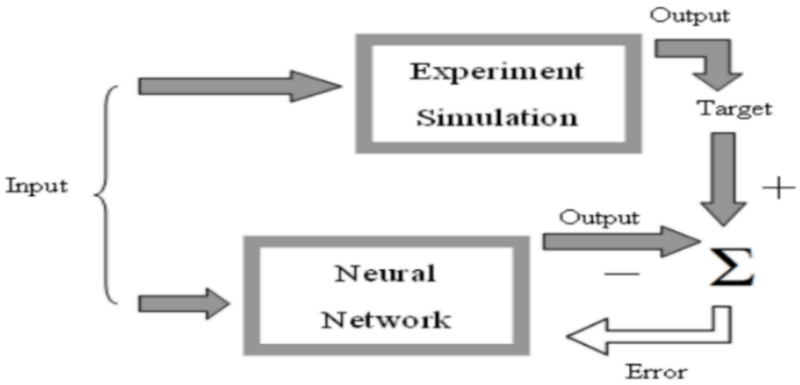

Figure 3-4: Schematic representation of error-correction learning [188]

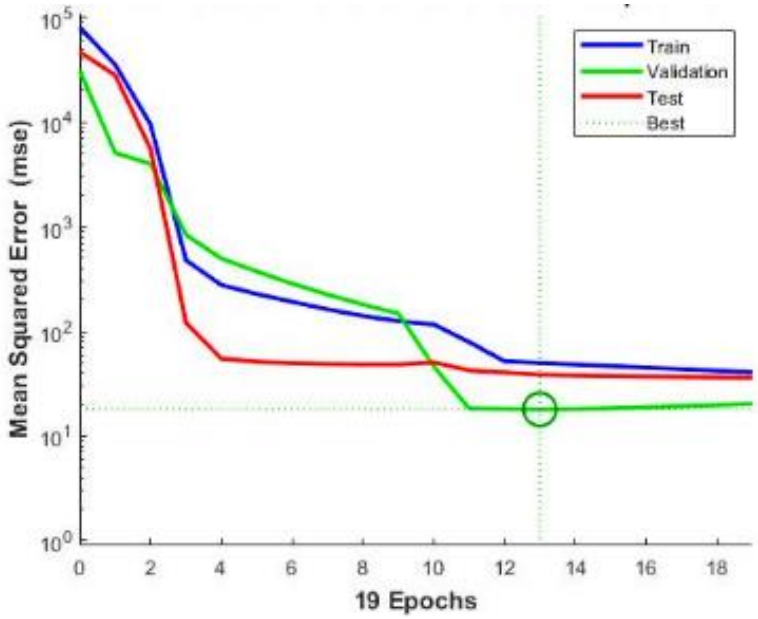

Figure 3-5: Mean square error versus epoch for the validation check

As for many functions, the most commonly used and efficient output feature is the mean square error. With a given number of input training datasets, reducing the mean squared error will improve the accuracy of a specific ANN. The mean square error versus the epoch of the ANN estimation of the Ni-modified alloy steels is shown in figure 3-5. Regression is also one more important performance measurement in the modeling of prediction. The variance of each sample output data from the target is found in regression. All sample performance training, validation, and testing of the Ni-modified alloy steels are near the fit line shown in figure 3-6. This means that the training network for the network parameter defined is between the experimental target and the prediction output at the best performance.

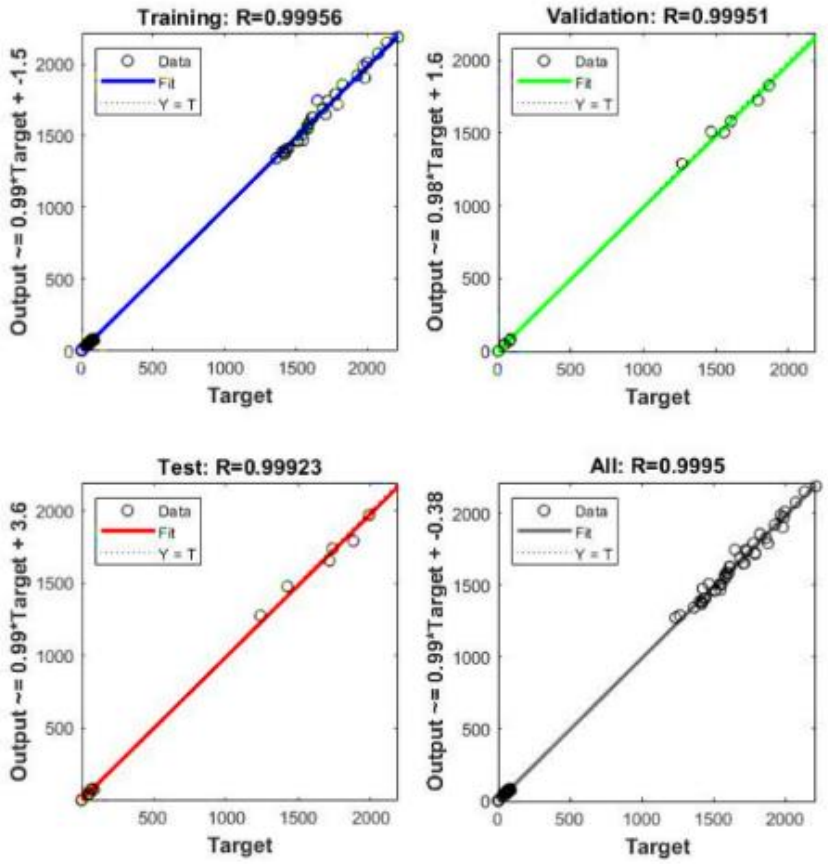

Figure 3-6: Regression fit and R values for training testing and validation

- Experimental Methods

The experimental investigations were carried out to characterize the mechanical properties of the Cr-Mo alloy steel and its Ni-modified alloy steels. To do this, it is started by manufacturing all test specimens for all experimental test scenarios. The manufacturing process to prepare the specimens are; commercially available transmission gear of Cr-Mo alloy steel (which is nearly the same in chemical composition as DIN 1.7243) as an ingot, hot forging and adding Nickel (Ni) powder, rolling the forged material to desired shape and size then normalizing and heat treatment. The surface hardening mechanism of all the test materials was case hardening conducted by gas nitriding, quenching, tempering, and fine finishing using an Electrical Discharge Machine (EDM). All the specimens were heat-treated in the same manner as the same tempering temperature and holding time.

The case hardening type used in this study was nitriding which is a universal thermo-chemical surface treatment process. Gas nitriding is a surface hardening process, where nitrogen is added to the surface of alloy steel parts using dissociated ammonia as the source. Nitriding is carried out at temperatures below the transformation temperature of alloy steels so that with proper manufacturing techniques, there is little or no distortion as a result of the process. The specimens to be nitrided are heat treated to the proper strength level, and finally machined by EDM type. The specimens are then exposed to active nitrogen at a carefully controlled temperature, typically in the range of 496 °C to 529.5°C. This temperature is typically below the final tempering temperature of the alloy steel so that nitriding does not affect the base metal mechanical properties. In the experimental test, specimens for mechanical property, dimensions, shapes, and types were determined and carried out based on the ASTM standards. Three experimental tests conducted in this research include tensile test, impact toughness test, and surface hardness test. However, the other parameters like fracture toughness and retained austenite were investigated by the ANN modeling prediction method only.

(a): Tensile test

The chemical composition of the sample materials for all the tensile tests of the developed specimens is shown in table 3-1. As per various norms, there are different types of tensile test specimens' shapes, dimensions, and types. The tensile test specimen most of the time used was uniform over the tensile specimen's gauge length. The specimen's cross-sections are typically circular, square, or rectangular. Thus, based on the ASTM E8-04 standard a round cross-section specimen and sizes were prepared as shown in figure 3-7 and figure 3-8(b).

To provide basic design details on the strength of materials, the tensile test is commonly used and is an approved test for the material specification. In this test, the specimens were made according to ASTM E8 standard and the tensile test was performed using HZ-1001 metal tensile tester of universal test machine (UTM) as shown in figure 3-8 (a). The UTM HZ-1001metal tensile tester has the following specifications: Max Testing Force: 100 KN, weight: 500-1000Kg, Power: 220V, 50Hz0.75kw, and testing speed from 0.001 to 500mm/Min, machine dimension: 1040*590*2000mm (L*W*H).

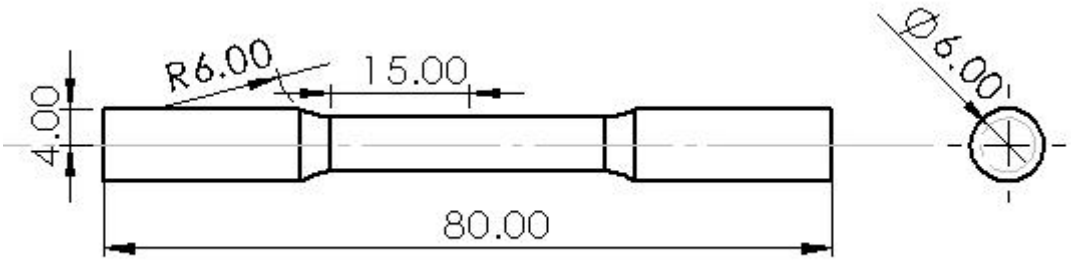

Figure 3-7: Size of tensile specimen

Figure 3-8: (a): universal tensile test machine (b): prepared specimens of the tensile test

(b): Charpy Impact test

The Charpy impact test measures the energy absorbed by a notched specimen while breaking under an impact load. The Charpy impact test was performed using an XJJ- 50J Charpy impact machine. The test is usually used to indicate the toughness of a material at a specified temperature. It is not a particularly accurate test but can give a general indication of the ability of a material to resist brittle fracture at its minimum design material temperature. According to the ASTM E23 standard, the test specimen consists of a bar of metal with 55x10x10mm^3 dimensions having a notch machined across one of the larger

dimensions as shown in figure 3-9 with a V-notch of 2mm deep, with 45° angle and 0.25 mm radius along the base. The Charpy impact test consists of striking a suitable specimen with a hammer on a pendulum arm while the specimen is held securely at each end. The energy absorbed by the specimen is determined by precisely measuring the decrease in motion of the pendulum arm. The pendulum impacts on the specimen and the start and finish heights of the pendulum are measured as shown in figures 3-10. The height difference equates to the energy absorbed by the specimen before it fractures.

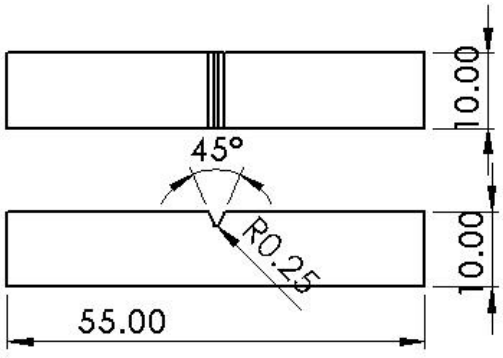

Figure 3-9: Size of V-notch Impact Specimen

The steps of experimental procedures involved in performing impact test using Charpy impact test as schematically represented in figure 3-10 are; determination of friction losses by releasing the hammer without a specimen inserted and this should result in zero energy used by the hammer as shown in figure 3-11 (a). If any difference is registered it is due to friction losses, set up the pendulum to its original position to have 450J (maximum energy) as shown in 3-11 (b), placing the specimen in the support at the base of the tester with the notch facing away from the direction of impact. The first notched bar is at room temperature which was 31˚C, after the specimen is well placed and the path of the pendulum swing is clear, release the hammer by pushing forward firmly on the release handle. The pendulum swings through and breaks the specimen into two halves. Record the energy consumed from the dial as indicated in figure 3-11 (b), data recorded from the dial should minus the energy due to friction losses to get the energy that caused the specimen to break.

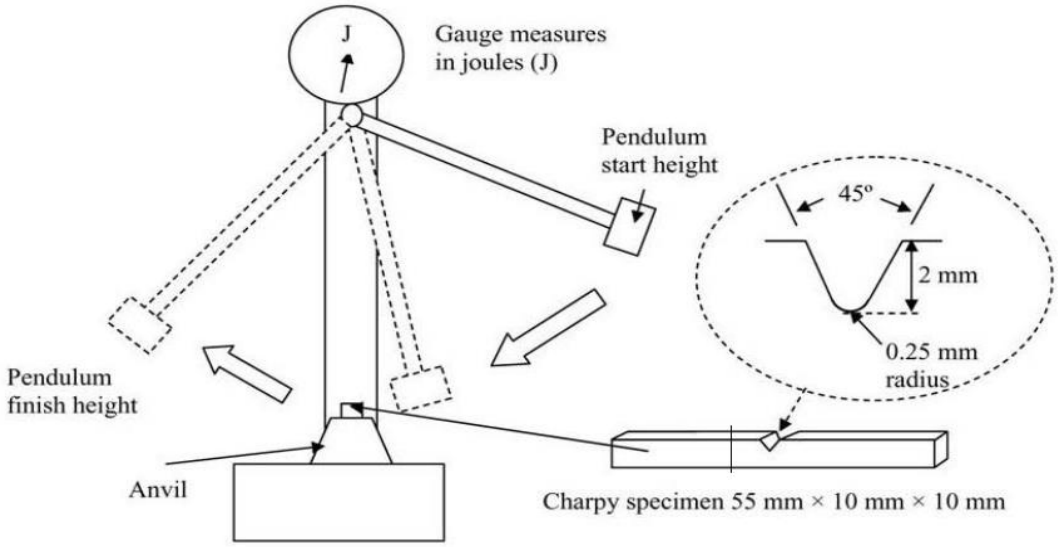

Figure 3-10: Schematic representation of Charpy impact test procedure [189]

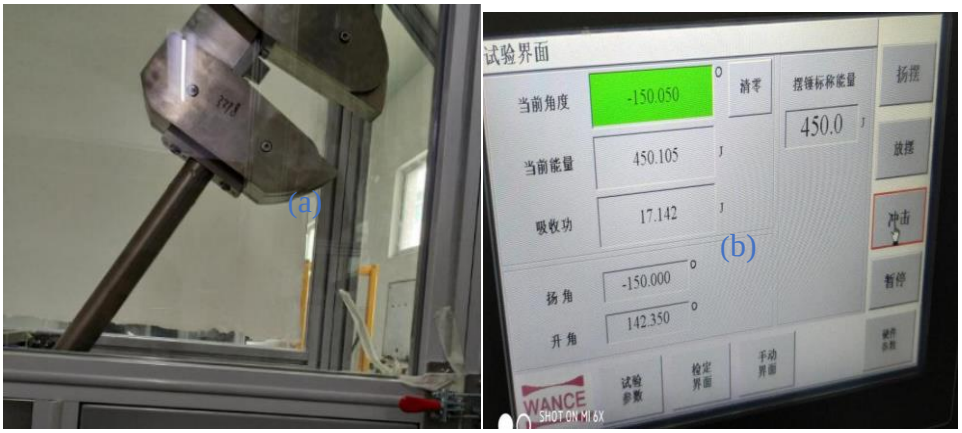

Figure 3-11: (a): Charpy impact tester machine (b): machine specification

(c): Hardness Test:

During the hardness test of sample materials using the Rockwell hardness C (HRC), it is usually necessary to prepare the surface of the specimen to be tested. The test specimen can be measured by using the EBP-R-150E analog Rockwell hardness machine as shown in figure 3-13 (a). The test specimen sizes for HRC hardness tests were prepared according to the ASTM E18 standard. The dimensions and type of the specimens are shown in Figures 3-12.

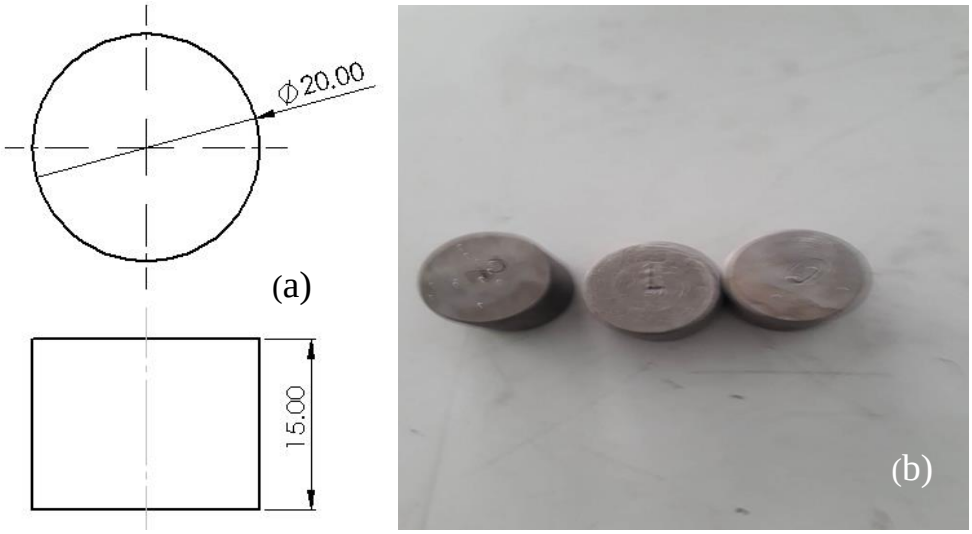

Figure 3-12:(a): Size of Rockwell hardness test specimen (b): prepared spacemen

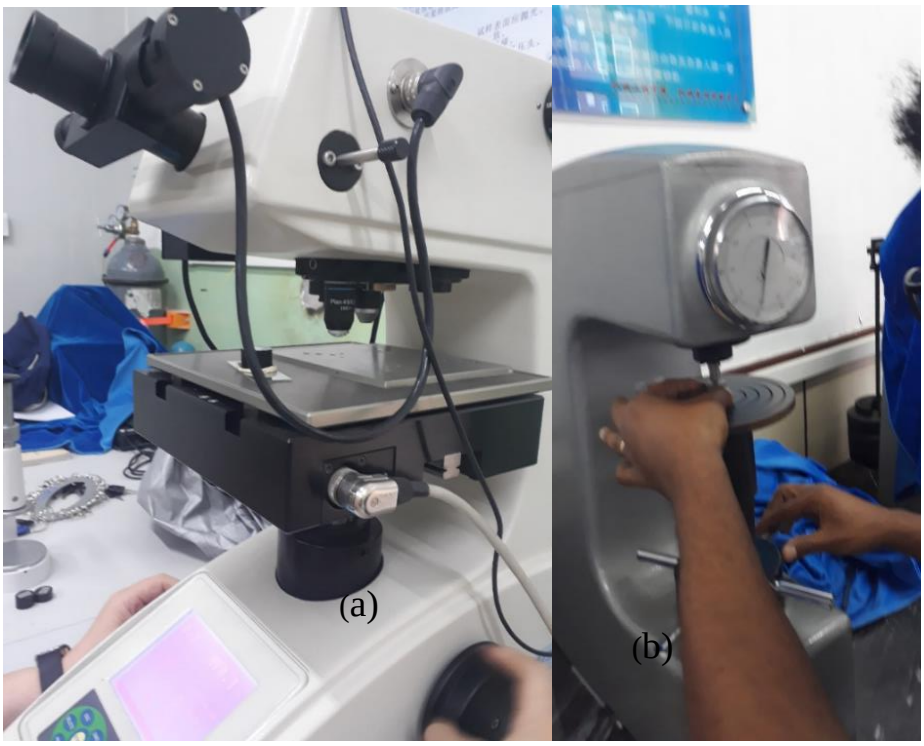

Figure 3-13: (a): Vickers hardness test machine (b): Rockwell hardness test machine

Very hard materials should be tested by the Vickers hardness testing method for precise values. The specimens were tested by using AFFRI-DM2 SEMI macro hardness tester as shown in figure 3-13 (a). During Vickers hardness testing, it is usually necessary to prepare the surface of the specimen to be tested. As the specimen surface quality requirements are

significantly stricter than those for the Rockwell method, it is sufficient for the surface to be free of impurities. To view an alloy steel specimen under an optical microscope, the specimen must be prepared as follows. It must be mounted onto a Bakelite pack as shown in figure 3-14 using a mounting press machine, polished the specimen as shown in figure 3-14 (c) using finer and finer grits as well as polishing machine as indicated in figure 3-15(a), and finally, it needs to be etched by echant as shown in figure 3-15 (b).

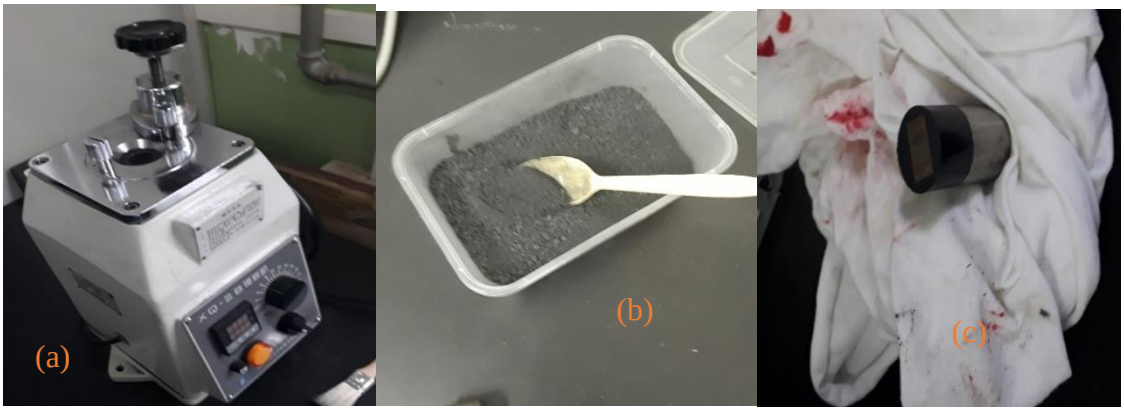

Figure 3-14: (a): Mounting Press machine (b): Bakelite powder (c): specimen

Figure 3-15: (a): polish machine (b): echant

(d): Microstructure

The microstructure of the selected specimens was characterized using an optical microscope NCM-V1000 metal alloy structure inverted optical microscope trinocular. The optical microscope, a non-destructive and real-time imaging technique, is the standard tool for characterizing the microstructure of developed specimens. The specimens for optical metallography were prepared the same as the sample for the microhardness test. The sample can be used interchangeably for both micro hardness and microstructure tests.

Microstructural and surface analysis of the specimen using optical microscopy was performed. The metallographic specimen mounting is achieved using a mounting press to encapsulate the specimen in plastic mounting material, such as Bakelite. The general procedures for the metallographic examination can summarize the steps necessary for sample preparation, as follows: an examination of the as-polished surface of the specimen with the metallographic microscope to observe features such as voids, corrosion, and chemical inhomogeneity of the metal and photographic recording of the etched structures from the computer as shown in figure 3-16.

Figure 3-16: Optical Microscope (OM) on microstructure analysis

After conducting experimental and ANN modeling for determination of mechanical property of the Ni-modified alloy steels a further study of design and fatigue stress analysis of the alloy steel materials of Cr-Mo and 1.55% Ni-modified Cr-Mo-Ni were considered. Hereafter, methods to design and fatigue analysis of transmission gear by employing gear calculation using AGMA standards and KISSsoft gear simulation software approaches. The AGMA standard Calculation is scripted in Matlab (see appendix C) to realize all possible solutions of gear geometries, lightweight, compactness, effective stress, and design safety factors by considering the given design parameters of the vehicle that fulfilled the constraints. The same parameters were done by KISSsoft gear simulation software by encoding the input parameters to the predefined interface. Various iterations mechanisms have been done using both approaches, out of which most optimum ones have been selected

in terms of load-carrying capacity, lightweight and smooth operation. The suitable values of the gear geometry were selected based on an iterative method by varying the geometrical parameters of helix angle, face width, and input load.

Finally, for simulating power transmission gear surface fatigue failure, conducting a rolling contact fatigue test on a twin-disc test rig is very mandatory. Rolling contact fatigue test of surface durability on twin-disc test machines of case hardened alloy steel specimens varies based on its specimen feature and test parameters. Testes are performed on a couple of roller specimens where one disc is crowned to achieve a point contact that affects uneven damage to the surface. Therefore, if micropitting or wear occurs, a groove may form on the contact surfaces and cause an uncontrolled reduction within the contact pressure for a given applied load. Hence, Despite point contact disc pairs tend to be more durable than line contact specimens, one of the discs was crowned to anticipate edge loading and to cut back the number of loads needed to come up with a given contact pressure to match the load capacity of the test rig.[190].

In this research, the test samples used contained low-speed specimens that are cylindrical-shaped discs, and high-speed specimens consisted of crowned-shaped discs to attain minimum effective contact area. Both samples (high speed and low-speed specimens) were made from low alloy steel materials, Cr-Mo alloy steel, and Ni-modified Cr-Mo alloy steel. In the sample preparation process, the study used cylindrical and crowned disk samples with the same surface finish and hardness. The chemical composition of both commercially available and the newly developed alloy steel is given in table 3-1.

The manufacturing process of the disc specimens of both the commercially available and the newly developed materials was following the same procedure like melting in a vacuum of the argon atmosphere, hot forging and applying Ni-content (for the newly developed material), rolling the forged material to the desired form, then normalizing and heat treatment (tempering, quenching, and nitriding) and finally surface finishing. As earlier researches have revealed that the load-carrying capacity of discs specimens surface finished by wire electro-discharge machining (EDM) is three times higher than ground finished discs for short-time contact fatigue tests [191]. Accordingly, the prepared

specimens shown in figure 3-18 of both candidate materials were finally finished by EDM as shown in figure 3-19.

In gear RCF testing, a tribological compatible disc-on-disc test is utilized to reduce the effort and costs of manufacturing complex geometries of gear. For this reason, the size of disc specimens of outer and inner diameters were 70 and 45 mm respectively, and 28 mm in thickness. It is observed that with the basic design of the twin-disc machine, the standard sample consists of two flat disks, resulting in a line contact configuration. In this experiment, the high-speed disc geometry is modified, in such a way that the effective contact surface of 8.5 mm is crowned on both sides of 3 degrees (3^0). For more clarity, the dimensions of the test discs shown in Figures 3-17 were adapted from [192].

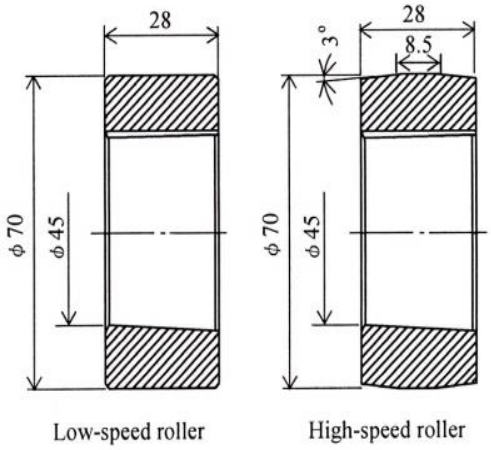

Figure 3-17: Dimension of test discs [192]

Figure 3-18: Prepared test discs

Figure 3-19: EDM finished specimens

As micropitting has occurred at the asperity level, it is not easy to define the occurrence and absence of micropitting in an analytical model. Micropitting has relied on applied loads, tooth geometry, surface roughness, lubricant property, and the metallurgy of the specimen. Consequently, there is no all-inclusive model that predicts the presence of micropitting on the surface of contact bodies [193]. Likewise, the presence of micropitting can be determined using the experimental methods by preparing gear specimens and testing them under the same working conditions.[194]. Nevertheless, gear spacemen preparation is expensive and time-consuming. So, to simulate transmission gears, research outputs recommend the use of easier and faster tests with rolling pairs of discs in loaded contact.

Multiple studies stated that disc specimens have been broadly adapted to evaluate the contact fatigue performances of various gear materials [195-198]. The use of disc specimen tests related to the surface fatigue performance of different materials to compare with each other is widely accepted, researchers like [199] are honored that disc specimens are more robust than gears. Thus, the best way to determine the micropitting level of a transmission gear is to conduct an experimental test using disc samples. To do this, sample preparation, size, and material type is very important parameter.

After test samples were manufactured and finally refined in the workshop, the specimens were marked and washed in an ultrasonic bath using industrial gasoline. The experimental tests were carried out on the adapted RCF twin-disc test rig at Ethiopian Technical

University (ETU). The twin-disc machine developed by the researchers is shown in figure 3-20.

For more detail, all components and lubrication control are shown in appendix figure D-1 to figure D-10. As indicated in figure 3-30, the setting up of disc-to-disc contact is very easy. Disc-to-disc has emerged as the standard test rig for rolling. The test specimens are mounted on independent shafts driven by separate AC motors. After adjusting both samples with the twin-disc test rig, load the specimens using a hydraulic hand pump and apply normal force (F_N) to the sliding rigid panel as a result contact pressure (Hertzian pressure) is generated at the contact point of the test rollers. According to the relevant test rig ISO 6336 standard specification of the test sample, the design, and development of the twin-disc contact fatigue test rig were ideally selected as per the concept design. The study used the specimen specification as described in [192].

Figure 3-20: Adapted twin-disc test rig

During the RCF test, a lubricant (oil or water) was applied to the inlet area using a forced lubrication method to maintain a stable meniscus of liquid. As literature shows, the disc-to-disc contact area had to be lubricated by supplying 1 drop of water per 3 seconds or 1 drop of transmission oil per second [200]. Also, the temperature of the lubricant is an important test parameter as it strongly affects the viscosity of the lubricant. Therefore, the lubricant was heated using an induction system built-in the system to achieve and maintain the desired temperature. In actual transmission gear, lubricant temperature does not exceed 150 ^{o}C [201]. So, in this study, the adapted twin-disc test rig was utilized a heavily saturated SAE 90 grade (property depicted in table 3-2) and the controlled lubricant temperature is from 80-90 ^{o}C.

Table 3-2: Given lubricant property of SAE90

Parameter	Value
Kinematic viscosity @40 ^{o}C	155
Kinematic viscosity @100 ^{o}C	15.5
Density	7.28 lbs/gal
Specific gravity	0.875

3.3. Test Conditions

The RCF experimental tests were carried out with a step load stage process i.e. gradually increasing the normal load applied up to 8.2 KN, and maximum Hertzian contact pressure was up to 1.5 GPa. The experimental tests are summarized in table 3-3. It can be seen that the normal load on the rollers (disks) has four different load levels (K3, K6, K8, and K9). These loads are divided into sub-levels and it is clearly stated in [202]. For high-speed discs to complete the test, each load phase takes several minutes and hours, which is equivalent to nearly ten million load cycles. In addition, approximately 5 million load cycles were needed to perform low-speed discs. During the experimental test, the test procedure for evaluating the RCF test is presented, as shown below:

Phase1: Load stage K3 (running-in) which is a new disc, with light loads until their roughness decrease for the first few hours.

Phase 2: For analysis, collect a lubricant

Phase 3: load stage K6,

Phase 4: For analysis, collect a lubricant

Phase 5: Dismounting rollers, measurement of mass loss, and surface photography,

Phase 6: Mount rollers with fresh lubricant

Phase 7: load stage K8,

Phase 8: Repeat steps 4 and step 5.

Phase 9: Load stage K9,

Phase 10: Repeat steps 4 and step 5.

The only lubricating oil was replaced at each load stage transition. However, the lubricating oil did not change from load sub-stage to load sub-stage. After each interruption, discs were taken out from the test bench, washed, weighed, measured before replacement, and proceeded with a new test specimen. The key parameter during the run-in and RCF testing is the SRR shown in table 3-4. SRR is characterized by the ratio of sliding speed (us) and rolling speed (ur). In a twin-disc machine with a fixed rotating shaft, the rolling speed corresponds to the entrainment speed of the lubricant. The SRR term can be calculated using Equation 1, where u1 and u2 are the surface velocities of the fast and the slow bodies. During the meshing process, the tooth profile is exposed to a wide range of SRR (from pure rolling to more than 50%). The effect of SRR on RCF testing is that the higher the SRR, the more pitting will appear[203]. As stated in the study, maturity indicates that micropitting susceptible is more likely to occur on surfaces with negative SRR values [204].

$$SRR = \frac{u_s}{u_r} = 2 \times \left(\frac{|u_1 - u_2|}{u_1 + u_2} \right) \qquad (1)$$

Where: $u_s = u_1 - u_2$ is the sliding speed, $u_r = \frac{u_1 + u_2}{2}$ is the mean rolling speed.

Another parameter that affects the life of the rolling contact is a slip that occurs between the contact surfaces. Note that Eq.2 gives the slip of entity 1. If there is a local negative slip in the main body 1. The presence and signs of slippage affect the number of cycles required to support the surface. Negative slip reduces the number of load cycles required to start surface wear and increases surface wear at a given load level, while positive slip counteracts contact fatigue cracks.

$$s_1 = \frac{u_1 - u_2}{u_1} \qquad (2)$$

.Table 3-3: RCF test and load stages

Load stage	Normal force (N)	Hertzian pressure (Mpa)	Half pressure width (mm)	Load sub stage	No_Cyles for high speed *10^3	No_Cyles for low speed *10^3	Time need (hr)	Oil T°
K3	1090.8	514	0.159	K3-1	20	10	7.15’	80
				K3-2	60	30	21.428’	
				K3-3	100	50	35.714’	
K6	3749.7	953	0.295	K6-1	200	100	71.428’	90
				K6-2	800	400	4.762hr	
				K6-3	1880	940	11.191hr	
K8	6513.131	1256	0.388	K8-1	200	100	71.428’	90
				K8-2	800	400	4.762hr	
				K8-3	1880	940	11.191hr	
K9	8184.95	1408	0.435	K9-1	2880	1440	17.143 hrs	90
Total					8820	= 4,410	52.5 hrs	

Table 3-4: controlled parameters during the run-in and RCF test

Test Stages	Description	High-speed disc(rpm)	Low-speed disc(rpm)	Slip ratio	SRR
K3, K6, k8 & k8	Run-in & RCF	2800	1400	-1 & 0.5	0.66

After completing the RCF tests, the damaged (tested) sample must be analyzed and inspected. To facilitate this analysis, a wheel cut-off machine or EDM machine was used to cut part of the damaged parts to take out the sample from the case hardened roller tested specimens as shown in Figure 3-23. In this study, the researchers used a wheel cut of a

machine equipped with a lubrication system so that the microstructure of the tested specimen material would not change due to heating. To prepare samples for optical microscope (OM), used coarse Sic paper as a diamond suspension. These samples were gradually polished in the direction of the rolling axis. In addition, perform surface analysis on the test samples parallel to the rolling plane on these cross-sections, as shown in Figure 3-21 (2).

Sample preparation for metallographic investigations of the roller samples produced by RCF is typically performed on both cross (transverse) and parallel sections. Therefore, the preparation of samples for OM involves the following: Determine the position and orientation of the target plane (axial or peripheral), as shown in Figure 3-22, cut off the elements to better approximate the target plane, and then install it in the resin, and polished with enough polishing foil, and the polished surface is etched to obtain clear micrographs. In addition, samples for SEM were prepared differently from OM samples.

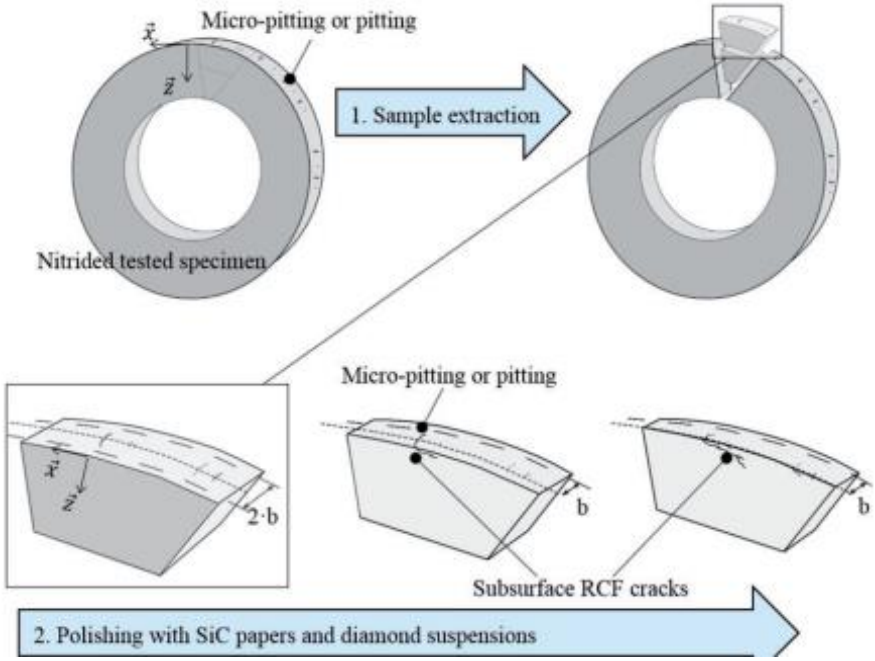

Figure 3-21: Cross-sectional preparation for metallographic analysis [201]

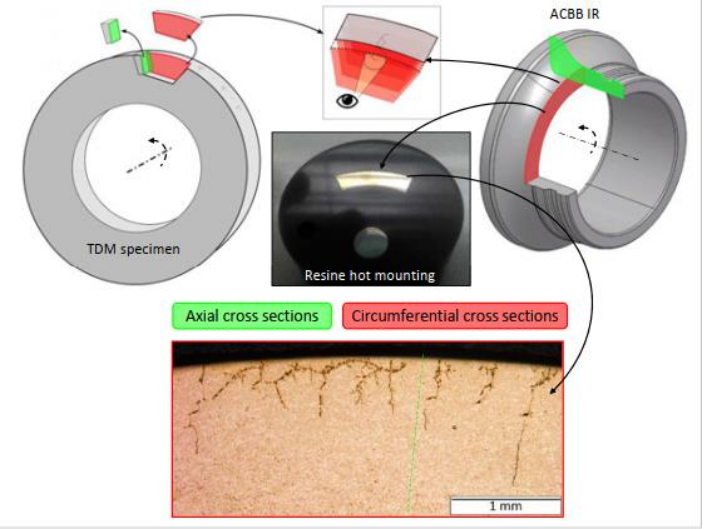

Figure 3-22:Axial and circumferential cross-sections polished after hot Mount [56]

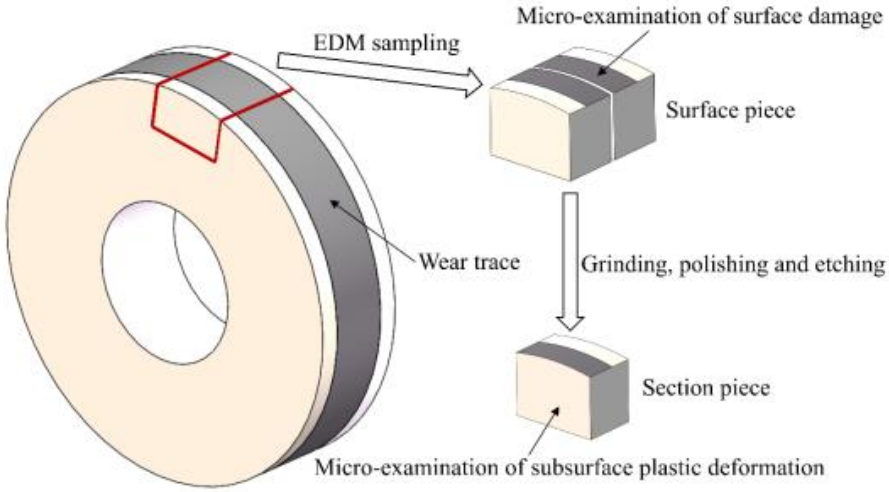

Figure 3-23: Surface and section sampling position [205-207]

SEM analysis was performed using a JCM-6000 Plus (BENCHTOP SEM) scanning electron microscope (see figure 3-24). The sample was sonicated in acetone, rinsed with ethyl alcohol, and placed in a high vacuum chamber. The acceleration voltage configuration was chosen to be 15.00 KV for all samples to extract the parts near the surface. Each sample was made using a 50×, 100×, 200×, 500×, 1000× , and 2000 × magnification. The Post-processing of SEM images and RMS roughness parameters (Sq) calculations were performed on the Mountains Map Premium 8.2 software (Digital Surf, France). MountanMap® is the surface analysis and metrology software used for Post-processing damaged surface of SEM micrograph. The software measures surface

parameters i.e. roughness/waviness, surface heights (topography), and SEM/SPM images. The cylindrical curvature of SEM images is removed by the 3rd-degree polynomial and the Gaussian low-pass filter with 0.8 mm cutoff is used to remove wavelengths. The process of determining the pitting factors is as follows: first, change the SEM micrograph into studiables topography, convert the topography into 3D view, using particle analysis (water detection segmentation) method, and finally determine the pit factors The Micropitted depth, equivalent diameter and area post-processed by particle analysis of water detection segmentation method as depicted in figure 3-25.

Figure 3-24: Scanning electron microscope

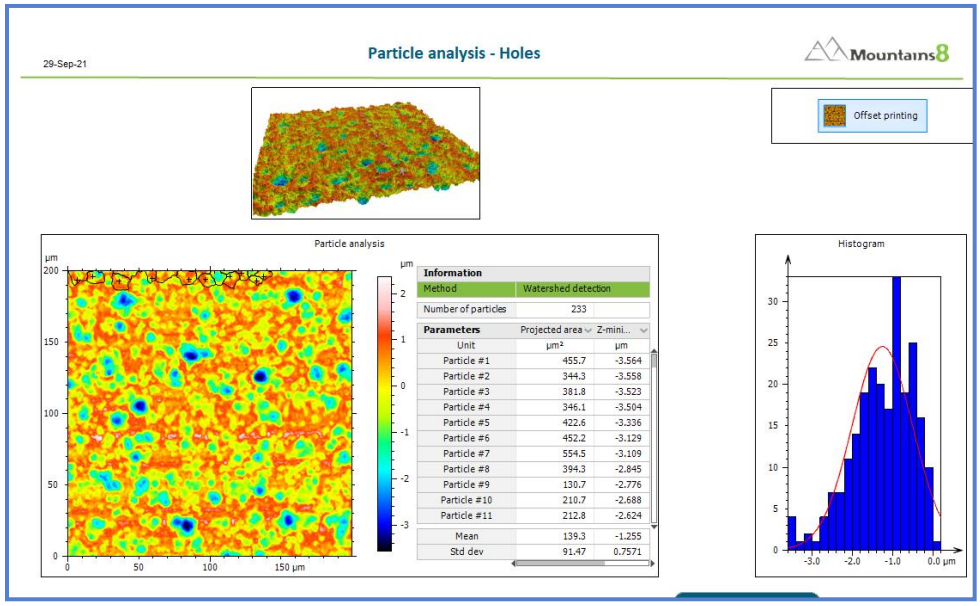

Figure 3-25: Particle analysis water segmentation

CHAPTER FOUR

4. Result and Discussion

4.1. Mechanical Property of Ni-modified Alloy Steels

Case hardened low alloy steels are the most utilized materials in power transmission gears where high surface hardness, good core toughness, and high yield strength are required. The vehicle transmission gears have been working under severe operating situations of loads and rotations. As result, the existing power transmission gear materials have a challenge in combating contact fatigue failure initiation. To improve the contact fatigue failure resistance, the property of the existing materials was improved through Ni-alloying modification. As in many works of literature presented, the mechanical properties of the alloy steel correlate with fatigue failure resistance. Fracture toughness has directly correlated with microstructure and cleanliness of alloy steel materials. Hence, improved microstructural property and cleanliness with fewer inclusion materials can have high fracture toughness.

So, determining the mechanical properties of Ni-alloyed-modified material is a very important concern. Literatures divulge that computational material science employs data analytics tools such as artificial neural networks that can achieve accurate prediction output which nearly the same is as experimental test results. Therefore, the ANN modeling prediction was used in this research to explore the mechanical properties of the Ni-modified Cr-Mo alloy steels and an experimental tests was also conducted to verify the ANN results.

Accordingly, test results indicate that tensile properties (yield strength, ultimate tensile strength, and percent of total elongation) of the Ni-modified alloy steels have been expressed as a function of tempering temperature for both predicted and experimental outputs as shown in figure 4-1, figure 4-2, and figure 4-3 respectively. The outputs in both ANN prediction modeling and experimental tests indicate that yield strength and ultimate tensile strength of Ni-modified Cr-Mo alloy steels gradually increase with the increasing addition of Ni- content. Moreover, the outputs of yield strength and ultimate tensile strength with tempering temperature (from AQ to 500 °C) were also investigated.

As it is noticed in figure 4-1, initial yield strength increases with increasing tempering temperature up to 200 °C, followed by a gradual decrease from 200 to 500 °C of tempering temperature. Similarly, the ultimate tensile strength of the Ni-modified alloy steel sharply decreases as tempering temperature increases from AQ to 500 °C as shown in figure 4-2.

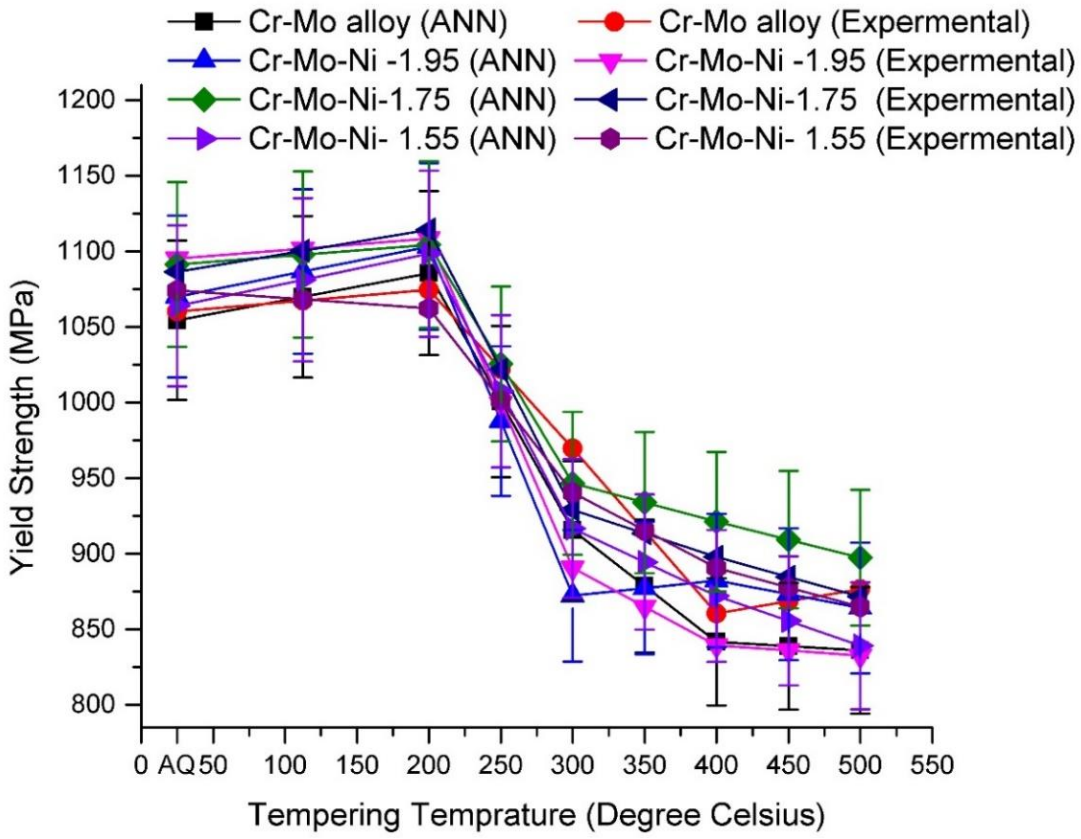

Figure 4-1: Influence of Ni-content on the yield strength

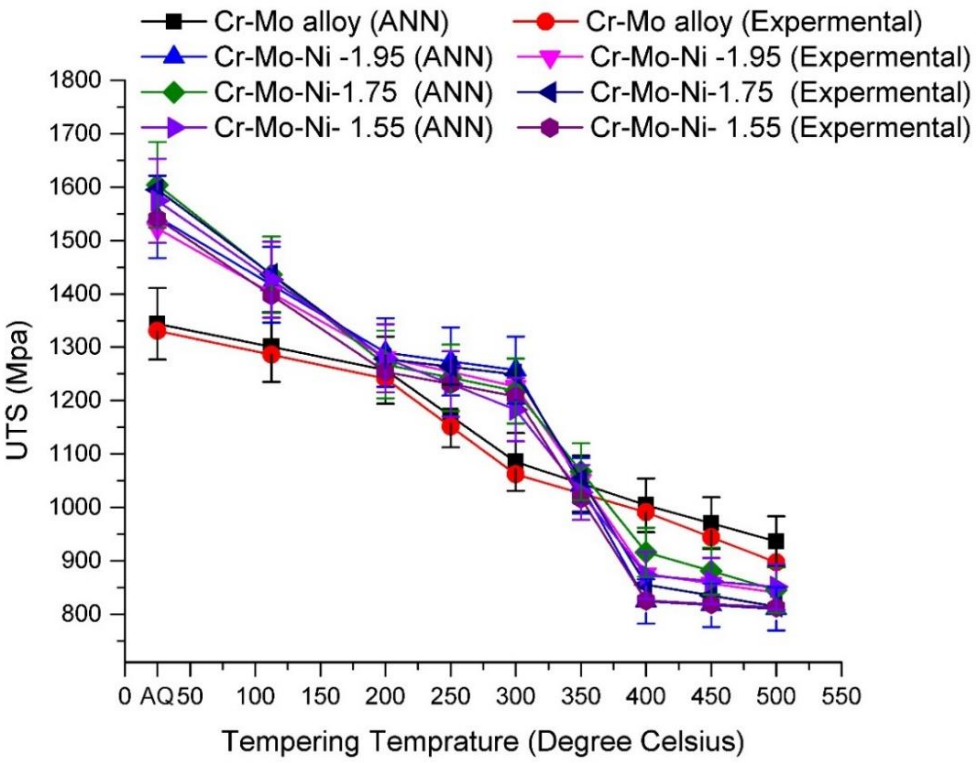

Figure 4-2: Influence of Ni-content on ultimate tensile strength (UTS)

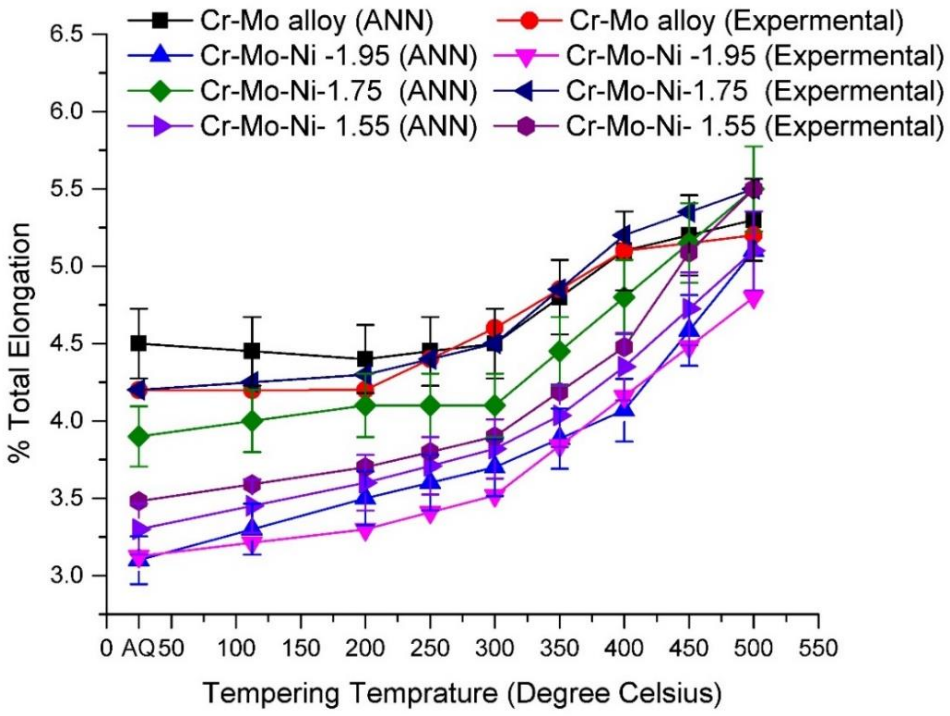

Figure 4-3: Influence of Ni-content on % total elongation

The percent total elongation of alloy steels indicates the ductility behavior of materials. Figure 4-3 illustrates the percent of total elongation versus tempering temperature, it increases as tempering temperature increases irrespective of the amount of Ni-content added to the base alloy steel. Likewise, the percentage of total elongation has been lowered as more Ni-content is added to the existing alloy steel

The toughness properties (Charpy impact toughness and fracture toughness) of the Ni-modified alloy steels have been expressed as a function of tempering temperature for both predicted and experimental outputs as shown in figure 4-4, and figure 4-5 respectively. Impact failure mode usually occurs in transmission gears due to the sudden impact and shock loading through operation [208]. So, investigating the impact toughness of Ni-modified Cr-Mo alloy steels plays a vital role in selecting transmission gear material that withstands this kind of failure mode. Therefore, the study carries out the ANN prediction modeling method to determine the impact toughness of 1.15%, 1.35%, 1.55%, 1.75%, and 1.95% of Ni-modified Cr-Mo alloy steels. Here the 1.15% and 1.35% of Ni-content were included in this prediction to address the behaviors of lower Ni-contents other than the manufactured Ni-modified Cr-Mo alloy steel combinations. To verify the prediction values, an experimental test was conducted on 1.55 %, 1.75%, and 1.95 % of Ni-modified Cr-Mo alloy steels. Results indicated that impact toughness increases when the added Ni-content increases from 1.15% to 1.55 %l meanwhile further increase of nickel content reduces the impact toughness. Normally, Ni-modified alloy steel showed higher impact toughness compared with Cr-Mo alloy steel. Figure 4-4 shows both predicted and experimental values of impact toughness versus tempering temperature. It indicates that the impact toughness increases gradually with an increase in tempering temperature from AQ to 300°C. However, the 1.55 % of Ni-modified Cr-Mo alloy steel shows a monotonously decrease from AQ to 200°C then increases up to 300°C, and then decreases slowly up to 500°C. However, for the base alloy steel, 1.15%, and 1.95% were increased its impact toughness as tempering temperature increased. Therefore, experimental and predicted results of impact toughness show that the 1.55 % Ni-modified Cr-Mo alloy steel has higher impact toughness compared with other Ni- content modified alloy steels.

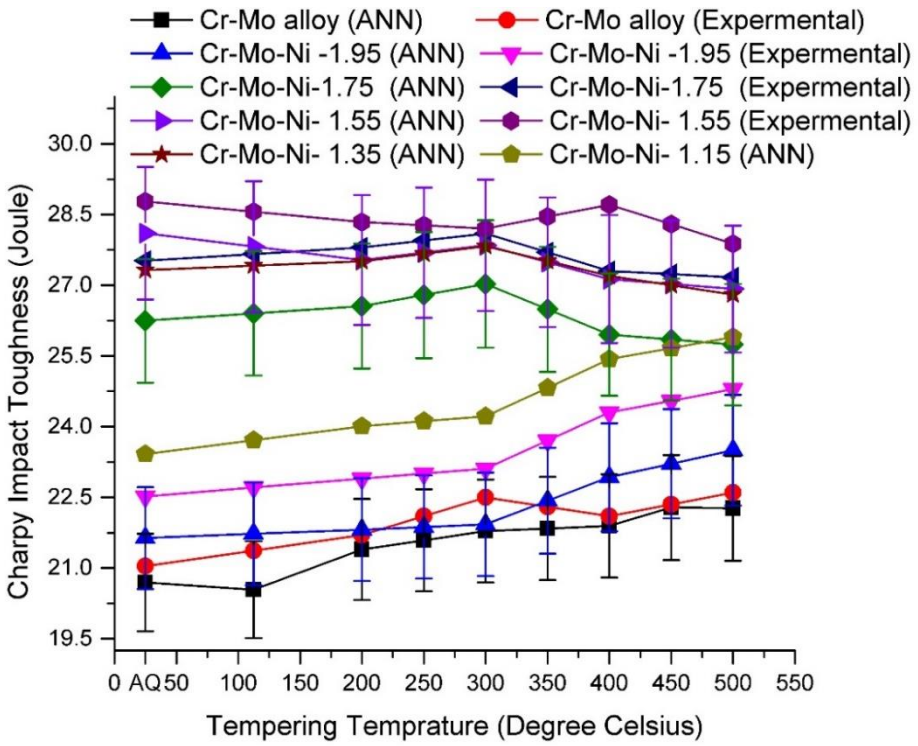

Figure 4-4: Influence of Ni-content on Charpy impact toughness

The fracture toughness is an essential material property that is overseen by various factors, the most significant of which is microstructure and nonmetallic inclusion size of materials. Furthermore, it has a direct correlation with microstructure refinement and nonmetallic inclusion size. Fracture toughness can be enhanced by modifying the alloying elements of the material as a result of the addition of nickel content to alloy steel leading to improved fracture toughness by reducing the susceptibility to cleavage fracture. [209].

Figure 4-5 shows that the predicted value of fracture toughness versus tempering temperature of 1.15%, 1.35%, 1.55%, 1.75%, and 1.95% Ni-modified alloy steels. As indicated in figure 4-5, fracture toughness increases as the tempering temperature increases from AQ to 200 °C. Then it decreases as the tempering temperature increases from 200 to 500 °C. Hence, Cr-Mo alloy steel modified by 1.55% Ni-content has higher fracture toughness compared with other Ni-content modifications that can endure fatigue failure. In this investigation researchers only employed ANN prediction modeling.

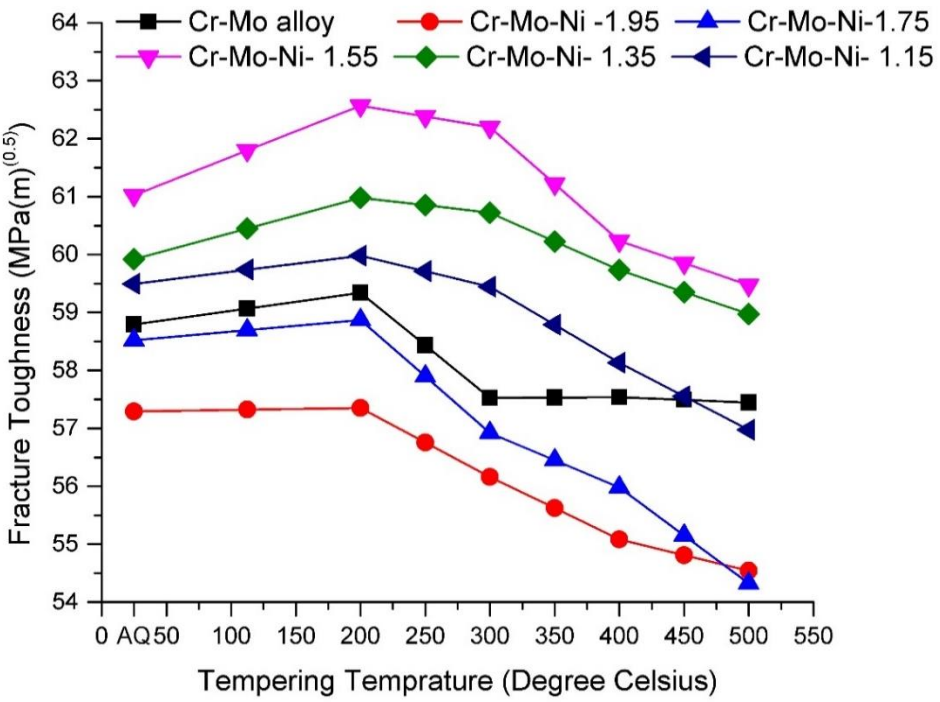

Figure 4-5: Influence of Ni-content on fracture toughness

The percent of the retained austenite was also investigated using the ANN prediction model. As identified in various research findings, retained austenite is normally advantageous for contact fatigue resistance [210] and the effect of retained austenite on the mechanical behavior of alloy steels varies in different fatigue regimes. Thus, moderate amounts of percent retained austenite less than (15%) do not have a damaging effect on material properties. Also, the tempering temperature of ANN prediction modeling plays an important role in influencing retained austenite content. Figure 4-6 indicates that as tempering temperature increases starting from 200°C to 500°C, the amount of percent retained austenite decreases sharply for 1.55% Ni Cr-Mo steels. However, for other sample alloy steels as the tempering temperature increase up to 300 °C, then the percent of retained austenite remains almost the same and then decreases sharply as tempering temperature goes beyond 300°C.

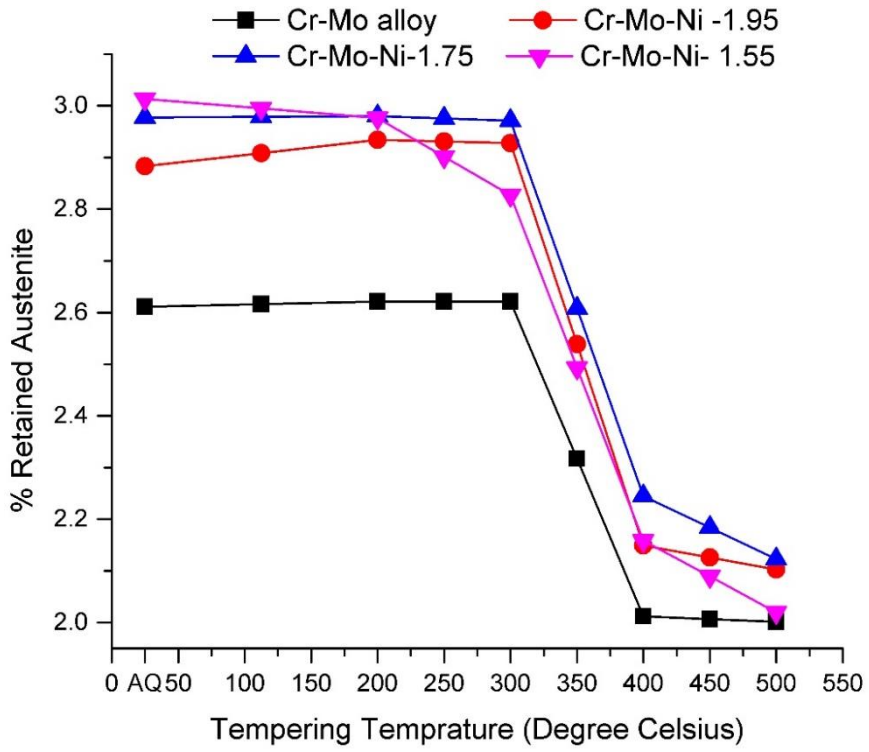

Figure 4-6: Influence of Ni-content on percent retained austenite

The surface hardness of the Ni-modified alloy steels was measured experimentally using the HRC hardness tester machine at various tempering temperatures. With the same tempering temperature, the alloy steels were also investigated using ANN perdition modeling. In both cases, as temperature increases, the surface hardness decreases as the alloy steel structure changes from martensite to ferrite and the dislocation density also decreases as shown figure 4-7. Likewise, as the amount of Ni-content added to Cr-Mo alloy steel increases, the surface hardness decreases slightly.

The test result of Vickers hardness was performed by microhardness test method using optical microscope measured from surface. To compare the hardness from surface hardness to core of the Cr-Mo alloy steel and Cr-Mo-1.55 Ni materials were used and results are shown in figure 4-8. From the results shown the hardness of the two materials is almost the same with a slight difference. This disparity has no significant effect on transmission gear fatigue failure.

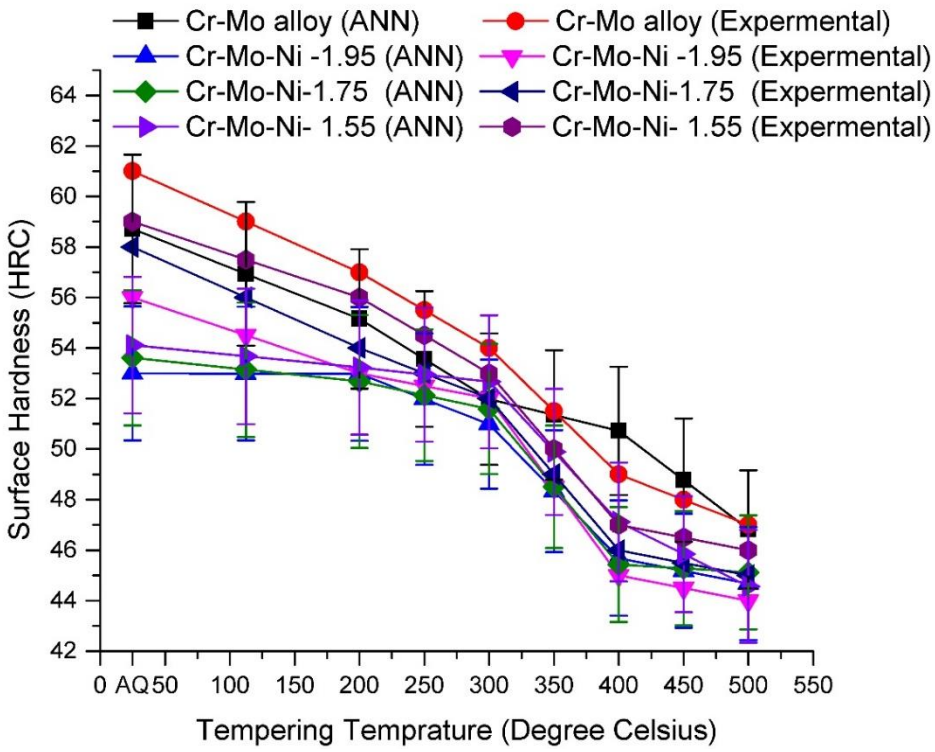

Figure 4-7: Influence of Ni-content on surface hardness

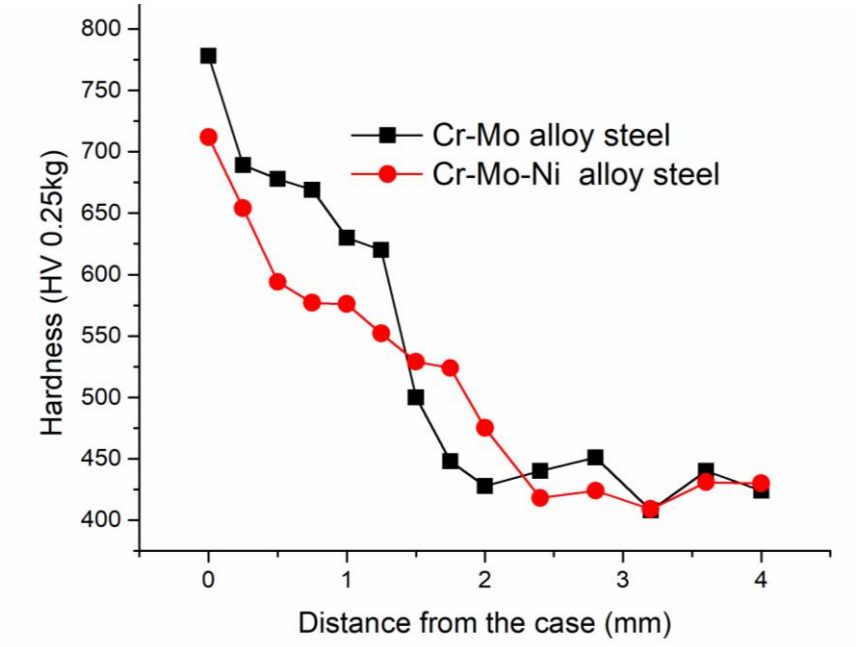

Figure 4-8: Vickers hardness of case depth

.

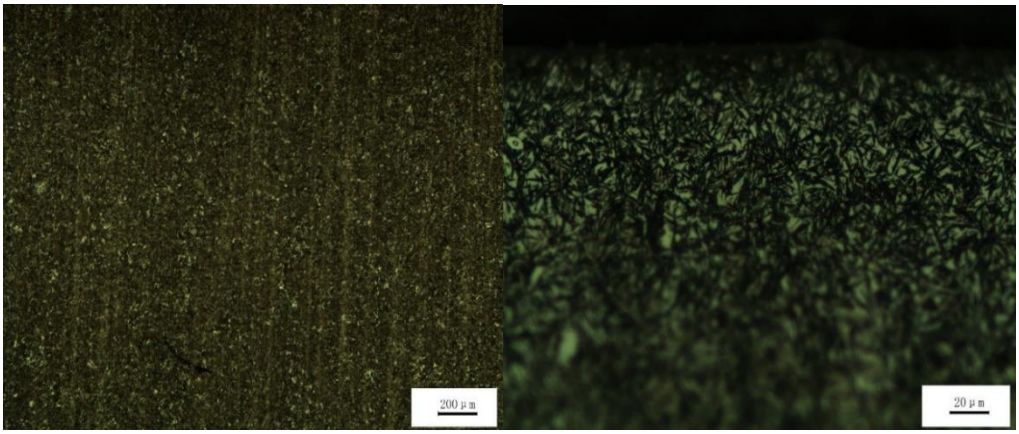

Figure 4-9: OM micrograph of Cr-Mo-Ni alloy steel

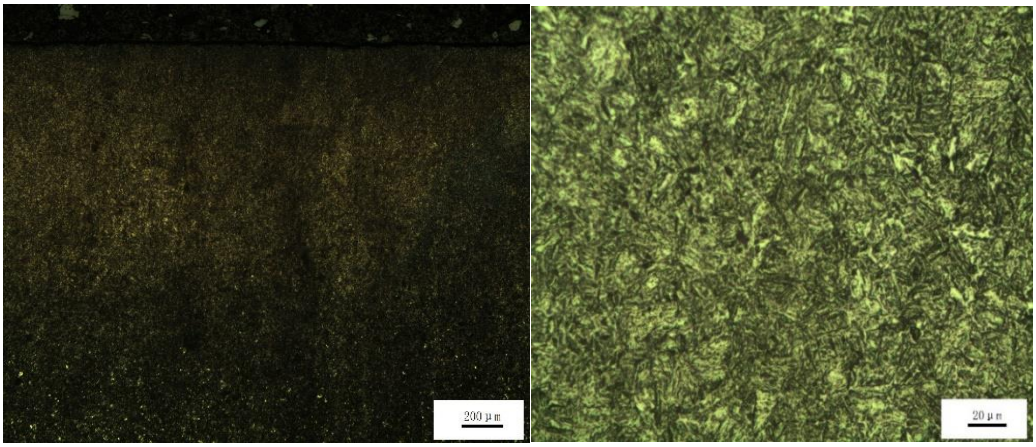

Figure 4-10: OM micrograph of Cr-Mo alloy steel

A variety of microscopy techniques have been used to observe the microstructure of the candidate materials of Cr-Mo and 1.55 percent Ni-modified Cr-Mo alloy steel, as shown in figures 4-9 and 4-10, respectively. When viewed at different length scales, the microstructural features of a given material can vary greatly. For this purpose, when explaining the microstructure of a material, it is important to note the length scale of the observations is made. An attempt was made to compare the microstructure of Cr-Mo alloy steel and Cr-Mo-1.55 Ni-alloy steel with the observed mechanical properties.

Figures 4-9 and 4-10 demonstrate the optical micrographs of the lightly etched specimens of the current alloy steel and nickel-modified alloy steels. It shows that the nickel-modified alloy steel microstructures differ greatly from the current alloy steel. The Ni-modified alloy steel microstructures include grain boundary ferrite (GBF) and acicular ferrite (AF) in the martensite matrix which indicates has good ductility.

4.2. Fatigue Analysis Ni-modified Alloy Steels

Transmission system and components, failure occurs mostly on gears under repeated loading due to fatigue such as bending on tooth root and micropitting on gear surface. The primary mode of failure for transmission gears is a failure by bending. In root bending failure mode, the crack starts at the weakest point of the tooth or the root fillet where the bending tensile stress and stress concentration is very high. The secondary mode of failure in transmission gear is surface damage which is caused by higher cyclic contact stress (Hertzian stress) than a surface can withstand. Contact fatigue failure is characterized by the fact that particles of material break off the surface/subsurface of the gear teeth after a certain number of meshing cycles have been reached.

Fatigue is considered a high cycle when the peak stresses in the material are held within the elastic range while low cycle fatigue occurs when stresses are above the elastic limit. This arbitrary division may vary from material to material depending upon tensile properties. The stress number is determined from the S-N (Wöhler) curve of bending stress and contact stress, which is the result of strength calculations of gears [211]. It is also possible to compute by KISSsoft gear simulation software depending on the material property and AGMA. In this study, an effort has been done to relate the fatigue stresses of transmission gear for a given set of constraints by varying helix angle and face width using AGMA standards and KISSsoft gear simulation software approaches. The influence of fatigue stresses on transmission gear was studied by varying the helix angle from (15^{o}-30^{o}) degree and face width from (14.5-28 mm) by keeping the gear ratio and pressure angle constant.

Figure 4-11 (KISSsoft result) shows typically the relationship between fatigue stress and helix angle, as the helix angle increases the fatigue stress decreases. At the same time, figure 4-11 explains the relationship between fatigue stresses and face width, as face width increases the fatigue stress decreases. In Figure 4-11, fig.4-12, (a) and (b) represents the disparity of fatigue stresses as the input torque varies from 50 Nm to 75 Nm respectively. Input torque has a great influence on fatigue stress of gear as presented in figure4-11, Figures 4-12, and fig 4-13 of (a) and (b). It is obvious that, as input torque increases fatigue stress also increases proportionally for the same helix angle and face width.

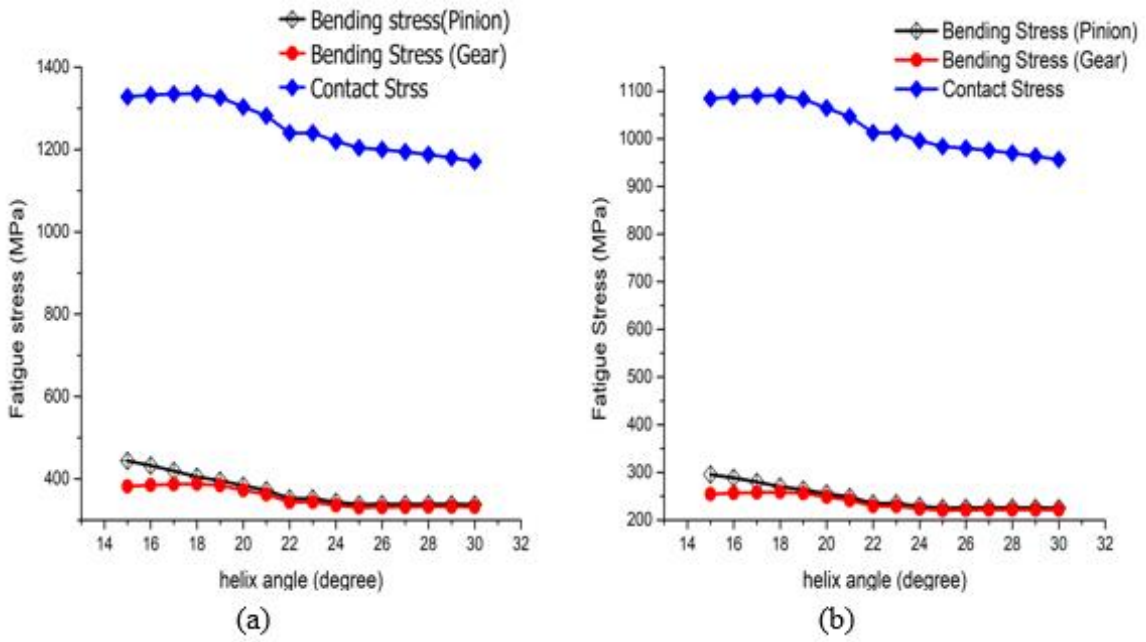

Figure 4-11: Fatigue stress VS helix angle at input torque of (a): 75 Nm (b): 50 Nm

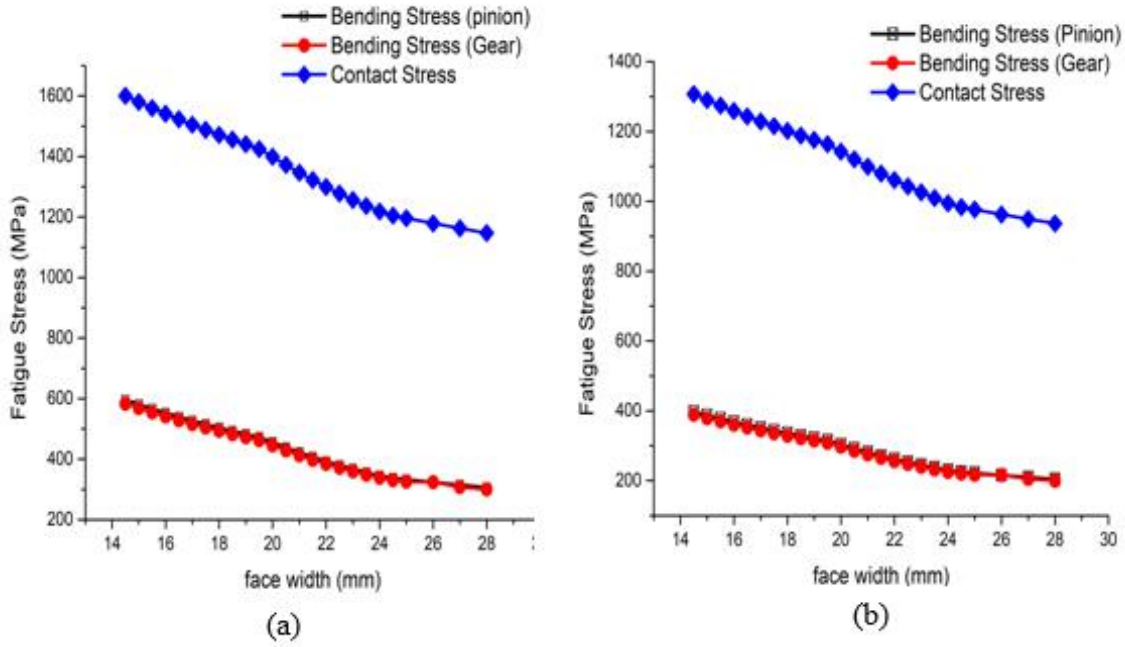

Figure 4-12: Fatigue stress VS face width at input torque of (a): 75 Nm (b): 50 Nm

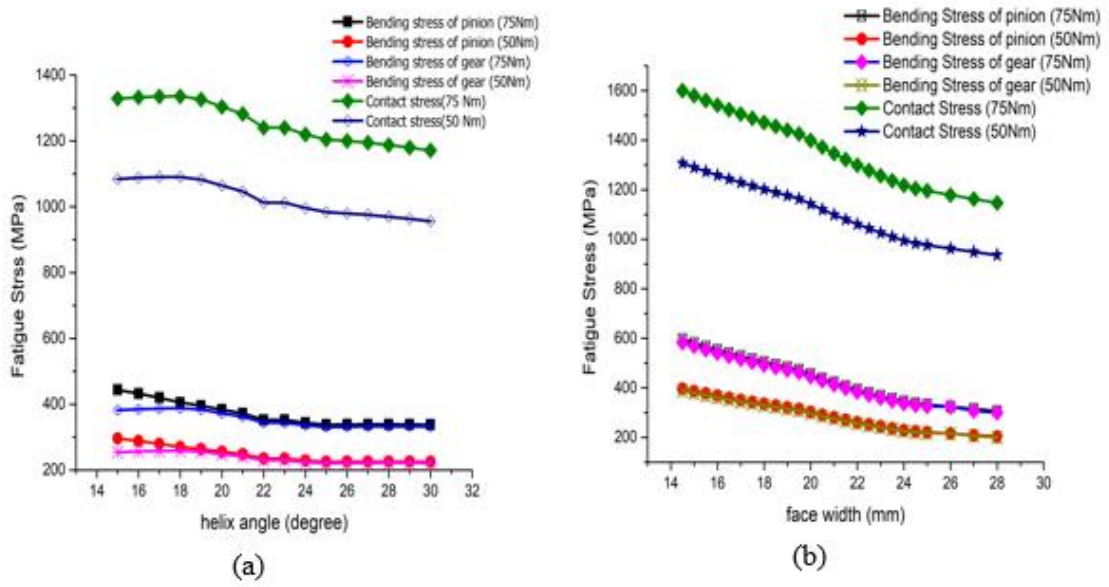

Figure 4-13: Fatigue stress versus (a): helix angle (b): face width

As it can be observed from figure 4-11 up to 4-13, in all cases, the results indicated that both fatigue stresses (bending and contact) decrease slowly with an increase in helix angle and face width by keeping the other parameters constant regardless of the input torque. Figure 4-13 summarizes how the fatigue stress of transmission gear is affected by input torque, helix angle, and face width as all in one approach. And it is shows that as the input torque increases the fatigue stress increases.

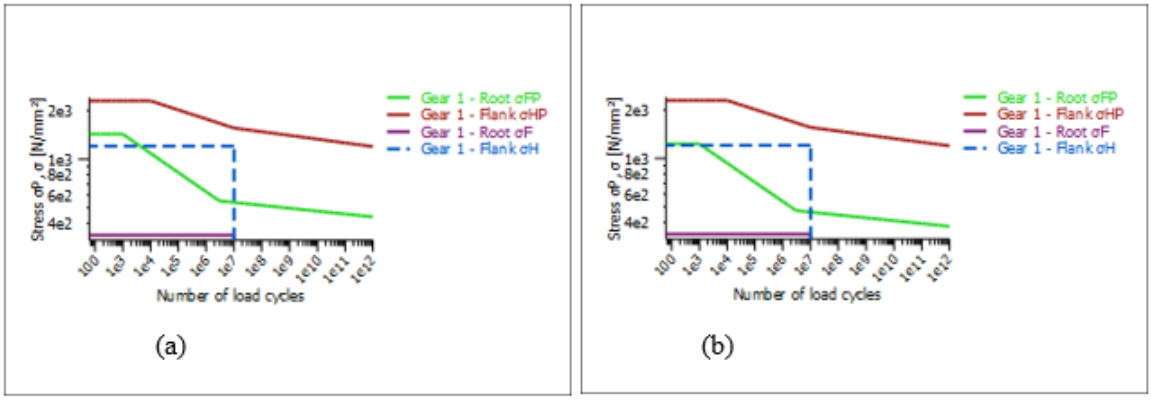

Figure 4-14**:** Simulation of the strength of material and number of Load Cycles by KISSsoft for (a): Cr-Mo-Ni (b): Cr-Mo alloy steels

Figure 4-14 (a) and (b), shows the relationship between allowable stresses based on material property and several load cycles S-N curves of Cr-Mo-Ni and Cr-Mo alloy steels. Calculation and making curves to the corresponding S-N graph of the candidate alloy steels can be done using KISSsoft gear simulation software based on the similar chemical composition of commercial steel materials. The curve defines the allowable stress versus the number of load cycles, since both pinion and gear are made up of the same material, the curve is also the same for both mating gears and it shows only the S-N curve of a pinion. The upper curve (red) indicates allowable stress for contact fatigue stress and the lower curve (green) is for allowable bending fatigue stress. As it can be shown in the curve the allowable stress varies as the number of load cycles varies. Based on the design life, it can find specific allowable stress for both contact and bending. The effective stress also is shown in Figures 4-14 above, effective bending stress (purple) and effective contact stress (blue). By comparing the S-N curve of the two candidate materials, Cr-Mo-Ni has higher allowable bending stress than Cr-Mo alloy steel. But they have the same allowable contact stress.

The safety factors against fatigue failure of bending and contact stresses in the gear is a key parameter to describe whether the designed gear withstands the load without failure or not. To define the appropriate gear design parameters, the effects of safety factors were investigated by varying helix angle, face width, and input torque. Results show that bending and contact safety factors vary at 50Nm and 75Nm of input torque, helix angle, and face width as shown in figure 4-15 to figure4-18. These results indicated that by increasing face width, both safety factors are increased consistently regardless of the input torque. Figure4-15 explicitly shows that as helix angle increases from (15^o-18^o) degrees the bending safety factor (KISSsoft software) of gear decreases because of gear geometry modification i.e. tip relief. This is applied to minimize the peak bending stress and contact stress at the start and end of the active profile. However, the bending safety factor of pinion increases as the helix angle increases linearly. The contact safety factor of both pinion and gear (KISSsoft software) decreases as helix angle increases from (15^o-18^o) degrees due to the stated gear modification. As can be noted from figure 4-15 up to 4-19 the safety factors of the transmission gear are revealed in both analytical and simulation approaches.

When comparing, the simulation values are a little higher than the analytical (AGMA standard) values as shown in all fatigue safety factors versus the variable gear design parameter. The error between the analytical (AGMA standard) of Matlab and KISSsoft software is negligible. For instance, at the selected parameter i.e. helix angle at 25^{o} degrees and face width at 24.5 mm, the error is 1.32% in bending safety factor and 1.03% in the contact safety factor.

Similarly, figures 4-15 to figure 4-18, (a) and (b) illustrate when input torque varies from 50Nm and 75Nm, the safety factors in both bending safety factor and contact safety factor increase respectively. This shows that the safety factor is a good manifestation of the load carrying capacity of power transmission gear.

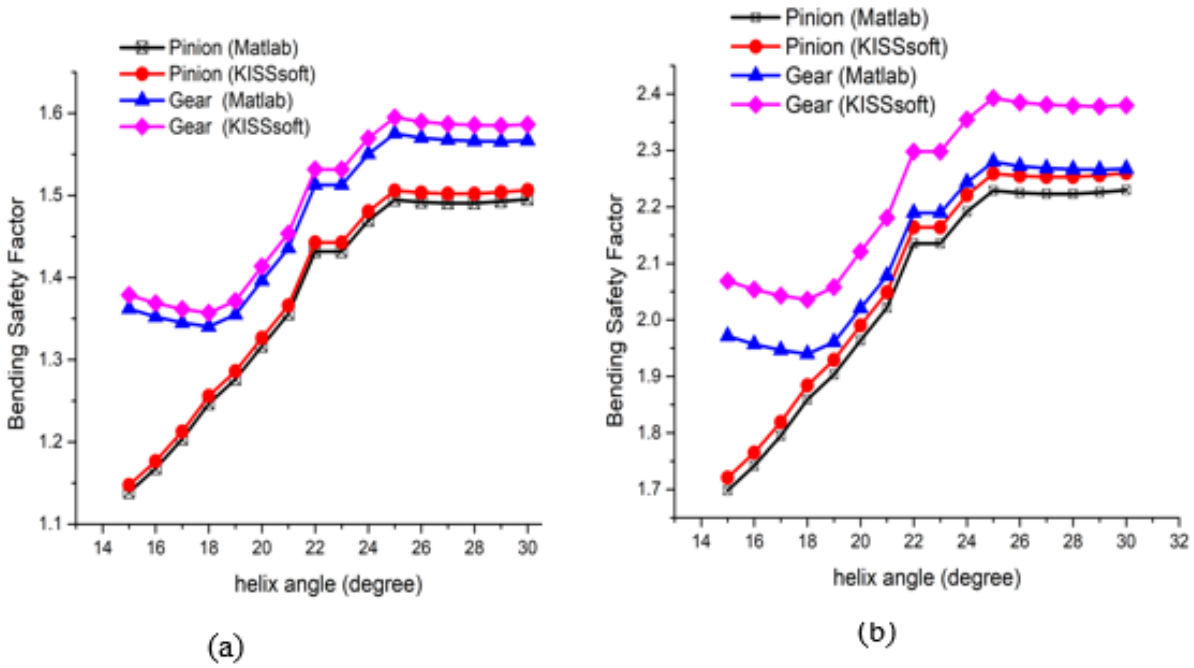

Figure 4-15: Bending safety factor versus helix angle at input torque (a):75 Nm (b):50 Nm

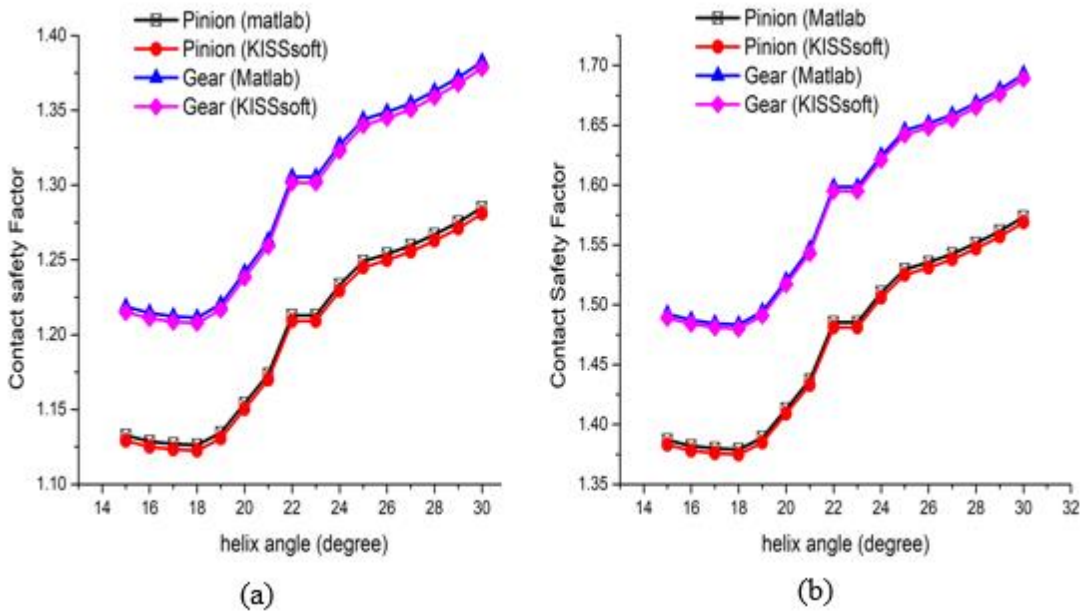

Figure 4-16: Contact safety factor versus helix angle at input torque (a):75 Nm (b):50 Nm

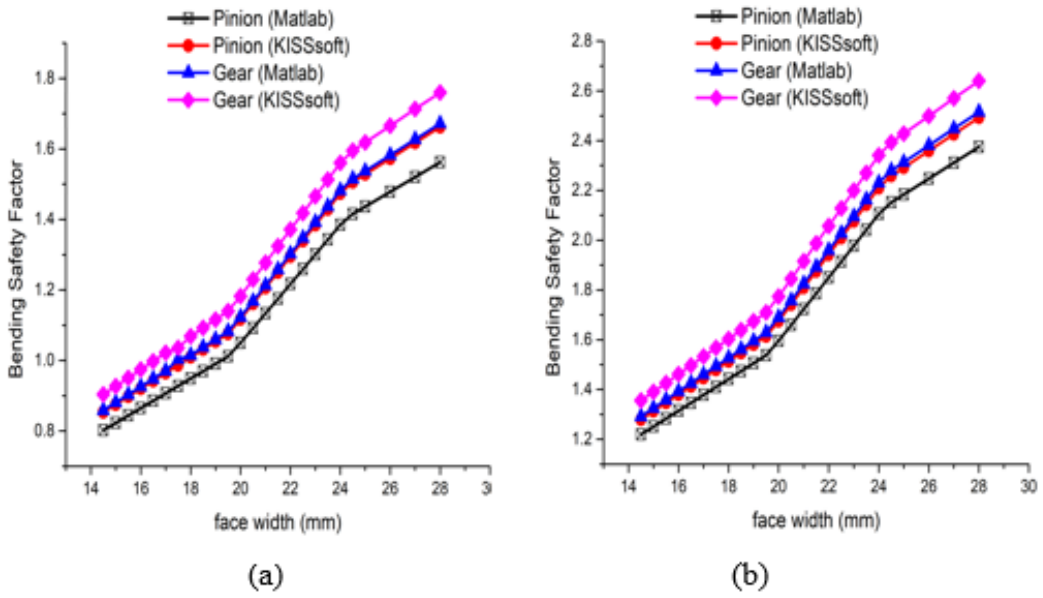

Figure 4-17: Bending safety factor versus face width at input torque (a):75 Nm (b): 50 Nm

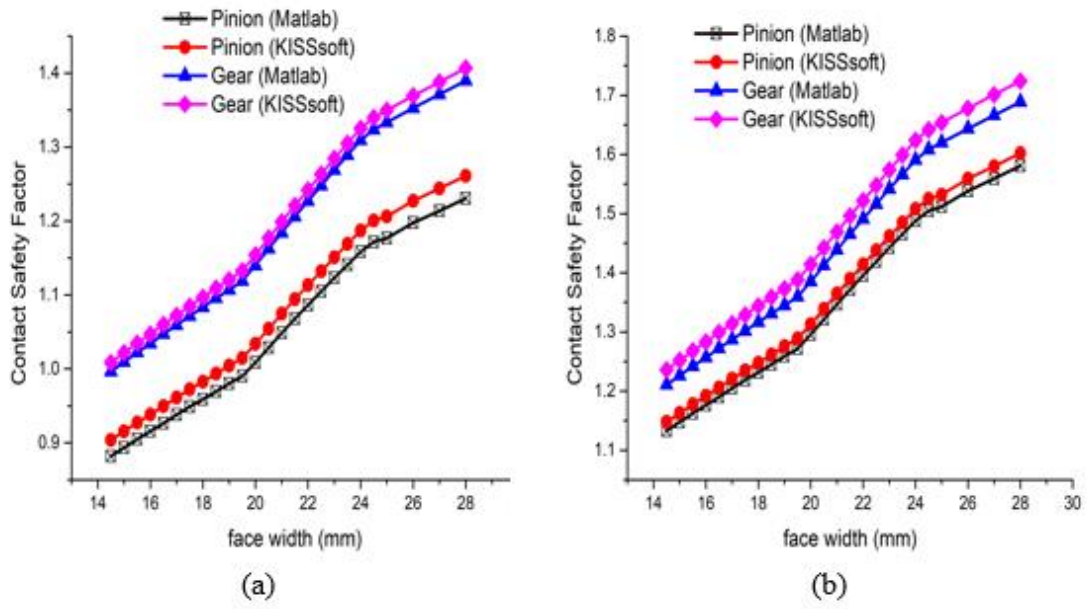

Figure 4-18: Contact safety factor versus face width at input torque (a):75 Nm (b): 50 Nm

Observing Figure4-19 (a) and (b), it is clear that, as the variable design parameter of helix angle and face width starts to increase, then all safety factors will increase while other parameters are kept constant. It shows all in one approach of bending safety factor with face width and helix angle at 75, 50 Nm of input torque.

Figure 4-20 and Figure 4-21 clearly show that the safety factors of the transmission gear with the candidate alloy steel materials and input torques after selecting the variable design parameter i.e. helix angle 25^0 and face width 24.5 mm. Besides, service life has also a great influence on both safety factors of bending (root) safety and contact (flank) safety factors. In this study the researchers select service life as 20,000 hours, as shown in figure 4-20 and figure 4-21 it is designated in a vertical line (H), at this specific service life the safety factors are above the minimum safety factors stated in AGMA standard. According to the AGMA standard so, for minimum bending safety (SF_{min}) and flank (contact) safety (SH_{min}), the corresponding values are 0.94 and 0.96 respectively. Comparing the safety factors of the two candidate materials, Cr-Mo-Ni has a higher bending safety factor (pinion and gear) than Cr-Mo alloy steel. In general, figure 4-22 summarize the fatigue safety factor of both candidate materials at 75 Nm.

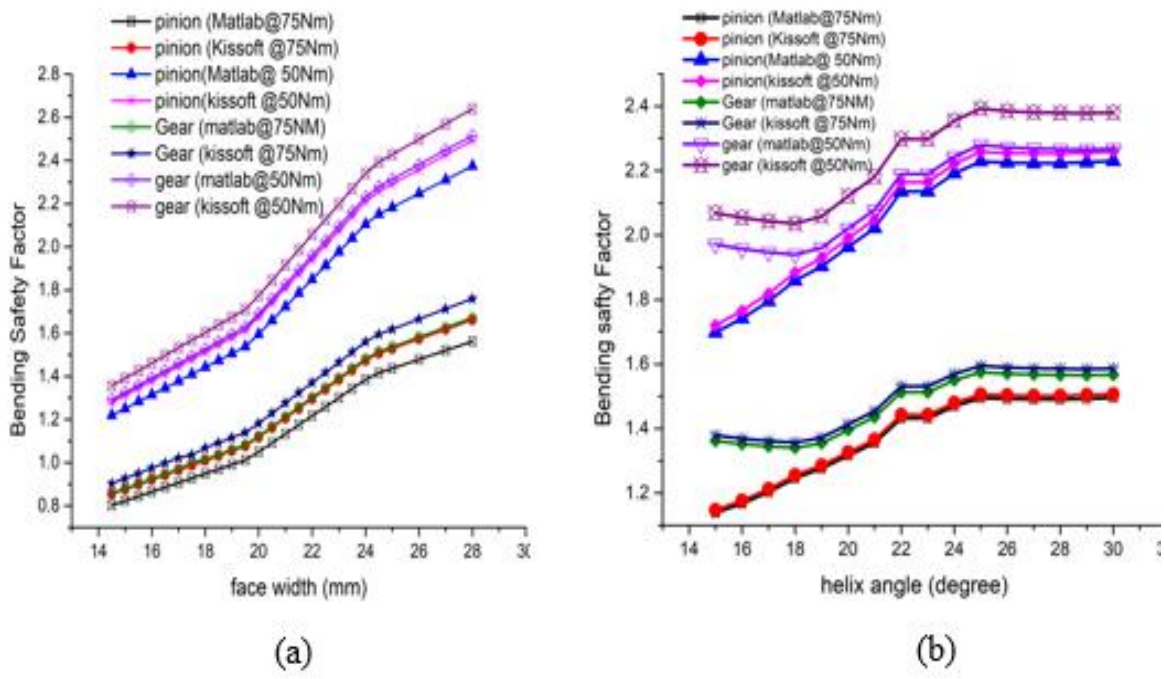

Figure 4-19: Bending safety factor versus (a): face width (b): helix angle

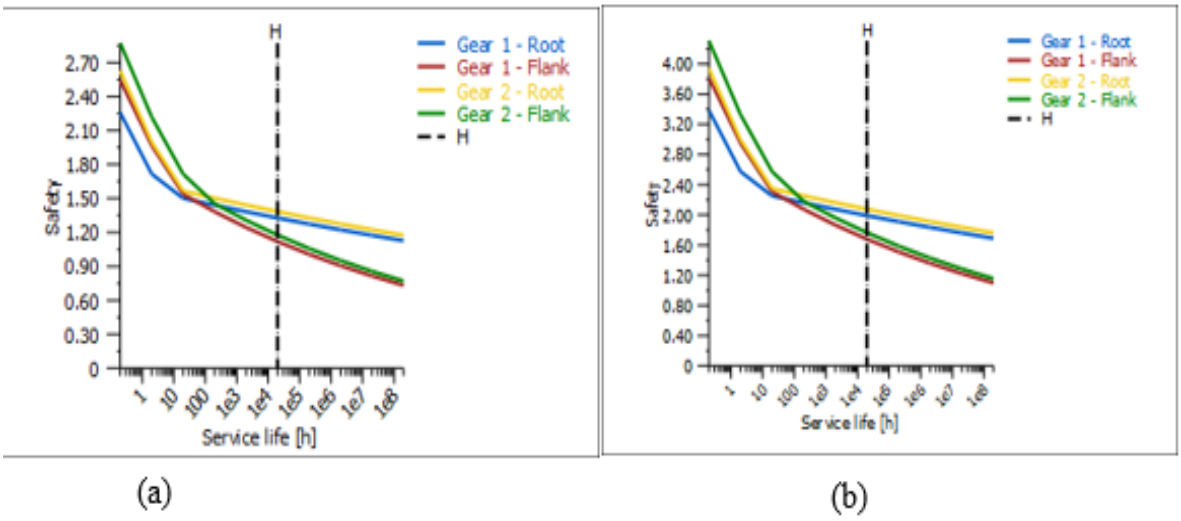

Figure 4-20: Service life of Cr-Mo-Ni alloy steel at input torque (a): 75 Nm (b): 50 Nm

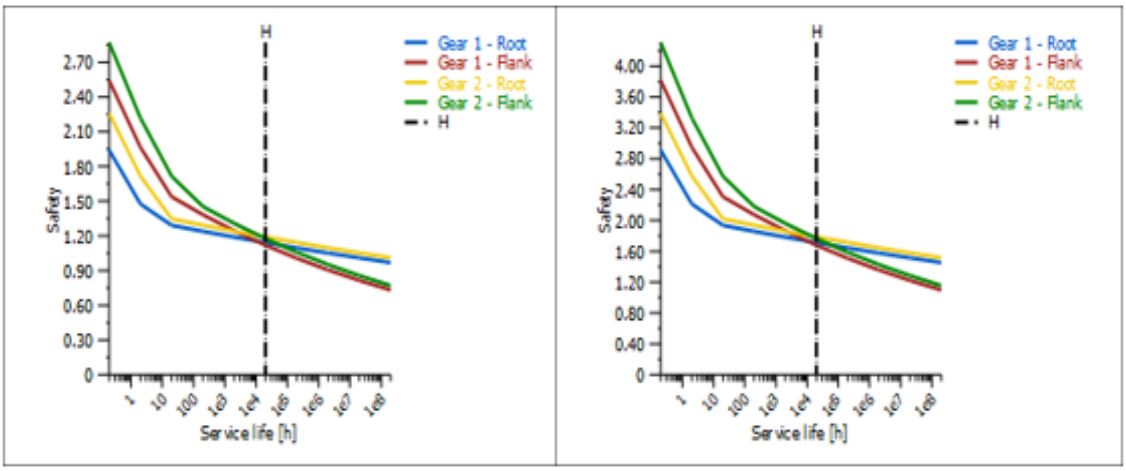

Figure 4-21: Service life of Cr-Mo alloy steel at input torque (a): 75 Nm (b): 50 Nm

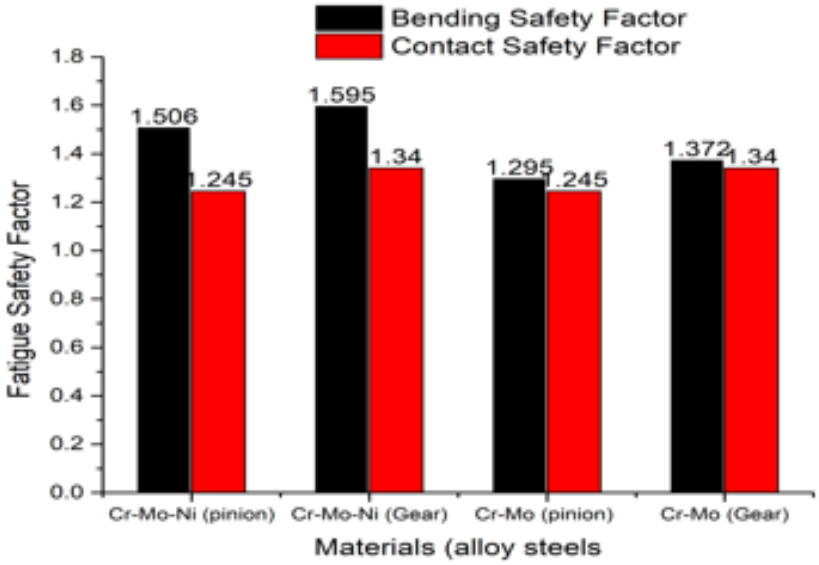

Figure 4-22: Safety factors of candidate alloy steels with input torque 75 Nm

Refer to compactness, lightweight, quiet and smooth operation of transmission gear is a very important issue in this research. Investigations have been done by both approaches at which geometric parameters compact, lightweight, and smooth operation without compromising the load-carrying capacity. When the total contact ratio increases, the load-carrying capacity also increases, while reducing the gear noise since it reduces the irregularity of resultant tooth rigidity and limits the meshing impact [212]. Figure 4-23 described the contact ratio of transmission gear which enables us to know the smooth

operation. Contact ratio has a larger effect on noise, the larger the contact ratio the smoother the gears operate, and the higher the helix angle the smoother the operation. Helical gears with an adequate total contact ratio, $\varepsilon\gamma$, (higher than 2.5) act as an active measure to reduce noise generation due to the more gradual engagement of the teeth during meshing. This meshing of the teeth and smooth transfer of load from one tooth to another gives helical gears the ability to transmit heavy loads at high speeds. Single-helical gears introduce both thrust and radial loads on the rolling bearings. By increasing the helix angle, thrust (axial) loads rise accordingly. An accurate choice of the helix angle is a key phrase since it will affect the subsequent bearing selection. The contact ratio of helical gear categorizes as follows [49].

a) The pair whose overlap ratio over 1.0 has good vibration characteristics.
b) If the total contact ratio is less than 2.0, the vibration characteristics are similar to spur gear
c) If the total contact ratio is greater than 2.0 and the overlap ratio is less than 1.0, it needs modification of the tooth profile and trace of the driven gear.

Therefore, increasing the overlap ratio reduces vibration, especially the effect that is remarkable when the overlap ratio is greater than 1.0. In this research, the total contact ratio and overlap ratio is 3.405 and 2.022 respectively.

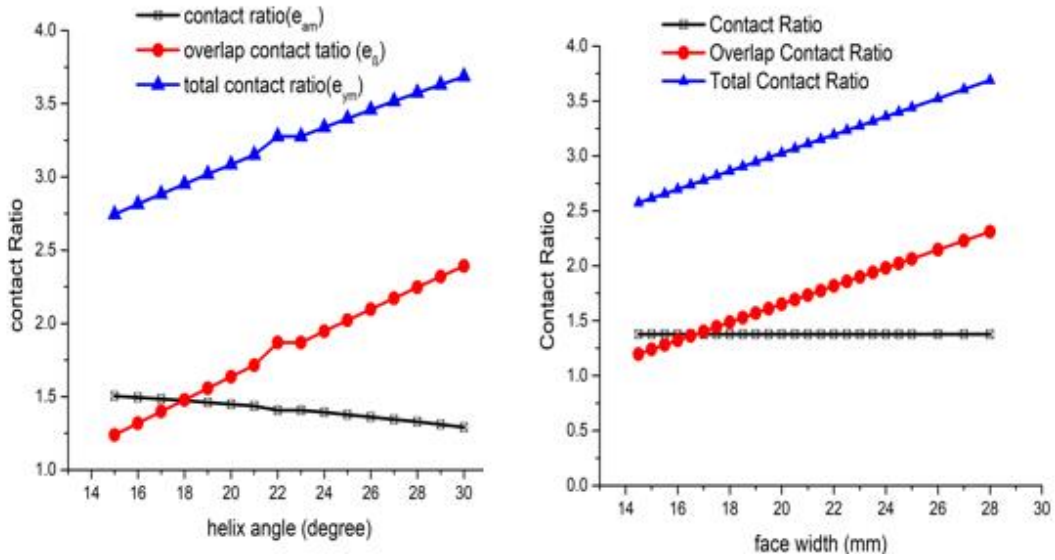

Figure 4-23: Contact ration versus variable design parameters

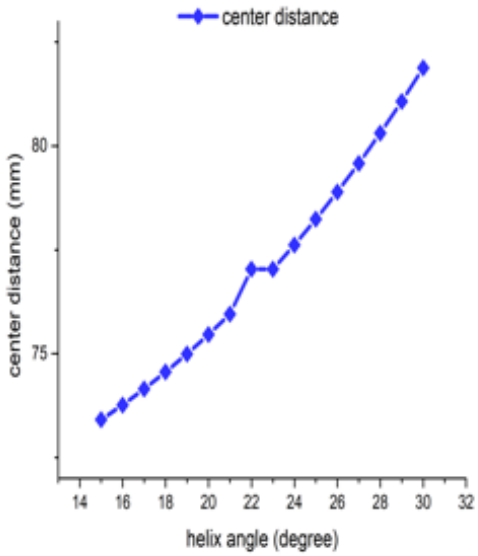

Figure 4-24: Center distance versus helix angle

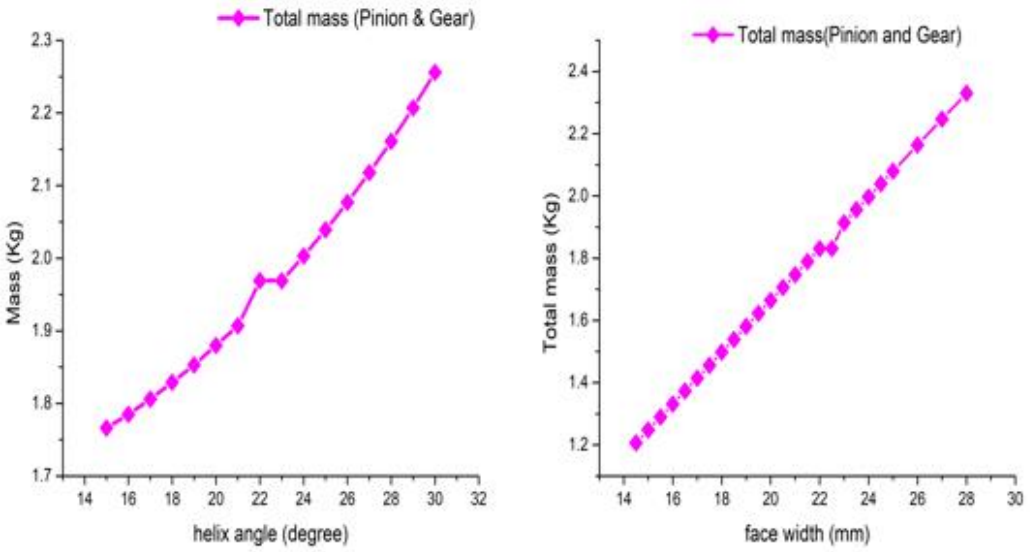

Figure 4-25: Mass versus parameters

Figure 4-24 shows the effect of the center distance when the helix angle varies. Center distance is directly related to the helix angle. At a face width of 24.5 mm and 25^{O} of helix angle, the center distance of the mating gears is 78.24 mm. Likewise, lightweight can be expressed by the total mass of the mating pairs. The total mass of both pinion and gear varies as helix angle changes. At a face width of 24.5 mm and 25^{O} of helix angle, the total max weight of the mating gears is calculated by KISSsoft as 2.04 Kg (see figure 4-25).

4.3. Surface Evaluation and Analysis

To ensure sufficient robustness of gear damage, RCF experimental tests were carried out on two materials (Cr-Mo and 1.55% Ni-modified Cr-Mo alloy steels) under the same operating conditions. The experimental test performance was accomplished by employing the same parameter for all samples. In this experiment, to occur surface damage on the sample discs, it is mandatory to run the test as per table 3-3. Moreover, the RCF test results have manifested the damage in the form of surface morphology, surface topography, and wear mass. After an accomplished experimental test, employ a scanning electron microscope (SEM) and an optical microscope (OM) to assess surface characterization and surface evaluation of the cutoff samples. Thus, fast RCF failure usually occurs in low-speed samples due to negative SRR. As research studies verified, the RCF failure was explained in terms of Micropitted area (A_p), Micropitted depth, and the equivalent diameter of the pitted surface to reveal RCF damage. So, the study evaluated the surface damage in the above-said parameters.

Knowingly, the systematic characterization of damaged surfaces can provide a good understanding of the tribological property of the material. In this work, after completing the RCF test, both candidate materials of the high-speed and the low-speed discs were measured and analyzed. Investigation of the damaged samples with SEM and OM by seeing and post-processing the micrographs of the damaged surface of the discs. The texture parameters in the micrographs were also calculated using mountain mapping software for SEM and OM imaging. The texture parameters were examined and reported as an average of different magnification and scale measurements. The cylindrical feature of the SEM image is removed from the image by applying leveling filter techniques. Accordingly, a third-order polynomial function was used to remove the cylinder feature from the SEM and OM micrographs.

The reconnoitered damaged surface texture of the disc samples of Cr-Mo alloy steel was shown in figures 4-26 (a) and (b). The surface maps of high-speed and low-speed discs of the Cr-Mo alloy steels were measured surface roughness. The surface map of the Root Mean Square (RMS) surface roughness (Sq) of Cr-Mo alloy steel is dignified at high speed

and low-speed disc samples. It is seen from the two surface maps that the low-speed disc has a slightly higher surface roughness than the high-speed disc.

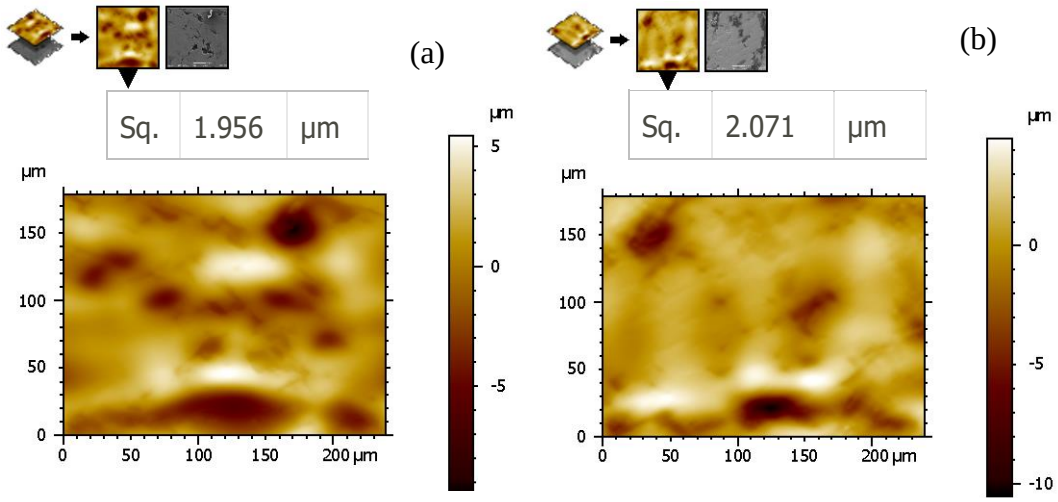

Figure 4-26: Surface map of Cr-Mo alloy steel (a): high-speed disc (b): low-speed disc

Similarly, the surface maps of RMS surface roughness (Sq) for high speed and low-speed discs of Ni-modified Cr-Mo alloy steel materials are shown in Figures 4-27 (a) and (b). As indicated in Figures 4-27 (a) and (b), surface maps of the surface roughness (Sq.) of the low-speed disc have almost the same as a high-speed disc. Therefore, the surface roughness of all the sampled materials was scrutinized at various positions and with different magnifications and the value of the surface roughness revealed in the figures is an average value. To verify the results, researchers check the surface roughness of micrographs in other similar open-access software called Gwydion. And the results are almost similar to the mountain surface map software.

Comparing the two candidate materials in terms of Sq after the RCF test, the Ni-modified Cr-mo alloy steel material has lower surface roughness than the Cr-Mo alloy steel. Therefore, from the surface damage point of view, the texture of root mean surface roughness is positively correlated with the damaged portion. The more surface RMS roughness, the more damaged portion.

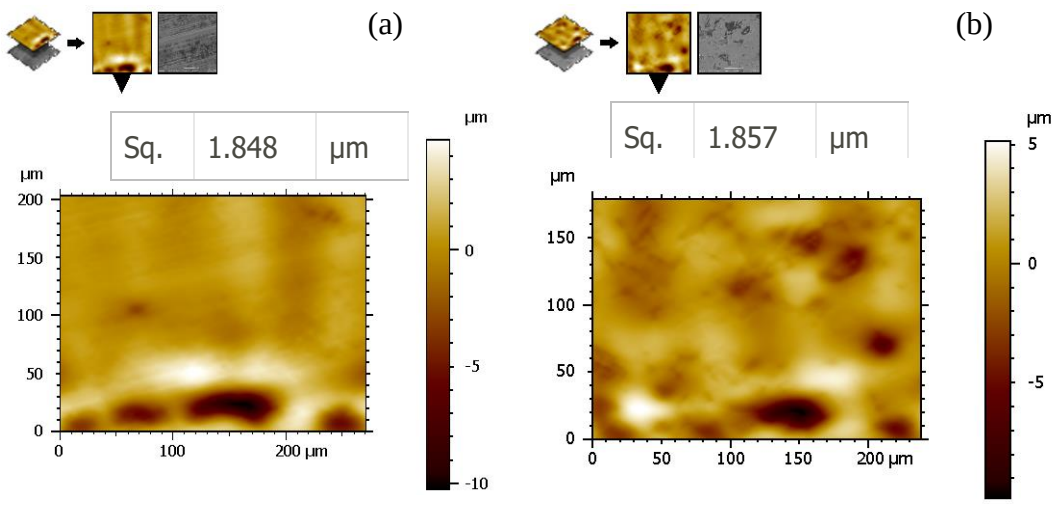

Figure 4-27: Surface map of Ni-modified Cr-Mo alloy steel (a): high-speed disc after (b): low-speed disc

Assessing wear mass (mass loss) in the RCF test is a very common and imperative parameter to determine the tribological behavior of the RCF test materials. Wear mass can affect by various factors such as lubricant type and system configuration and response which can bring a significant influence on wear mass. In this study, all the sample materials utilized the same transmission gear lubricant of SAE 90 and system configuration for the entire test.

The wear mass results for both materials of Cr-Mo and 1.55% Ni-modified Cr-Mo alloy steels of the high-speed and low-speed discs were measured at every load stage as shown in figure 4-28. It is visible that, figure 4-28 indicates the wear rates (mass loss per stage) of the high-speed disc of Ni modified Cr-Mo alloy steel has a smaller value when compared with other counterpart sample materials. From the test result, the 1.55% Ni-modified Cr-Mo alloy steels have a lower wear rate due to their mechanical property enhancement. In addition, the geometric kinematics of the samples can affect the wear mass of the samples. Regarding the geometric kinematics of high-speed discs, samples were crowned and they gained less wear mass compared with the low-speed disc sample.

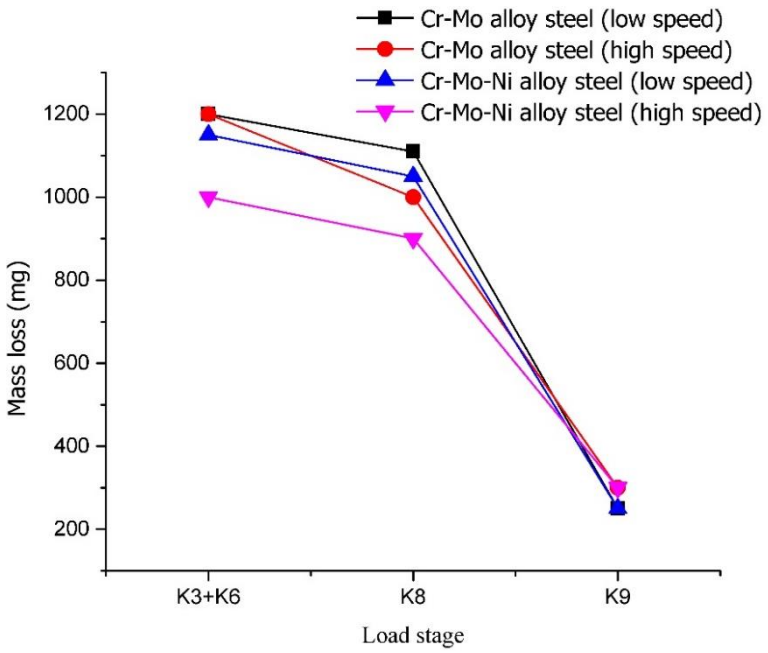

Figure 4-28: Wear mass at each load stage

After the RCF tests, the discs were removed from the twin-disc test bench, extract a small portion of the tested disc specimens were, cleaned with an ultrasonic cleaner, and dried by using hot air. Thereafter, the extracted sample discs were examined by SEM at different scales (200μm, 100 μm, 50 μm, 20 μm, and 10 μm) and magnifications of each sample. Also, this study extracts a small portion from the tested disc for optical microscope (OM) purposes. Figures 4-29 to figure 4-32 showed, OM and SEM micrographs of the high-speed and low-speed disks of Cr-Mo and Ni-modified Cr-Mo alloy steels. Figures 4-29 (a) & (b) and figure 4-30 (a) & (b) represent SEM micrograph of 50 μm scale and ×500 magnification among the plenty of SEM images of high speed and low-speed discs of Cr-Mo alloy steel materials. On both micrographs, it can be seen that pits already exist. Once mating bodies are subjected to rolling/sliding motion, strong plastic deformation occurs on these contacting bodies after run-in [203, 213].

Figure 4-29 showed the damaged portion of Cr-Mo alloy steel of high-speed disk micrographs after 10 million stress cycles. As a result, some micro pits are seen on the surface. Similarly, figures 4-30 display the Cr-Mo alloy steel of low-speed disk SEM micrographs at nearly 5million stress cycles. It can be seen that micro pits are visible when the disk is seen in high magnification.

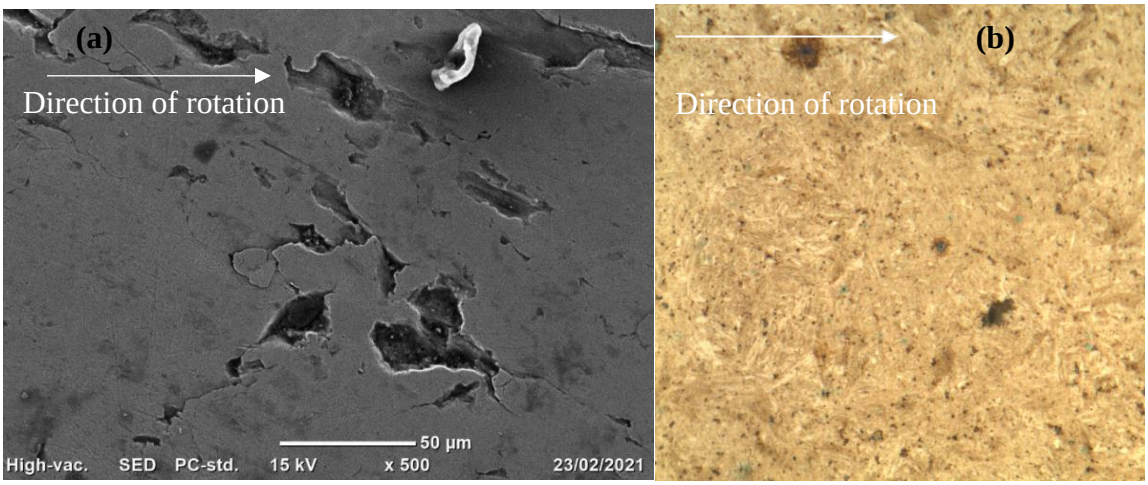

Figure 4-29: High-speed Cr-Mo alloy steel after RCF test: (a): SEM Micrograph (b): OM Micrograph

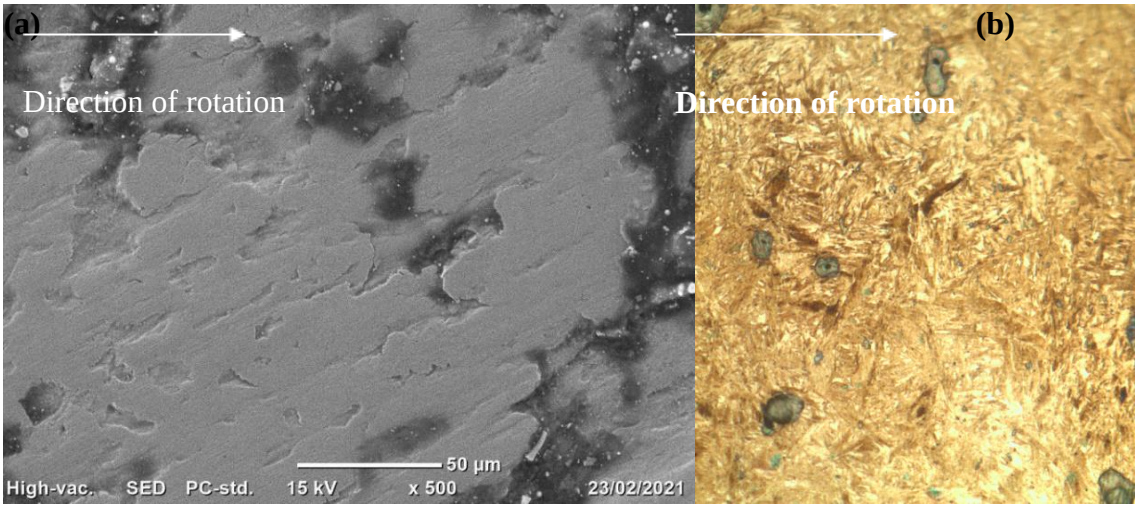

Figure 4-30: Low-speed Cr-Mo alloy steel after RCF test (a): SEM Micrograph (b): OM Micrograph

Likewise, Figures 4-31 and figure 4-32 represented SEM micrographs of 50 µm scale and ×500 magnification among the SEM images of high speed and low-speed discs of Ni-modified Cr-Mo alloy steel materials. Figure 4-31 (a) & (b) demonstrates the pitted portion of Ni-modified Cr-Mo alloy steel of high-speed disk micrographs after 10 million stress cycles for high-speed disc and 5 million stress cycles for the low-speed disc. Hence, micro pits are seen on both surfaces. Likewise, figures 4-32 presented the Ni-modified Cr-Mo alloy steel of low-speed disk SEM micrographs at nearly 5million stress cycles. It can be comprehended that micro pits are noticeable when the disk is seen in high magnification.

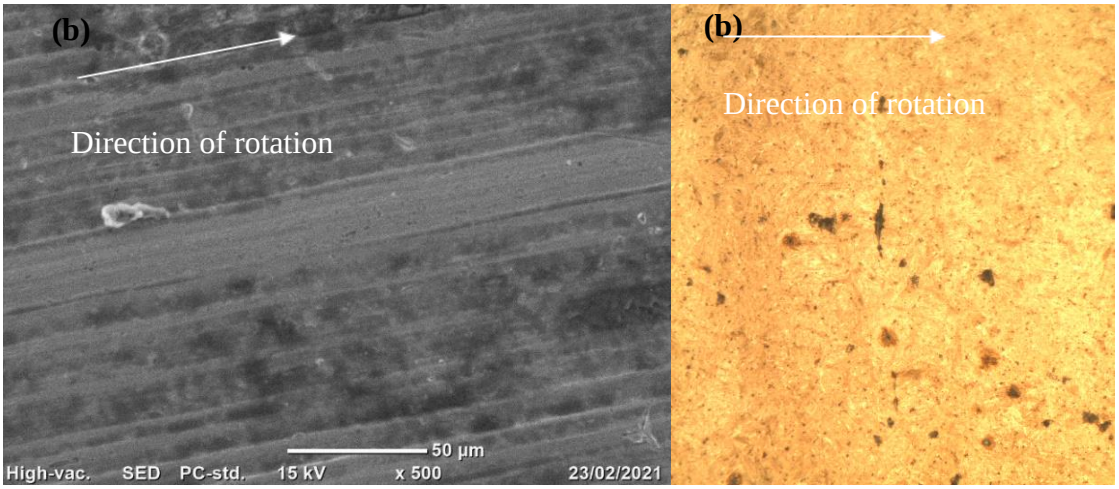

Figure 4-31: High-speed Ni-modified Cr-Mo alloy steel after RCF test (a): SEM Micrograph (b): OM Micrograph

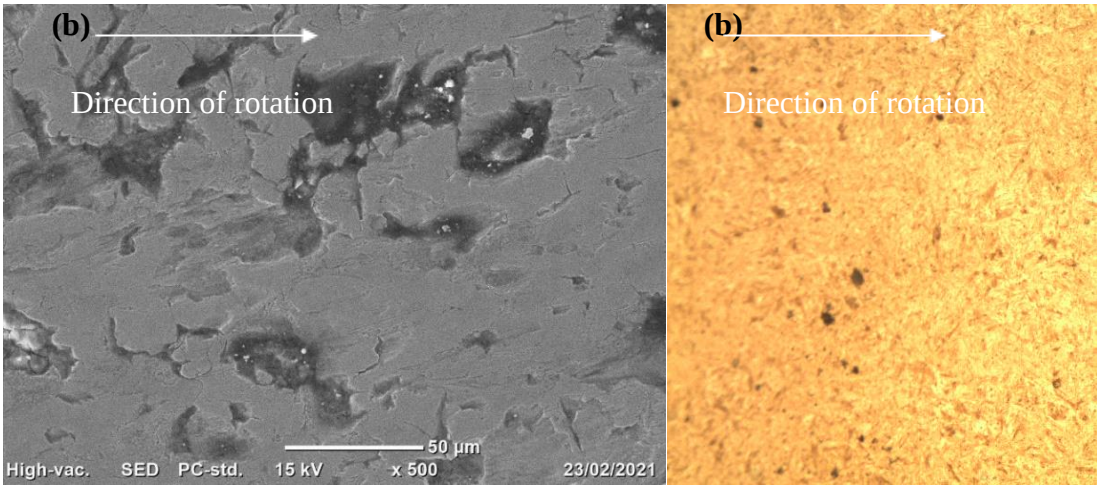

Figure 4-32: Low-speed Ni-modified Cr-Mo alloy steel after RCF (a): SEM Micrograph (b): OM Micrograph

For more clarity on the surface damage, micropitting can be categorized into various pitting determinant factors. Literatures categorized pits as the micro pit, pit, and macro pit based on pitted depth, the equivalent pitted diameter values. Thus, the surface defect is said to be a micro pit if it has a depth >1 µm and equivalent diameter in the range of 10–50 µm, below the mean plane of the surface [214, 215]. As well in this study, damaged surfaces with a pitted depth greater than or equal to 1 µm, equivalent diameter between 10–40 µm are regarded as micropitting. Else if the values are beyond the stated values, it is considered as small pitting.

The micropitting parameters like pitted depth pitted equivalent diameter and pitted roundness of the high speed and low speed of the two candidate materials are reported in Figures 4-33, figure 4-34, figure 4-35, and figure 4-36 in terms of a histogram. As shown in all figures, most micron-level depths range from -1.0 μm to -10 μm and equivalent pit diameter ranges from 10-40 μm, which indicates that there is pitting in the micro and macro level.

A further increase in the fatigue cycle will lead to an increase in the macro-scale depth and equivalent diameter. However, for both high speed and low speed of Cr-Mo alloy steel material, pits of large depth (up to 12 μm) and equivalent diameter (up to 50 μm) are observed as shown in Figure 4-35 (a) and (b) and figure 4-36(a) and (b). As illustrated in Figure 4-33 (a) and (b), figure 4-34 (a) and (b), figure 4-35 and figure 4-36, the severity of surface damage is more in Figure 4-36(a) and (b). Since in figure 4-36(a) and (b) some pits appear deeper than pits observed in another similar figure.

Similarly, figures 4-33 (c), 4-34 (c), 4-35 (c), and 4-36 (c) show the shape of the micro pits of the candidate materials indicated. The shape of micro pits if is a round shape the value becomes 1. As indicated in the figures, the more nearer to 1 indicates the shape of the pits are circular, if far apart from 1 this shows the shape is not circular.

One more factor to identify the areas of the micro pitted and the macro pitted, a correlation is established between the depth of the micro pitting and its equivalent diameter. As revealed in Figure 4-33 (d), Figure 4-34 (d), Figure 4-35 (d), and Figure 4-36 (d), the correlation between pit depth and equivalent diameter were seen. In this study, a pit is said to be a macro pit, if the diameter of the pit exceeds 50. In Figure 4-36 (d), the pitted depth of the Cr-Mo alloy low-speed disc pit is limited to 10 μm. Although the maximum pit depth of a low-speed disc with 12 μm (see Figure 4-36(b)), it is much deeper than that of a high-speed disc.

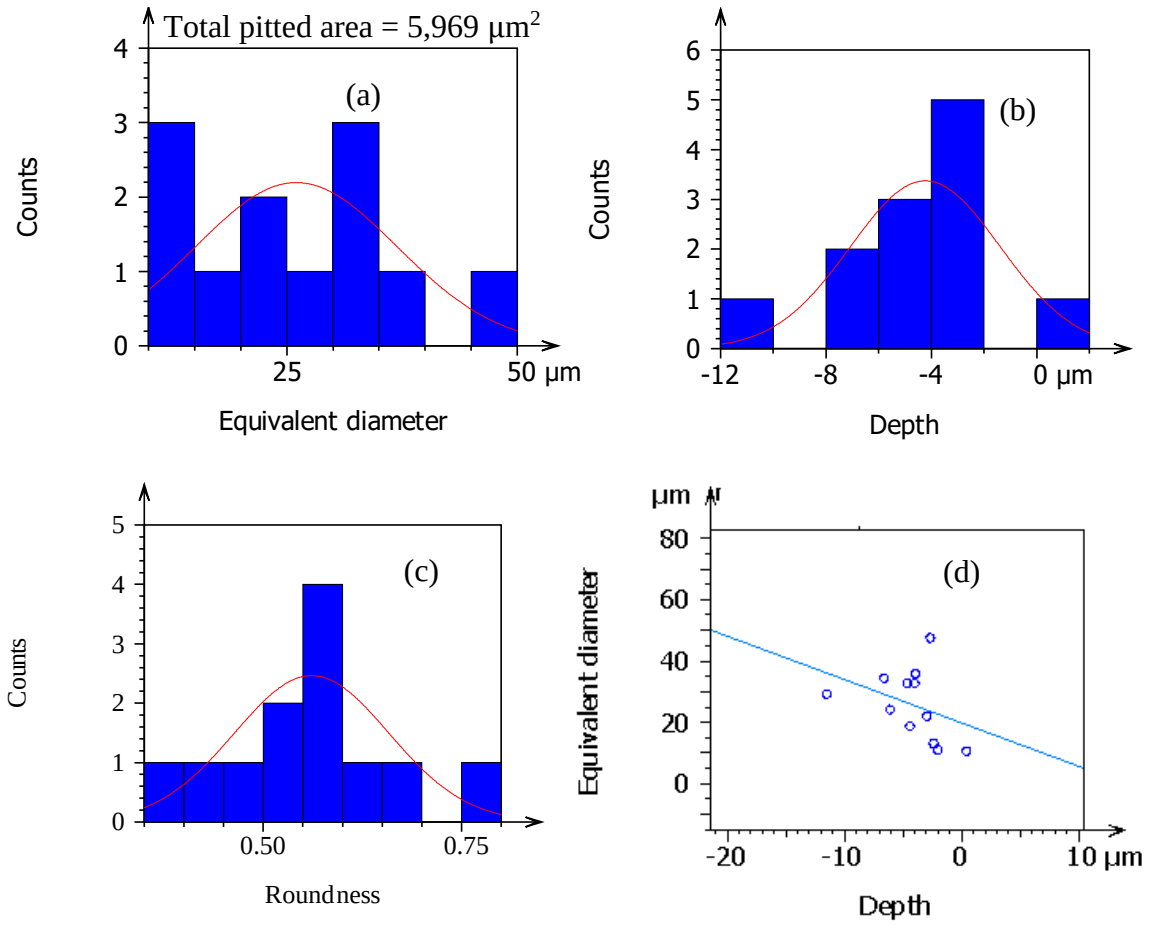

Figure 4-33: Ni-Modified Cr-Mo alloy steel of low-speed micropits of (a): equivalent diameter (b): depth (c): shape (d): correlation b/n micropits depth and micropits equivalent diameter

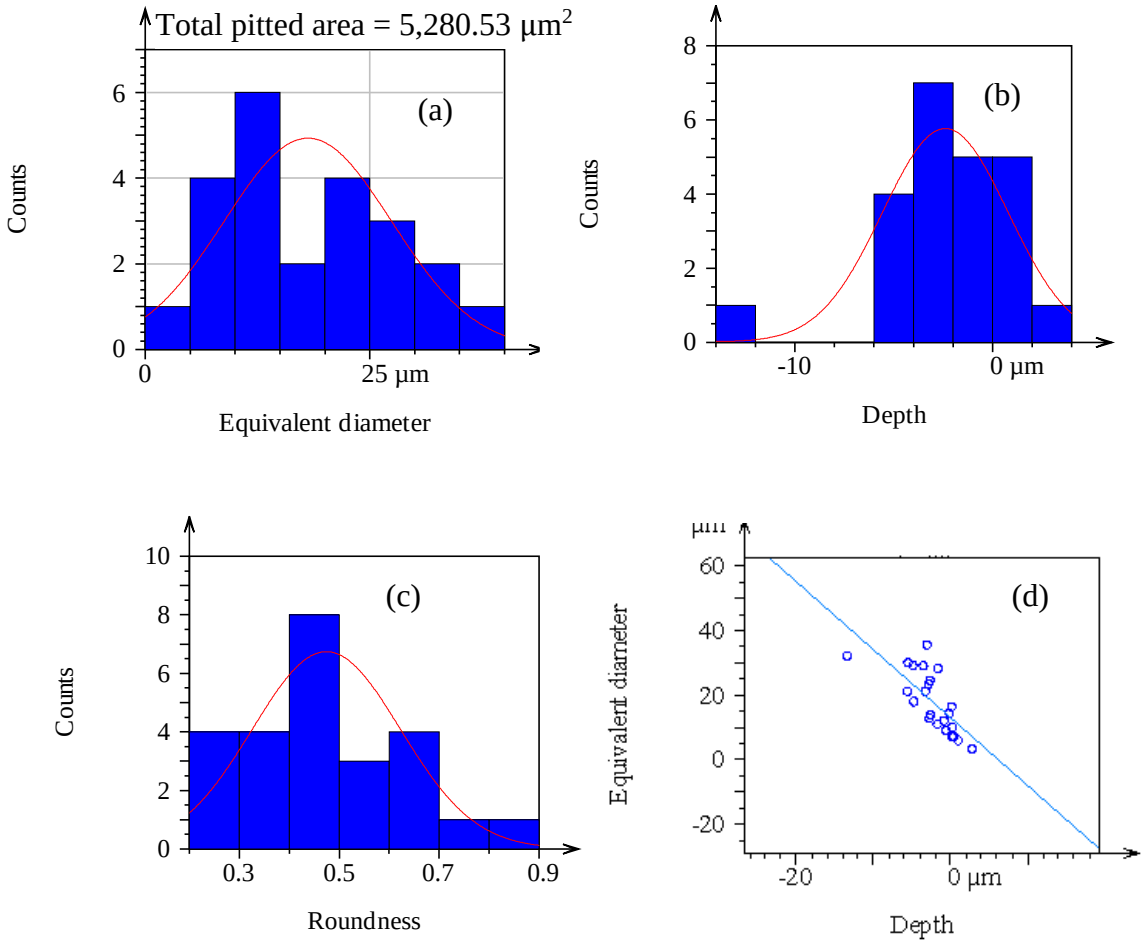

Figure 4-34: Ni-Modified Cr-Mo alloy steel of high-speed micropits of (a): equivalent diameter (b): depth (c): shape (d): correlation b/n micropits depth and micropits equivalent diameter

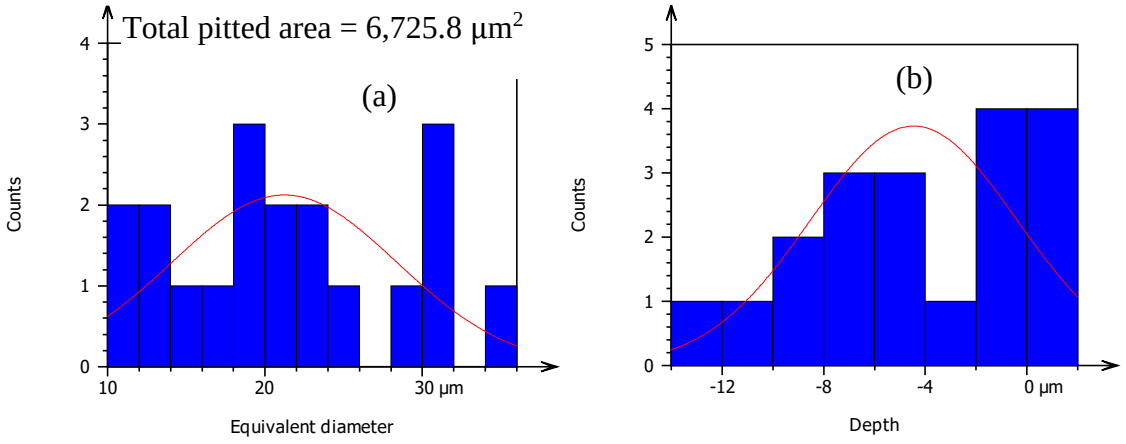

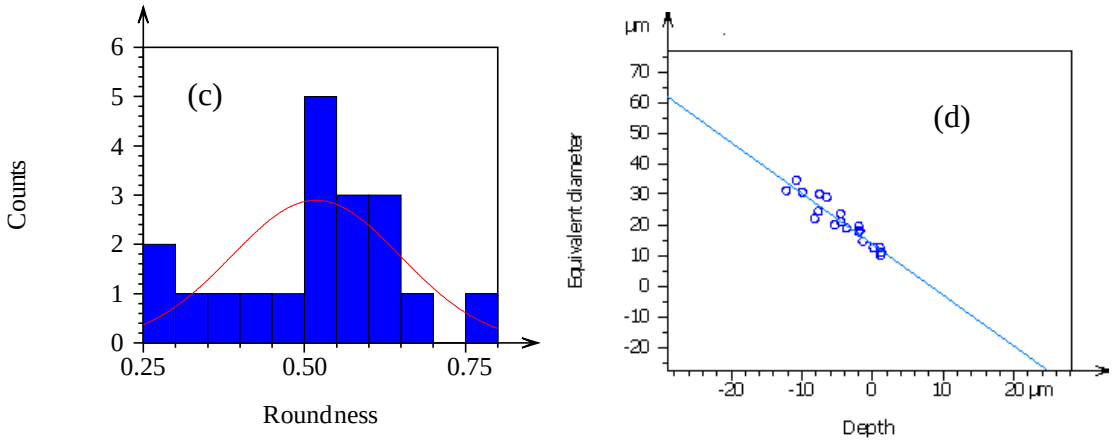

Figure 4-35: Cr-Mo alloy steel of low-speed micropits of (a): equivalent diameter (b): depth (c): shape (d): correlation b/n micropits depth and micropits equivalent diameter

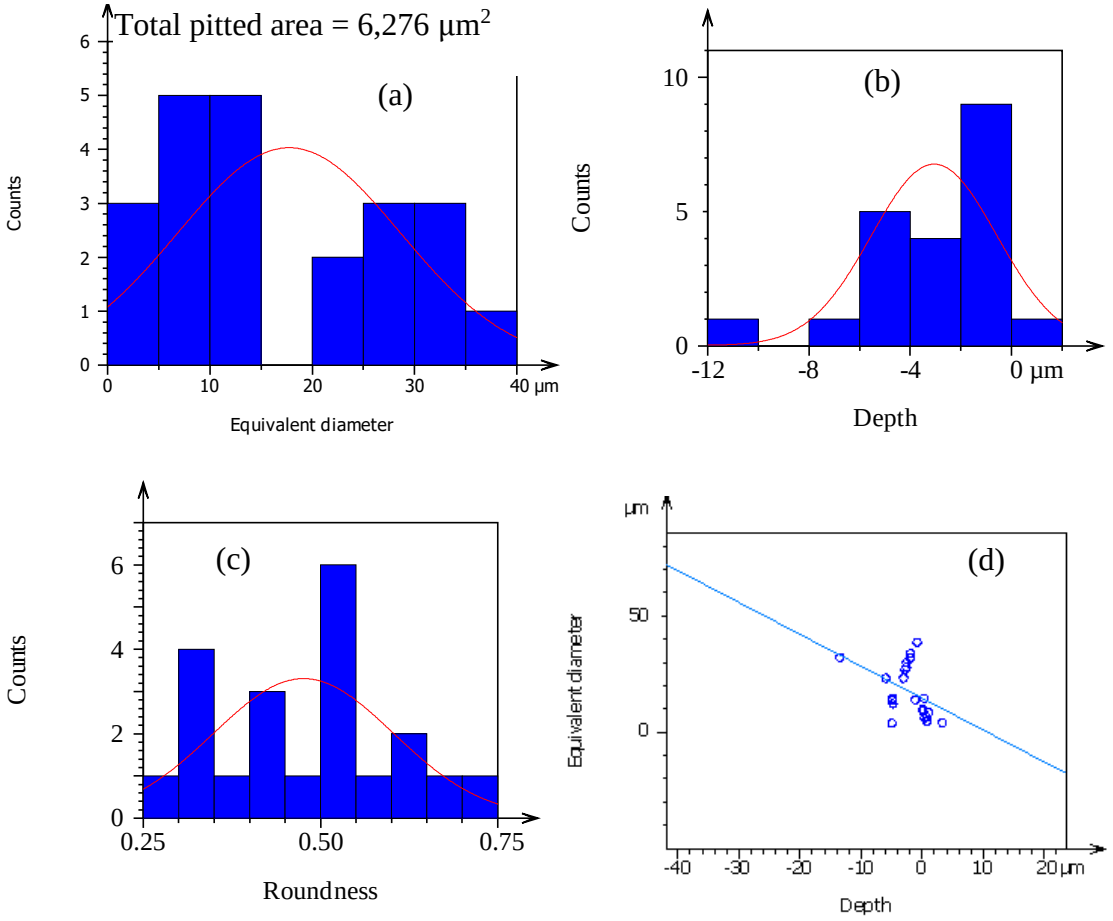

Figure 4-36: Cr-Mo alloy steel of high-speed micropits of (a): equivalent diameter (b): depth (c): shape (d): correlation b/n micropits depth and micro pit equivalent diameter

The images from Figures 4-37 and figure 4-38 are rainbow topography scale images, where the blue (watershed segmentation) area represents the pitted area, and the reddish area represents the undamaged area. The damage portion is expressed as a percentage of micro pitted area ratio (Ap) and the AP is also shown on the top side of Figure 4-37 and Figures 4-38. The percentage of the Micropitted area can be computed as the total pitted area by the total surface scanned by SEM. The total image area for all candidate materials is 120,000 μm^2. Figure 4-37 (b) shows with larger micropitting area ratio which is 5.66 % while the same condition in figure 4-37 (a) decreased its ratio which is 5.23%.

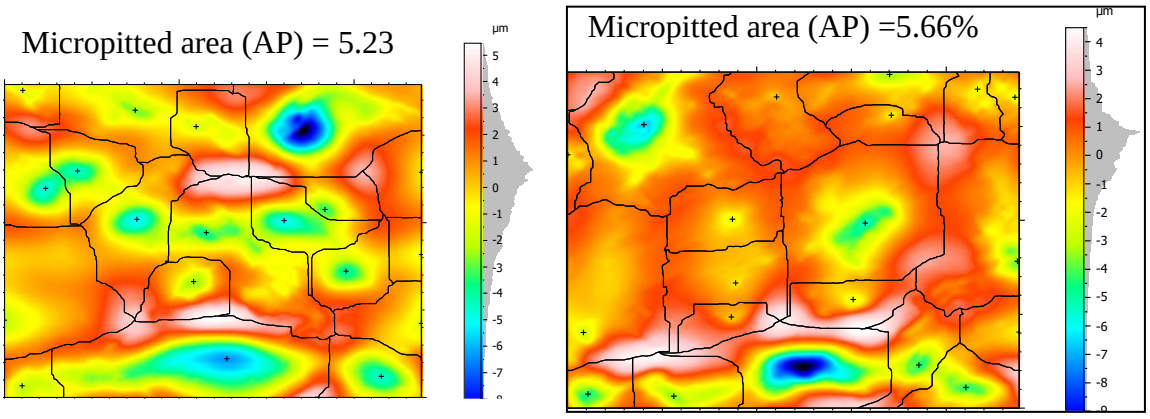

Figure 4-37: Evaluation of Surface damage of Cr-Mo alloy steel of (a): high-speed disc (b): low-speed disc

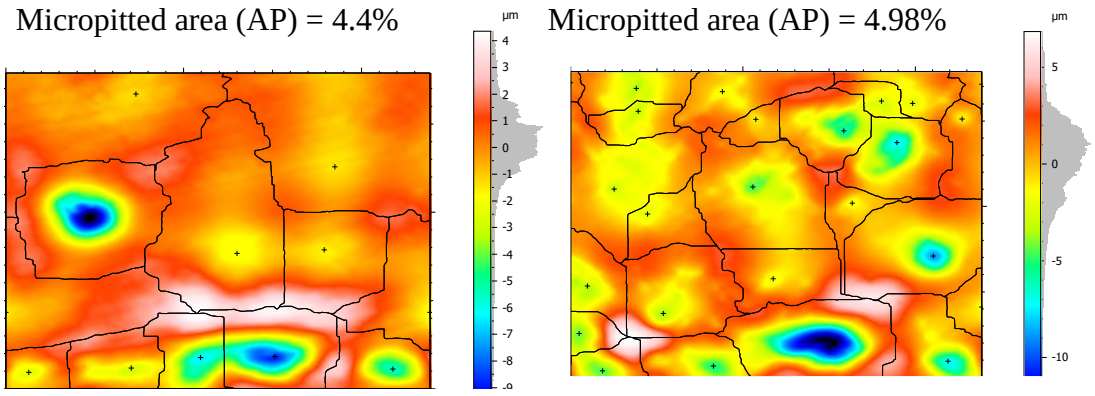

Figure 4-38: Evaluation of Surface damage of Ni-modified Cr-Mo alloy steel (a) high-speed disc (b): low-speed disc

Generally, this study examines the effects of adding Ni-content in different proportions to existing Cr-Mo alloy steel to develop new alloy steel for power transmission gears. Thus, experimental tests were carried out on 1.55 %, 1.75%, and 1.95 % Ni-modified Cr-Mo alloy steels. To address and study the behavior of lower alloying Ni content addition to Cr-Mo alloy steel, the study includes 1.15% and 1.35% Ni-contents and explored with ANN modeling. Then, the results still indicate that a Ni-content of 1.55 % has good fatigue failure resistance. As an additional rationale, studies supported these results having a higher Ni-content (2% Ni) modification than the candidates in this study.

Literature suggests that the addition of Si or Ni to the existing Cr-Mo alloy steel of transmission gear material can improve surface durability. Daniel et.al [102] figured out that, micropitting area ratio of the developed alloy steels reduces owing to wear and plastic deformation that occurs on rolling-sliding surfaces under high load conditions. They reported that the micropitting area ratio of 2%Ni-modified Cr-Mo alloy steel under the same heat treatment and loading conditions was less than that of the existing Cr-Mo alloy steel. At this point, compare the sectional hardness and surface fatigue results of Ni-modified Cr-Mo alloy steel containing 2%Ni-modified and 1.55% Ni-modified alloy steels. The sectional hardness of the 2% Ni-modified Cr-Mo alloy steel was 710HV, while the 1.55% Ni-Modified Cr-Mo alloy steel is 714 HV. Likewise, the effective case depth (a position with a hardness of 550HV) was 1.7 mm for 2% Ni-Modified alloy steel and 1.4 mm for 1.55% Ni-modified alloy steel, this is due to the amount of nickel content in the alloy chemical composition. The value of the micropitting area ratio for 2% Ni-modified Cr-Mo alloy steel was 5%. In comparison to this, the 1.55% Ni-modified Cr-Mo alloy steel owes a micropitting ratio of 4.4%. Hence, it is reasonable to conclude that 1.55 % Ni-modified alloy steel is a better material for power transmission gears to withstand surface fatigue failure.

CHAPTER: FIVE

5. General Conclusions and Recommendations

5.1. General Conclusion

In this study, an investigation was carried out on the determination of the mechanical properties of Cr-Mo alloy steel and its modification with the Ni-content using ANN and experimental tests. During the experiment, each material sample has been reputed three times and takes the average result. From both results of ANN and experimental, the following conclusions were drawn:

The more Ni-content added to the existing alloy steel, the higher yield strength and tensile strength were obtained. At the same time, as the content of Nickel added to Cr-Mo alloy steel increases from 0% to 1.55%, the impact and fracture toughness increase, however, with a further increase in the content of Nickel, the alloy steel drastically decreases toughness. It is interesting to note that alloy steels have a Ni-content greater than 1.55% consist of less grain boundary ferrite and acicular ferrite compared to 1.55% Ni-modified Cr-Mo alloy steel. Moreover, according to ANN and experimental results, 1.55% of Ni-modified Cr-Mo alloy steel shows improved fracture toughness and impact toughness without sacrificing yield strength. As a result, 1.55% Ni-modified Cr-Mo alloy steel is resistant to fatigue failure and can be used for transmission gears working under severe conditions. For further study, design, and fatigue stress analysis of the alloy steel materials of Cr-Mo and 1.55% Ni-modified Cr-Mo-Ni were considered. By using KISSsoft simulation software and AGMA standard iterating approach were carried out to investigate safety factors, fatigue stresses, lightweight, compactness, and smooth operation by altering helix angle, face-width, and input torque. Thus, from the attained results, contact stresses increase as helix angle increases from (15-18 degrees) due to the geometric modification, then it decreases as helix angle increases from (18-30 degrees). Furthermore, the effect of helix angle and face width on fatigue safety factors of gears has been investigated and the fatigue safety factors are positively correlated with the face width. Similarly, contact ratio affects noise, the larger the contact ratio the smoother the gears operate, and the higher the helix angle the smoother the operation. Comparing the two materials the 1.55% Ni-modified alloy steel has a higher impact load-carrying capacity manifested in terms of

bending safety factor. However, there is no significant difference in terms of contact load-carrying capacity demonstrated as a contact fatigue safety factor. As a result, further surface durability test was needed to verify the results obtained from mechanical property. Experimental studies were carried out on the evaluation of Cr-Mo and Ni-modified Cr-Mo alloy steels. All the samples of alloy steels were from the same manufacturing and heat treatment batch, and the same surface finish. The rolling contact fatigue of the sample materials was investigated using a twin-disc test rig. Consequently, the damaged portion of the tested disc samples has been examined using SEM and OM. With the micrographs obtained from OM and SEM, it was convenient to study the damage occurrence on both the sample materials with Micropitted parameters.

The surface texture topography (Sq) values are positively correlated with surface damage, Ni-modified Cr-Mo alloy steels have 5.52% lower in Sq compared with Cr-Mo alloy steel. Regarding mass loss, the Ni-modified Cr-Mo alloy steel has high wear mass resistance compared with counter Cr-Mo alloy steels. Considering the initial load stage Cr-Mo alloy steel has 4.16% higher mass loss compared to Ni-modified Cr-Mo alloy steel. Similarly, the Ni-modified Cr-Mo alloy steel has high micropitting resistance than the Cr-Mo alloy steels in terms of Micropitted area ratio, pitted depth, and pitted diameter. The Ni-Modified Cr-Mo alloy steel has 12.01% higher in Micropitted resistance compared to Cr-Mo alloy steel. Thus, the scientific contribution of this research is an investigation of the optimal Ni-content value (mass in %) to be added to the existing Cr-Mo alloy steel as a power transmission material to achieve better resistance to fatigue failure on surface contact. However, the study did not empirically address the thermal effect on micropitting fatigue failure. This paper only accessed the thermal influence by controlling the lubricant temperatures. Taking the thermal phenomenon into account in gear design would enable a better understanding of the mechanisms of contact fatigue failure modes.

5.2. Recommendations

In vehicles, power transmission gear is a very important component, but due to severe operating conditions, fatigue failure of gear surface is a common phenomenon. Exploring gear material, fatigue analysis, development of twin-disc test rig, and investigation of a rolling contact fatigue test on the gear materials were addressed using experimental and analytical approaches. Thus, a better material for combating contact fatigue failure was discovered by adding Ni content to the existing Cr-Mo alloy steel and performing a rolling contact fatigue test on the locally manufactured twin-disc test rig. As a result, the 1.55% Ni-modified Cr-Mo alloy steel can withstand rolling fatigue failure and this research recommends transmission gear material that operates under severe working conditions and is more prone to surface fatigue failure.

The following actions should be considered by power transmission gear manufacturers and researchers:

- Prior to experimental testing, use ANN models that can accurately predict the mechanical properties of transmission gear materials.
- In conducting experiment test on surface durability of gears using the twin-disc machine, assessing the influence of factors like gear steel material, lubricant properties, surface finish, load, thermal effect, speed, and slide-roll ratio should be taken into account.
- The locally developed twin-disc test rig found out that it works successfully and is possible to conduct a rolling contact fatigue test by applying different load conditions and other factors. However, to be more precise and in line with the standard, some modifications are required, that is, contact pressure should be applied automatically via a servo-hydraulic control valve, and it should also be equipped with a vibration sensor and data acquisition software that enables the machine to be switched off when micropitting lead to strong machine vibrations.

This research can be extended and further study will be conducted on:

- Further developments in gear design for vehicle transmission gear can be achieved considering defined road profiles. This would lead to less oversized gear concerning the required safeties;

- Due to the increased fatigue life of transmission gears, testing of additional increased load levels may be required for chemically polished gears to avoid suspending multiple tests without failure and to keep testing time to a reasonable length of time.
- Perform RCF tests on the twin-disc machine for a wider range of lubricants to test more accurately the influence of lubricants on transmission gear fatigue failure.
- Explore the impact of thermal effect on micropitting and investigate the mechanisms of micropitting crack initiation and propagation.

Reference

[1] F. Bottiglione, S. De Pinto, G. Mantriota, and A. Sorniotti, "Energy consumption of a battery electric vehicle with infinitely variable transmission," *Energies*, vol. 7, pp. 8317-8337, 2014.

[2] H. N. Hailu and D. T. Redda, "The Open Mechanical Engineering," *Open Mechanical Engineering Journal*, vol. 12, pp. 81-94, 2018.

[3] N. REGULATION, "510/2011 of the European parliament and o the council," *May, 11th*, 2011.

[4] B. Ciuffo and G. Fontaras, "Models and scientific tools for regulatory purposes: The case of CO2 emissions from light duty vehicles in Europe," *Energy Policy*, vol. 109, pp. 76-81, 2017.

[5] J. Savoy, "Light-Weight Assembled Gears: A green design solution for passenger and commercial vehicles," *Gear Technology*, pp. 64-71, 2013.

[6] D. Brasil, "Resolution no. 315, dated October 29, 2002," *Provides for the new stage of the Vehicle Emission Control Program-PROCONVE*, vol. 20.

[7] L. De Novellis, A. Sorniotti, and P. Gruber, "Design and comparison of the handling performance of different electric vehicle layouts," *Proceedings of the institution of mechanical engineers, part d: journal of automobile engineering*, vol. 228, pp. 218-232, 2014.

[8] A. Sorniotti, S. Subramanyan, A. Turner, C. Cavallino, F. Viotto, and S. Bertolotto, "Selection of the optimal gearbox layout for an electric vehicle," *SAE International Journal of Engines*, vol. 4, pp. 1267-1280, 2011.

[9] P. Sathyanarayana and G. S. Kumar, "Optimization of single speed EV drivetrain for commercial electric vehicles," in *2017 IEEE Transportation Electrification Conference (ITEC-India)*, 2017, pp. 1-3.

[10] V. Heuer, K. Loeser, and G. Schmitt, "Improved Materials and Enhanced Fatigue Resistance for Gear Components," in *Fall Technical Meeting. American Gear Manufacturers Association*, 2015.

[11] R. J. Drago, *Fundamentals of gear design*: Butterworth-Heinemann, 1988.

[12] P. S. Houghton, *Gears: spur, helical, bevel, and worm: a treatise for draughtsmen, shop superintendents, foremen, mechanics, and students*: Technical Press, 1961.

[13] B.-R. Höhn, K. Stahl, J. Schudy, T. Tobie, and B. Zornek, "FZG rig-based testing of flank load-carrying capacity internal gears," *Gear Technology, June/July*, pp. 60-69, 2012.

[14] L. Zhang, B. G. Thomas, X. Wang, and K. Cai, "Evaluation and control of steel cleanliness-Review," in *Steelmaking Conference Proceedings*, 2002, pp. 431-452.

[15] T. Krantz, M. Alanou, H. Evans, and R. Snidle, "Surface fatigue lives of case-carburized gears with an improved surface finish," *Journal of tribology*, vol. 123, pp. 709-716, 2001.

[16] G. W. Stachowiak and A. W. Batchelor, "Engineering Tribology (2005)," ed: Elsevier, 2004.

[17] Y. Suzuki, "Trend of transmission and gear technology [J]," in *The JSME Symposium on Motion and Power Transmission, Japan*, 2004, pp. 1-4.

[18] M. B. Karamış, K. Yıldızlı, and G. Ç. Aydın, "Sliding/rolling wear performance of plasma nitrided H11 hot working steel," *Tribology International*, vol. 51, pp. 18-24, 2012.

[19] S. Hassani-Gangaraj, "Moridi a., Guagliano M, Ghidini a., Boniardi M. The effect of nitriding, severe shot peening and their combination on the fatigue behavior and micro-structure of a low-alloy steel," *Int J Fatigue*, vol. 62, pp. 67-76, 2014.

[20] J. Wu, H. Liu, J. Li, X. Yang, and J. Hu, "Comparative study of plasma oxynitriding and plasma nitriding for AISI 4140 steel," *Journal of Alloys and Compounds*, vol. 680, pp. 642-645, 2016.

[21] G. Wang, S. Qu, F. Lai, X. Li, Z. Fu, and W. Yue, "Rolling contact fatigue and wear properties of 0.1 C–3Cr–2W–V nitrided steel," *International Journal of Fatigue*, vol. 77, pp. 105-114, 2015.

[22] C. Madhavan, "Effects of heat treatments on the surface durability of ferrous based powder metal spur gears," *Department of Mechanical Engineering, liT Madras*, 1991.

[23] H. Soyama, "Comparison between the improvements made to the fatigue strength of stainless steel by cavitation peening, water jet peening, shot peening and laser peening," *Journal of Materials Processing Technology*, vol. 269, pp. 65-78, 2019.

[24] H. Akyıldız, M. Kulekci, and U. Esme, "Influence of shot peening parameters on high-cycle fatigue strength of steel produced by powder metallurgy process," *Fatigue & Fracture of Engineering Materials & Structures*, vol. 38, pp. 1246-1254, 2015.

[25] S.-C. Hwang, J.-H. Lee, D.-H. Lee, S.-H. Han, and K.-H. Lee, "Contact stress analysis for a pair of mating gears," *Mathematical and Computer Modelling*, vol. 57, pp. 40-49, 2013.

[26] B. Venkatesh, S. P. Vattikuti, and S. D. Prasad, "Investigate the Combined Effect of Gear Ratio, Helix Angle, Facewidth and Module on Bending and Compressive Stress of Steel Alloy Helical Gear," *Procedia materials science*, vol. 6, pp. 1865-1870, 2014.

[27] G. Karadere and I. Yilmaz, "Investigation of the Effects of Profile Shift in Helical Gear Mechanisms with Analytical and Numerical Methods," *World Journal of Mechanics*, vol. 8, pp. 200-209, 2018.

[28] H. Jamali, "Analysis of helical gear performance under elastohydrodynamic lubrication," Cardiff University, 2015.

[29] S. Nakkeeran, "Performance Analysis of Helical Gear," *International Journal of Psychosocial Rehabilitation*, vol. 23, 2019.

[30] P. Wagaj and A. Kahraman, "Impact of tooth profile modifications on the transmission error excitation of helical gear pairs," in *Proceedings of ESDA2002: 6th biennial conference on engineering systems design and analysis*, 2002.

[31] S. Gabroveanu, S. Cananau, and R.-F. Mirica, "Numerical study concerning the influence of contact ratio at helical involute gears," in *MATEC Web of Conferences*, 2019, p. 01005.

[32] J. S. Kang and Y.-S. Choi, "Optimization of helix angle for helical gear system," *Journal of mechanical science and technology*, vol. 22, pp. 2393-2402, 2008.

[33] H. Zeyin, L. Tengjiao, L. Tianhong, D. Tao, and H. Qiguo, "Parametric modeling and contact analysis of helical gears with modifications," *Journal of Mechanical Science and Technology*, vol. 30, pp. 4859-4867, 2016.

[34] H. Jiang, Y. Shao, C. K. Mechefske, and X. Chen, "The influence of mesh misalignment on the dynamic characteristics of helical gears including sliding

friction," *Journal of Mechanical Science and Technology,* vol. 29, pp. 4563-4573, 2015.

[35] S. Brauer, "High Speed Electric Vehicle Transmission: Investigation how noise vibration harshness are affected at high speeds in an electric vehicle transmission," ed, 2017.

[36] D. Kong, J. Meagher, C. Xu, X. Wu, and Y. Wu, "Nonlinear contact analysis of gear teeth for malfunction diagnostics," 2008.

[37] F. Antoine and J. Besson, "Simplified modellization of gear micropitting," *Proceedings of the Institution of Mechanical Engineers, Part G: Journal of Aerospace Engineering,* vol. 216, pp. 291-302, 2002.

[38] J. Colbourne, "The Kinematics of Crossed Helical Gears," 1982.

[39] F. L. Litvin and J. Zhang, "Topology of modified helical gears and tooth contact analysis (TCA) program," ILLINOIS UNIV AT CHICAGO CIRCLE DEPT OF MECHANICAL ENGINEERING1989.

[40] B. Shotter, "Experiences with conformal/WN gearing," *Machinery and Production Engineering,* pp. 322-326, 1977.

[41] Y.-j. Wu, J.-j. Wang, and Q.-k. Han, "Static/dynamic contact FEA and experimental study for tooth profile modification of helical gears," *Journal of mechanical science and technology,* vol. 26, pp. 1409-1417, 2012.

[42] G. M. Maitra, *Handbook of gear design*: Tata McGraw-Hill Education, 1994.

[43] K. L. Johnson, "Contact mechanics," *Proceedings of the Institution of Mechanical Engineers,* vol. 223, p. 254, 2009.

[44] W. A. Tuplin, *Involute gear geometry*: F. Unger Pub. Co., 1962.

[45] S. Li, A. Vaidyanathan, J. Harianto, and A. Kahraman, "Influence of design parameters on mechanical power losses of helical gear pairs," *Journal of Advanced Mechanical Design, Systems, and Manufacturing,* vol. 3, pp. 146-158, 2009.

[46] P. Velex, *International Gear Conference 2014: 26th-28th August 2014, Lyon*: Chandos Publishing, 2014.

[47] S.-H. Wu and S.-J. Tsai, "Contact stress analysis of skew conical involute gear drives in approximate line contact," *Mechanism and Machine Theory,* vol. 44, pp. 1658-1676, 2009.

[48] S. M. Jadhav, "Powertrain NVH analysis including clutch and gear dynamics," SAE Technical Paper 0148-7191, 2014.

[49] G. G. Rey, "Higher contact ratios for quieter gears," *Gearssolutions. com, January*, 2009.

[50] Y. Zhang, J. Du, J. Mao, and M. Xu, "Dynamic Analysis of High-Speed Helical Gear Transmission in Pure Electric Vehicle Gearbox," *Shock and Vibration*, vol. 2020, 2020.

[51] G. Stachowiak and A. Batchelor, "Engineering Tribology, Vol. 24 of Tribology Series," ed: Elsevier Science Publishers BV, 1993.

[52] B. Alfredsson, "A study on contact fatigue mechanisms," KTH, 2000.

[53] B. Alfredsson and M. Olsson, "Inclined standing contact fatigue," *Fatigue & Fracture of Engineering Materials & Structures*, vol. 26, pp. 589-602, 2003.

[54] M.-L. Dumont, "Etude des endommagements de surface induits par fatigue de roulement dans les contacts elastohydrodynamiques pour des aciers M50 et 100Cr6," Thèse de doctorat, INSA de Lyon, 197 p, 1997.

[55] D. Girodin, F. Ville, R. Guers, and G. Dudragne, "Rolling contact fatigue tests to investigate surface initiated damage using surface defects," 2002.

[56] A. R. Du Crehu, "Tribological analysis of White Etching Crack (WEC) failures in rolling element bearings," 2014.

[57] S. Alshahrany, "Rolling contact fatigue in heavily loaded gear transmission contacts," Cardiff University, 2015.

[58] S. Sankar and M. Nataraj, "Profile modification—a design approach for increasing the tooth strength in spur gear," *The International Journal of Advanced Manufacturing Technology*, vol. 55, pp. 1-10, 2011.

[59] G. Morales-Espejel, P. Rycerz, and A. Kadiric, "Prediction of micropitting damage in gear teeth contacts considering the concurrent effects of surface fatigue and mild wear," *Wear*, vol. 398, pp. 99-115, 2018.

[60] A. R. Hassan, "Contact stress analysis of spur gear teeth pair," *World Academy of Science, Engineering and Technology*, vol. 58, pp. 597-602, 2009.

[61] R. D. Arnell, P. Davies, J. Halling, and T. Whomes, *Tribology: Principles and Design Applications: Principles and Design Applications*: Macmillan International Higher Education, 1991.

[62] A. Clarke, H. P. Evans, and R. Snidle, "Understanding micropitting in gears," *Proceedings of the Institution of Mechanical Engineers, Part C: Journal of Mechanical Engineering Science,* vol. 230, pp. 1276-1289, 2016.

[63] P. Fernandes and C. McDuling, "Surface contact fatigue failures in gears," *Engineering Failure Analysis,* vol. 4, pp. 99-107, 1997.

[64] J. A. Williams, "The influence of repeated loading, residual stresses and shakedown on the behaviour of tribological contacts," *Tribology international,* vol. 38, pp. 786-797, 2005.

[65] N. Myshkin, M. Petrokovets, and A. Kovalev, "Tribology of polymers: adhesion, friction, wear, and mass-transfer," *Tribology International,* vol. 38, pp. 910-921, 2005.

[66] K. Johnson, "Contact mechanics cambridge univ," *Press, Cambridge,* vol. 95, p. 365, 1985.

[67] C. Mohan, C. Divakar, K. Venkatesh, K. Gopalakrishna, K. M. Lohith, and T. Naveen, "Design and development of an advanced linear reciprocating tribometer," *Wear,* vol. 267, pp. 1111-1116, 2009.

[68] G. Meneghetti, A. Terrin, and S. Giacometti, "A twin disc test rig for contact fatigue characterization of gear materials," *Procedia Structural Integrity,* vol. 2, pp. 3185-3193, 2016.

[69] T. NAKANISHI, D. T. REDDA, and G. DENG, "GSD-09 INFLUENCES OF SURFACE TEXTURE AND LUBRICATING OIL TEMPERATURE ON SURFACE FAILURE OF ROLLING-SLIDING CONTACT IN THE CASE OF CASE-CARBURIZED ALLOY STEELS (GEAR STRENGTH AND DURABILITY, INCLUDING GEAR MATERIALS AND HEAT TREATMENT TECHNIQUES)," in *The Proceedings of the JSME international conference on motion and power transmissions 2009,* 2009, pp. 350-355.

[70] N. F. Strey, A. B. Rezende, R. da Silva Miranda, S. T. da Fonseca, P. R. Mei, and C. Scandian, "Comparison of rolling contact fatigue damage between railway

wheels and twin-disc test specimens," *Tribology International*, vol. 160, p. 107037, 2021.

[71] J. Wei, A. Zhang, and P. Gao, "A study of spur gear pitting under EHL conditions: Theoretical analysis and experiments," *Tribology International*, vol. 94, pp. 146-154, 2016.

[72] A. Milani, A. Shanian, R. Madoliat, and J. Nemes, "The effect of normalization norms in multiple attribute decision making models: a case study in gear material selection," *Structural and multidisciplinary optimization*, vol. 29, pp. 312-318, 2005.

[73] A. Milani and A. Shanian, "Gear material selection with uncertain and incomplete data. Material performance indices and decision aid model," *International Journal of Mechanics and Materials in Design*, vol. 3, pp. 209-222, 2006.

[74] F. Hippenstiel, K. Johann, and R. Caspari, "Tailor Made Carburizing Steels for Use in Power Generation Plants," in *Proceedings of the International European Conference on Heat Treatment, Strasbourg, France*, 2009.

[75] K. Klenke, R. Kohlmann, P. Reinhold, and W. Schweinebraten, "Improved performance by high temperature carburizing shown by the example of VW4521+ Nb," *Proceedings Steels in Cars and Truck*, pp. 173-183, 2008.

[76] F. Hippenstiel, "Tailored solutions in microalloyed engineering steels for the power transmission industry," in *Materials science forum*, 2007, pp. 4131-4136.

[77] M. Wu and K. Hwang, "Formation mechanism of weak ferrite areas in Ni-containing powder metal steels and methods of strengthening them," *Materials Science and Engineering: A*, vol. 527, pp. 5421-5429, 2010.

[78] K. Nikolov, V. Ivanov, O. Cankaya, and L. Dimitrov, "Use of carbon nanotube composites in gearing," in *Proceedings of the 5-th International Conference on Power Transmission, October*, 2016, pp. 05-08.

[79] D. W. Dudley and S. P. Radzevich, *Dudley's handbook of practical gear design and manufacture*: CRC press, 2012.

[80] H. IMATAKA, M. YUYA, K. TANAKA, A. KOBAYASHI, and S. MAEDA, "Development of High-strength Nitriding Steel for Gear."

[81] M. F. Ashby, "Materials selection in mechanical design.: Kidlington," ed: Oxford, UK: Butterworth-Heinemann, cop, 2011.

[82] M. Ashby, H. Shercliff, and D. Cebon, "Materials Engineering, science, processing and design, Second Editions, Editorials Elsevier Ltd," ed: Oxford, 2010.

[83] H. Mohrbacher, "Metallurgical concepts for optimized processing and properties of carburizing steel," *Advances in Manufacturing*, vol. 4, pp. 105-114, 2016.

[84] D. Khan, R. Shukla, and B. Gautham, "In Silico Design of Materials and Processes: An Application of ICME to Carburizing Steels," *Transactions of the Indian Institute of Metals*, vol. 72, pp. 2179-2185, 2019.

[85] S. A. Miller, M. D. Lepech, and S. L. Billington, "Application of multi-criteria material selection techniques to constituent refinement in biobased composites," *Materials & Design (1980-2015)*, vol. 52, pp. 1043-1051, 2013.

[86] P. Karande and S. Chakraborty, "Application of multi-objective optimization on the basis of ratio analysis (MOORA) method for materials selection," *Materials & Design*, vol. 37, pp. 317-324, 2012.

[87] H. Delibaş, Ç. Uzay, and N. Geren, "Advanced material selection technique for high strength and lightweight spur gear design," *European Mechanical Science*, vol. 1, pp. 133-140, 2017.

[88] G. E. Dieter and L. C. Schmidt, *Engineering design*: McGraw-Hill Higher Education Boston, 2009.

[89] C. Renzi, F. Leali, and L. Di Angelo, "A review on decision-making methods in engineering design for the automotive industry," *Journal of Engineering Design*, vol. 28, pp. 118-143, 2017.

[90] S. Sapuan and M. R. Mansor, "Concurrent engineering approach in the development of composite products: A review," *Materials & Design*, vol. 58, pp. 161-167, 2014.

[91] J. Kaspar and M. Vielhaber, "Cross-component systematic approach for lightweight and material-oriented design," *DS 85-1: Proceedings of NordDesign 2016, Volume 1, Trondheim, Norway, 10th-12th August 2016*, pp. 332-341, 2016.

[92] C. R. Gagg and P. R. Lewis, "Wear as a product failure mechanism–overview and case studies," *Engineering Failure Analysis*, vol. 14, pp. 1618-1640, 2007.

[93] A. Krell, T. Hutzler, and J. Klimke, "Transmission physics and consequences for materials selection, manufacturing, and applications," *Journal of the European Ceramic Society,* vol. 29, pp. 207-221, 2009.

[94] D. Zhang, Y. Mao, Y. Li, J. Li, M. Yuan, and J. Lin, "Effect of ternary alloying elements on microstructure and superelastictity of Ti–Nb alloys," *Materials Science and Engineering: A,* vol. 559, pp. 706-710, 2013.

[95] G. Bonny, C. Domain, N. Castin, P. Olsson, and L. Malerba, "The impact of alloying elements on the precipitation stability and kinetics in iron based alloys: An atomistic study," *Computational Materials Science,* vol. 161, pp. 309-320, 2019.

[96] M. D. Bambach, A. Stieben, and W. Bleck, "18CrNiMo7-6 with TRIP-Effect for Increasing the Damage Tolerance of Gear Components—Part II: Microstructure and Mechanical Properties," in *Materials Science Forum*, 2014, pp. 639-643.

[97] M. D. Bambach, A. Stieben, and W. Bleck, "18CrNiMo7-6 with TRIP-Effect for Increasing the Damage Tolerance of Gear Components—Part I: Alloy Design," in *Materials Science Forum*, 2014, pp. 633-638.

[98] F. B. Abudaia, "Microstructure and fatigue strength of high performance gear steels," Newcastle University, 2003.

[99] M. A. d. Souza, B. d. O. Fiorin, T. M. Hashimoto, A. P. Rosifini, C. A. Nunes, C. A. R. P. Baptista, *et al.*, "Influence of Niobium or Molybdenum Addition on Microstructure and Tensile Properties of Nickel-Chromium Alloys," *Metals*, vol. 9, p. 589, 2019.

[100] D. E. Sievers and P. J. Bocchini, "Steel Alloy and Method for Heat Treating Steel Alloy Components," ed: Google Patents, 2020.

[101] Y. Deng, Y. Li, H. Di, and R. Misra, "Effect of Heating Rate during Continuous Annealing on Microstructure and Mechanical Properties of High-Strength Dual-Phase Steel," *Journal of Materials Engineering and Performance,* vol. 28, pp. 4556-4564, 2019.

[102] D. T. Redda, T. Nakanishi, and G. Deng, "Softening behavior of hardness and surface fatigue of rolling-sliding contact in the case of developed alloy steels," *Journal of Advanced Mechanical Design, Systems, and Manufacturing,* vol. 3, pp. 85-92, 2009.

[103] M. Agnani, O. DeNonno, K. Findley, and S. Thompson, "Quantitative Analysis of Microstructural Refinement in Simulated Carburized Microstructures," *Journal of Materials Engineering and Performance*, pp. 1-9, 2020.

[104] M. Shah, S. Das, and S. G. Chowdhury, "Effect of alloying elements on microstructure and mechanical properties of air-cooled bainitic steel," *Metallurgical and Materials Transactions A*, vol. 50, pp. 2092-2102, 2019.

[105] T. Sourmail, V. Smanio, F. G. Caballero, J. Cornide, C. Capdevilla, and C. García-Mateo, "Evolution of Microstructure and Mechanical Properties during Tempering of Continuously Cooled Bainitic Steels," in *Materials Science Forum*, 2012, pp. 2308-2313.

[106] E. Bagherpour, N. Pardis, M. Reihanian, and R. Ebrahimi, "An overview on severe plastic deformation: research status, techniques classification, microstructure evolution, and applications," *The International Journal of Advanced Manufacturing Technology*, vol. 100, pp. 1647-1694, 2019.

[107] H. Aghajani and M. Pouranvari, "A pathway to produce strong and tough martensitic stainless steels resistance spot welds," *Science and Technology of Welding and Joining*, vol. 24, pp. 185-192, 2019.

[108] D. K. Ganji and G. Rajyalakshmi, "Influence of Alloying Compositions on the Properties of Nickel-Based Superalloys: A Review," in *Recent Advances in Mechanical Engineering*, ed: Springer, 2020, pp. 537-555.

[109] H. Wang, B. Wang, Z. Wang, Y. Tian, and R. Misra, "Optimizing the low-pressure carburizing process of 16Cr3NiWMoVNbE gear steel," *Journal of Materials Science & Technology*, vol. 35, pp. 1218-1227, 2019.

[110] S. Maláková, A. Guzanová, D. Draganovská, G. Fedorko, and V. Molnár, "A case study of gear wheel material and heat treatment effect on gearbox strength calculation," *Journal of Mechanical Science and Technology*, vol. 33, pp. 5817-5827, 2019.

[111] T. Tobie, F. Hippenstiel, and H. Mohrbacher, "Optimizing gear performance by alloy modification of carburizing steels," *Metals*, vol. 7, p. 415, 2017.

[112] R. Gundlach, M. Meyer, and L. Winardi, "Influence of Mn and S on the properties of cast iron part III—testing and analysis," *International Journal of Metalcasting*, vol. 9, pp. 69-82, 2015.

[113] J. Garcia, V. C. Cipres, A. Blomqvist, and B. Kaplan, "Cemented carbide microstructures: a review," *International Journal of Refractory Metals and Hard Materials*, vol. 80, pp. 40-68, 2019.

[114] J. R. Davis, *Gear materials, properties, and manufacture*: ASM International, 2005.

[115] S. P. Radzevich, *Dudley's handbook of practical gear design and manufacture*: CRC Press, 2016.

[116] J. Jiang and Z. Fang, "High-order tooth flank correction for a helical gear on a six-axis CNC hob machine," *Mechanism and Machine Theory*, vol. 91, pp. 227-237, 2015.

[117] C. Özel, "A study on cutting errors in the tooth profiles of the spur gears manufactured in CNC milling machine," *The International Journal of Advanced Manufacturing Technology*, vol. 59, pp. 243-251, 2012.

[118] K. Kawasaki, I. Tsuji, and H. Gunbara, "Manufacturing method of double-helical gears using CNC machining center," *Proceedings of the Institution of Mechanical Engineers, Part C: Journal of Mechanical Engineering Science*, vol. 230, pp. 1149-1156, 2016.

[119] K. Gupta, N. Jain, and R. Laubscher, "Conventional and Advanced Finishing of Gears," *Advanced Gear Manufacturing and Finishing*, pp. 127-165, 2017.

[120] G. Hyatt, M. Piber, N. Chaphalkar, O. Kleinhenz, and M. Mori, "A review of new strategies for gear production," *Procedia CIRP*, vol. 14, pp. 72-76, 2014.

[121] D. T. Pham, S. S. Dimov, S. Bigot, A. Ivanov, and K. Popov, "Micro-EDM—recent developments and research issues," *Journal of materials processing technology*, vol. 149, pp. 50-57, 2004.

[122] A. Raj, B. Goswami, S. Kumar, and A. Ray, "Forge and Heat-treatments in Microalloyed Steels–A Review," *High Temperature Materials and Processes*, vol. 32, pp. 517-531, 2013.

[123] P. Jacquot, "Nitriding, Boriding and Carburizing of Steels," in *Advanced Techniques for Surface Engineering*, ed: Springer, 1992, pp. 69-82.

[124] S. Hock, J. Kleff, I. Kellermann, and M. Schulz, "Temperature—the key to optimize cost and result in carburizing vehicle driveline parts," *Proceedings of steel in cars and trucks*, pp. 245-255, 2005.

[125] P. Wei, H. Zhou, H. Liu, C. Zhu, W. Wang, and G. Deng, "Modeling of contact fatigue damage behavior of a wind turbine carburized gear considering its mechanical properties and microstructure gradients," *International Journal of Mechanical Sciences*, vol. 156, pp. 283-296, 2019.

[126] Z. Pang, S. Yu, and J. Xu, "Study of effect of quenching deformation influenced by 17CrNiMo6 gear shaft of carburization," *Physics Procedia*, vol. 50, pp. 103-112, 2013.

[127] M. A. Muraro, F. Koda, U. Reisdorfer Jr, and C. H. d. Silva, "The influence of contact stress distribution and specific film thickness on the wear of spur gears during pitting tests," *Journal of the Brazilian Society of Mechanical Sciences and Engineering*, vol. 34, pp. 135-144, 2012.

[128] S. P. Kumar, K. Suman, B. Nagaraju, and S. Ramanjaneyulu, "Contact Stress Analysis of Structural Steel Gears Under Misalignment of Shafts," in *Recent Advances in Material Sciences*, ed: Springer, 2019, pp. 283-296.

[129] E. Dehner and F. Weber, "Experience with Large, High-Speed Load Gears," *Gear Technology*, pp. 42-52, 2007.

[130] W. Musial, S. Butterfield, and B. McNiff, "Improving wind turbine gearbox reliability," National Renewable Energy Lab.(NREL), Golden, CO (United States)2007.

[131] C. Borri, P. Biagini, and E. Marino, "Large wind turbines in earthquake areas: structural analyses, design/construction & in-situ testing," in *Environmental Wind Engineering and Design of Wind Energy Structures*, ed: Springer, 2011, pp. 295-350.

[132] M. Sumida and I. Nomura, "Trend and challenge in Carburized Forged parts of Drivetrain," *JOURNAL-JAPAN SOCIETY FOR HEAT TREATMENT*, vol. 45, p. 76, 2005.

[133] M. Hiroki, M. Hideki, and Y. Ayumu, "Development of High-strength and High-wear Resistance Nitrocarburizing Steel by Precipitation Strengthening of Mo-V Carbonitride," *Honda R&D Technical Review,* vol. 24, pp. 111-119, 2012.

[134] K. Inoue and Y. Matsumura, "Influence of alloying elements on hardness distribution after nitrocarburizing in medium carbon steel," *Denki Seiko(Electric Furnace Steel),* vol. 75, pp. 11-18, 2004.

[135] N. Ishikawa, "Pitting fatigue behavior of gas nitrided spur gear (Development of high strength nitriding steel for gears-5)," *CURRENT ADVANCES IN MATERIALS AND PROCESSES,* vol. 10, pp. 474-474, 1997.

[136] T. Umeda and K. Miyabe, "Development of Manufacturing Technology for Nitriding Processes Using Nitriding Potential Control," Komatsu Technical Report, 60, 167, 2014, 17-232014.

[137] A. Mihailidis, V. Bakolas, K. Panagiotidis, K. Poulios, and C. Sachanas, "Influence of the bushing geometry on the thermohydrodynamic performance of a misaligned journal bearing," *Proceedings of the Institution of Mechanical Engineers, Part J: Journal of Engineering Tribology,* vol. 224, pp. 37-53, 2010.

[138] J. Koenig, S. Hoja, T. Tobie, F. Hoffmann, and K. Stahl, "Increasing the load carrying capacity of highly loaded gears by nitriding," in *MATEC Web of Conferences*, 2019, p. 02001.

[139] R. W. K. Honeycombe, "Steels microstructure and properties," *Metallurgy and materials science,* vol. 1, 1995.

[140] O. Mohanty, "On the stabilization of retained austenite: mechanism and kinetics," *Materials Science and Engineering: B,* vol. 32, pp. 267-278, 1995.

[141] C. Hardwick, R. Lewis, and R. Stock, "The effects of friction management materials on rail with pre existing rcf surface damage," *Wear,* vol. 384, pp. 50-60, 2017.

[142] G. Girsch and R. Heyder, "Kopfgehärtete HSH®-Schienen für den Hochgeschwindigkeitsverkehr," *Eisenbahningenieur,* vol. 54, pp. 6-15, 2003.

[143] R. Heyder and G. Girsch, "Testing of HSH® rails in high-speed tracks to minimise rail damage," *Wear,* vol. 258, pp. 1014-1021, 2005.

[144] R. Stock and R. Pippan, "RCF and wear in theory and practice—The influence of rail grade on wear and RCF," *Wear,* vol. 271, pp. 125-133, 2011.

[145] R. Stock, D. T. Eadie, D. Elvidge, and K. Oldknow, "Influencing rolling contact fatigue through top of rail friction modifier application–A full scale wheel–rail test rig study," *Wear,* vol. 271, pp. 134-142, 2011.

[146] R. Halama, R. Fajkoš, P. Matušek, P. Bábková, F. Fojtík, and L. Václavek, "Contact defects initiation in railroad wheels–Experience, experiments and modelling," *Wear,* vol. 271, pp. 174-185, 2011.

[147] E. A. Gallardo-Hernandez and R. Lewis, "Twin disc assessment of wheel/rail adhesion," *Wear,* vol. 265, pp. 1309-1316, 2008.

[148] M. Kráčalík, G. Trummer, and W. Daves, "Application of 2D finite element analysis to compare cracking behaviour in twin-disc tests and full scale wheel/rail experiments," *Wear,* vol. 346, pp. 140-147, 2016.

[149] C. Kammerhofer, A. Hohenwarter, and R. Pippan, "A novel laboratory test rig for probing the sensitivity of rail steels to RCF and wear–first experimental results," *Wear,* vol. 316, pp. 101-108, 2014.

[150] U. Olofsson and T. Telliskivi, "Wear, plastic deformation and friction of two rail steels—a full-scale test and a laboratory study," *Wear,* vol. 254, pp. 80-93, 2003.

[151] R. Lewis, E. Magel, W.-J. Wang, U. Olofsson, S. Lewis, T. Slatter, *et al.*, "Towards a standard approach for the wear testing of wheel and rail materials," *Proceedings of the Institution of Mechanical Engineers, Part F: Journal of Rail and Rapid Transit,* vol. 231, pp. 760-774, 2017.

[152] L. Buckley-Johnstone, M. Harmon, R. Lewis, C. Hardwick, and R. Stock, "A comparison of friction modifier performance using two laboratory test scales," *Proceedings of the Institution of Mechanical Engineers, Part F: Journal of Rail and Rapid Transit,* vol. 233, pp. 201-210, 2019.

[153] R. Lewis and U. Olofsson, "Mapping rail wear regimes and transitions," *Wear,* vol. 257, pp. 721-729, 2004.

[154] J. Li, J. Liang, G. Chen, and Y. Yang, "Research on Key Control Technology of Intelligent Rolling Contact Fatigue Test Facility," *Journal of Control Science and Engineering,* vol. 2020, 2020.

[155] D. Glover, "A ball-rod rolling contact fatigue tester," in *Rolling contact fatigue testing of bearing steels*, ed: ASTM International, 1982.

[156] D. I. Fletcher and J. H. Beynon, "Development of a machine for closely controlled rolling contact fatigue and wear testing," *Journal of testing and evaluation*, vol. 28, pp. 267-275, 2000.

[157] R. Dwyer-Joyce, R. Lewis, N. Gao, and D. Grieve, "Wear and fatigue of railway track caused by contamination, sanding and surface damage," 2003.

[158] W. L. Guesser, F. Koda, J. A. B. Martinez, and C. H. da Silva, "Austempered ductile iron for gears," *SAE International, Sao Paulo*, vol. 36, p. 305, 2012.

[159] R. Michalczewski, W. Piekoszewski, M. Szczerek, and J. Wulczyński, "A method for the assessment of the rolling contact fatigue of modern engineering materials in lubricated contact," *Transactions of FAMENA*, vol. 36, pp. 39-48, 2012.

[160] H. Ozturk, I. Yesilyurt, and M. Sabuncu, "Detection and advancement monitoring of distributed pitting failure in gears," *Journal of Nondestructive Evaluation*, vol. 29, pp. 63-73, 2010.

[161] W. Wang, S. Lewis, R. Lewis, A. Beagles, C. He, and Q. Liu, "The role of slip ratio in rolling contact fatigue of rail materials under wet conditions," *Wear*, vol. 376, pp. 1892-1900, 2017.

[162] P. Rycerz, A. Olver, and A. Kadiric, "Propagation of surface initiated rolling contact fatigue cracks in bearing steel," *International Journal of Fatigue*, vol. 97, pp. 29-38, 2017.

[163] D. Franklin, "Concept design and market screening of a surface fatigue test rig," ed, 2015.

[164] A. E. Desjardins, R. Proctor, G. Bai, S. McCormick, G. Shaner, G. Buechley, *et al.*, "Reduced virulence of trichothecene-nonproducing mutants of Gibberella zeae in wheat field tests," 1996.

[165] E. Lainé, A. Olver, M. Lekstrom, B. Shollock, T. Beveridge, and D. Hua, "The effect of a friction modifier additive on micropitting," *Tribology Transactions*, vol. 52, pp. 526-533, 2009.

[166] A. Oila, B. Shaw, C. Aylott, and S. Bull, "Martensite decay in micropitted gears," *Proceedings of the Institution of Mechanical Engineers, Part J: Journal of Engineering Tribology,* vol. 219, pp. 77-83, 2005.

[167] A. Oila and S. Bull, "Assessment of the factors influencing micropitting in rolling/sliding contacts," *Wear,* vol. 258, pp. 1510-1524, 2005.

[168] T. Ahlroos, H. Ronkainen, A. Helle, R. Parikka, J. Virta, and S. Varjus, "Twin disc micropitting tests," *Tribology International,* vol. 42, pp. 1460-1466, 2009.

[169] V. Moorthy and B. Shaw, "An observation on the initiation of micro-pitting damage in as-ground and coated gears during contact fatigue," *Wear,* vol. 297, pp. 878-884, 2013.

[170] F. D'Errico, "Micropitting damage mechanism on hardened and tempered, nitrided, and carburizing steels," *Materials and Manufacturing Processes,* vol. 26, pp. 7-13, 2011.

[171] H. P. Evans, R. W. Snidle, and K. Sharif, "Analysis of micro-elastohydrodynamic lubrication and surface fatigue in gear micropitting tests," in *ASME 2011 International Design Engineering Technical Conferences and Computers and Information in Engineering Conference*, 2011, pp. 585-591.

[172] M. Rackov and S. Kuzmanović, "Analysis of the most common failures of gears in universal gear reducers," *J Eng Ann Fac Eng Hunedoara,* vol. 7, pp. 67-74, 2009.

[173] C. J. Davis and M. Perea, "BuscaPalabras: A program for deriving orthographic and phonological neighborhood statistics and other psycholinguistic indices in Spanish," *Behavior Research Methods,* vol. 37, pp. 665-671, 2005.

[174] G. Fajdiga, J. Flašker, S. Glodež, and T. K. Hellen, "Numerical modelling of micro-pitting of gear teeth flanks," *Fatigue & fracture of engineering materials & structures,* vol. 26, pp. 1135-1143, 2003.

[175] K. Gopinath and M. Mayuram, "Machine Design II," *Indian Institute of Technology, Madras,* 2010.

[176] L. E. Alban, *Systematic analysis of gear failures*: ASM International, 1985.

[177] J. Halme and P. Andersson, "Rolling contact fatigue and wear fundamentals for rolling bearing diagnostics-state of the art," *Proceedings of the Institution of*

Mechanical Engineers, Part J: Journal of Engineering Tribology, vol. 224, pp. 377-393, 2010.

[178] R. W. Snidle and H. P. Evans, "Some aspects of gear tribology," *Proceedings of the Institution of Mechanical Engineers, Part C: Journal of Mechanical Engineering Science*, vol. 223, pp. 103-141, 2009.

[179] R. A. Abrahams, "The development of high strength corrosion resistant precipitation hardening cast steels," 2010.

[180] S. Hosseini, A. Zarei-Hanzaki, M. Y. Panah, and S. Yue, "ANN model for prediction of the effects of composition and process parameters on tensile strength and percent elongation of Si–Mn TRIP steels," *Materials Science and Engineering: A*, vol. 374, pp. 122-128, 2004.

[181] M. Miller, "Fatigue life prediction on nickel base superalloys," University of Southamtpon, 2007.

[182] M. Yamada, L. Yan, R. Takaku, S. Ohsaki, K. Miki, K. Kajikawa, *et al.*, "Effects of alloying elements on the hardenability, toughness and the resistance of stress corrosion cracking in 1 to 3 mass% Cr low alloy steel," *Isij International*, vol. 54, pp. 240-247, 2014.

[183] Y. Ge and K. Wang, "Influence of Microalloying Element on the Microstructure and Mechanical Properties of 34CrNiMo6 Steel for Wind Turbine Main Shaft," *Advances in Materials Science and Engineering*, vol. 2018, 2018.

[184] S. Maity and R. Kawalla, "Ultrahigh strength steel: development of mechanical properties through controlled cooling," *Heat Transfer–Engineering Applications*, pp. 309-336, 2011.

[185] M. S. Bhat, "Microstructue and mechanical properties of AISI 4340 steel modified with aluminum and silicon," California Univ., Berkeley (USA). Lawrence Berkeley Lab.1977.

[186] L. Cavaleri, P. G. Asteris, P. P. Psyllaki, M. G. Douvika, A. D. Skentou, and N. M. Vaxevanidis, "Prediction of surface treatment effects on the tribological performance of tool steels using artificial neural networks," *Applied Sciences*, vol. 9, p. 2788, 2019.

[187] P. G. Asteris, P. C. Roussis, and M. G. Douvika, "Feed-forward neural network prediction of the mechanical properties of sandcrete materials," *Sensors*, vol. 17, p. 1344, 2017.

[188] B. Denizer, "Artificial neural network analysis of the mechanical properties of tungsten fiber/bulk metallic glass matrix composites via neutron diffraction and finite element modelling," 2008.

[189] W. Grellmann, S. Seidler, and W. Hesse, "Procedure for determining the crack resistance behaviour using the instrumented Charpy impact test," in *Deformation and Fracture Behaviour of Polymers*, ed: Springer, 2001, pp. 71-86.

[190] S. Li and A. Kahraman, "A fatigue model for contacts under mixed elastohydrodynamic lubrication condition," *International Journal of Fatigue*, vol. 33, pp. 427-436, 2011.

[191] T. Bergs, U. Tombul, D. Mevissen, A. Klink, and J. Brimmers, "Load Capacity of Rolling Contacts Manufactured by Wire EDM Turning," *Procedia CIRP*, vol. 87, pp. 474-479, 2020.

[192] D. T. Redda, T. Nakanishi, and G. Deng, "Surface Durability of Developed Cr-Mo-Si Steel under Rolling-Sliding Contact," *Journal of Advanced Mechanical Design, Systems, and Manufacturing*, vol. 2, pp. 214-221, 2008.

[193] J. Keller, R. Olson, and M. Michaud, "Case Study of ISO/TS 6336-22 Micropitting Method," National Renewable Energy Lab.(NREL), Golden, CO (United States)2020.

[194] B. Standard and B. ISO, "Calculation of load capacity of spur and helical gears—," *ISO*, vol. 6336, p. 1996, 2006.

[195] C. Wilkinson and A. Olver, "The durability of gear and disc specimens—part i: The effect of some novel materials and surface treatments," *Tribology transactions*, vol. 42, pp. 503-510, 1999.

[196] C. Wilkinson and A. Olver, "The Durability of Gear and Disc Specimens—Part II: Post Failure Examination and Gear-Disc Correlation," *Tribology transactions*, vol. 42, pp. 610-618, 1999.

[197] G. Niemman and H. Winter, "Maschinenelemente Band II Getriebe allgemein, Zahnradgetriebe-Grundlagen, Stirnradgetriebe," ed: Springer-Verlag, 1985.

[198] L. Flamand, D. Berthe, and M. Godet, "Simulation of Hertzian contacts found in spur gears with a high performance disk machine," 1981.

[199] J. Kleemola and A. Lehtovaara, "Experimental simulation of gear contact along the line of action," *Tribology International,* vol. 42, pp. 1453-1459, 2009.

[200] N. Gao, R. Dwyer-Joyce, and D. Grieve, "Disc machine testing to assess the life of surface-damaged railway track," *Proceedings of the Institution of Mechanical Engineers, Part F: Journal of Rail and Rapid Transit,* vol. 215, pp. 261-275, 2001.

[201] M. Le, F. Ville, X. Kleber, J.-Y. Buffière, J. Cavoret, M.-C. Sainte-Catherine, *et al.*, "Rolling contact fatigue crack propagation in nitrided alloyed steels," *Proceedings of the Institution of Mechanical Engineers, Part J: Journal of Engineering Tribology,* vol. 231, pp. 1192-1208, 2017.

[202] J. A. Brandao, R. Martins, J. H. Seabra, and M. J. Castro, "Surface damage prediction during an FZG gear micropitting test," *Proceedings of the Institution of Mechanical Engineers, Part J: Journal of Engineering Tribology,* vol. 226, pp. 1051-1073, 2012.

[203] P. Rabaso, T. Gauthier, M. Diaby, and F. Ville, "Rolling contact fatigue: experimental study of the influence of sliding, load, and material properties on the resistance to micropitting of steel discs," *Tribology transactions,* vol. 56, pp. 203-214, 2013.

[204] A. Terrin and G. Meneghetti, "A comparison of rolling contact fatigue behaviour of 17NiCrMo6-4 case-hardened disc specimens and gears," *Fatigue & Fracture of Engineering Materials & Structures,* vol. 41, pp. 2321-2337, 2018.

[205] Y. Chen, C. He, X. Zhao, L. Shi, Q. Liu, and W. Wang, "The influence of wheel flats formed from different braking conditions on rolling contact fatigue of railway wheel," *Engineering Failure Analysis,* vol. 93, pp. 183-199, 2018.

[206] J. Santa, P. Cuervo, P. Christoforou, M. Harmon, A. Beagles, A. Toro, *et al.*, "Twin disc assessment of wear regime transitions and rolling contact fatigue in R400HT–E8 pairs," *Wear,* vol. 432, p. 102916, 2019.

[207] P. Liu, Y. Quan, J. Wan, and L. Yu, "Experimental Investigation on the Wear and Damage Characteristics of Machined Wheel/Rail Materials under Dry Rolling-Sliding Condition," *Metals,* vol. 10, p. 472, 2020.

[208] I. A. B. A. Aziz, D. M. N. B. D. Idris, M. H. A. B. Hassan, and M. F. B. Basrawi, "Finite element analysis of impact energy on spur gear," in *MATEC Web of Conferences*, 2018, p. 06011.

[209] J. Krawczyk, J. Pacyna, and P. Bała, "Fracture toughness of steels with nickel content in respect of carbide morphology," *Materials Science and Technology*, vol. 31, pp. 795-802, 2015.

[210] C. Sidoroff, M. Perez, P. Dierickx, and D. Girodin, "Advantages and shortcomings of retained austenite in bearing steels: a review," in *Bearing Steel Technologies: 10th Volume, Advances in Steel Technologies for Rolling Bearings*, ed: ASTM International, 2015.

[211] S. Beermann, "Reliability, Lifetime and Safety Factors."

[212] M. Rameshkumar, G. Venkatesan, and P. Sivakumar, "Finite Element Analysis of High Contact Ratio Gear," *AGMA Technical Paper, 10FTM06*, 2010.

[213] Y.-R. Jeng, Z.-W. Lin, and S.-H. Shyu, "Changes of surface topography during running-in process," *J. Trib.*, vol. 126, pp. 620-625, 2004.

[214] S. Roy, G. T. C. Ooi, and S. Sundararajan, "Effect of retained austenite on micropitting behavior of carburized AISI 8620 steel under boundary lubrication," *Materialia*, vol. 3, pp. 192-201, 2018.

[215] S. Roy, D. White, and S. Sundararajan, "Correlation between evolution of surface roughness parameters and micropitting of carburized steel under boundary lubrication condition," *Surface and Coatings Technology*, vol. 350, pp. 445-452, 2018.

APPendix

Appendix A: Input data

Table A1:Input data set (chemical composition and heat treatment condition) of alloy steels

Name of alloy	Chemical composition mass (%)											Austenite Temp. (°C)	Tempering Temp. (°C)
	C	P	S	Si	Mn	Cr	Ni	Mo	Al	cu	Fe		
AISI 4340	0.39	0.007	0.003	0.2	0.74	0.81	1.81	0.25	0	0.18	95.61	900.00	AQ
	0.39	0.007	0.003	0.2	0.74	0.81	1.81	0.25	0	0.18	95.61	900.00	250.00
	0.39	0.007	0.003	0.2	0.74	0.81	1.81	0.25	0	0.18	95.61	900.00	300.00
	0.39	0.007	0.003	0.2	0.74	0.81	1.81	0.25	0	0.18	95.61	900.00	400.00
	0.39	0.007	0.003	0.2	0.74	0.81	1.81	0.25	0	0.18	95.61	900.00	500.00
AISI 4340+Al	0.38	0.007	0.003	0	0.74	0.81	1.81	0.25	0.98	0.18	94.84	900.00	AQ
	0.38	0.007	0.003	0	0.74	0.81	1.81	0.25	0.98	0.18	94.84	900.00	250.00
	0.38	0.007	0.003	0	0.74	0.81	1.81	0.25	0.98	0.18	94.84	900.00	300.00
	0.38	0.007	0.003	0	0.74	0.81	1.81	0.25	0.98	0.18	94.84	900.00	350.00
	0.38	0.007	0.003	0	0.74	0.81	1.81	0.25	0.98	0.18	94.84	900.00	400.00
AISI 4340+2Al	0.37	0.007	0.003	0	0.74	0.81	1.81	0.25	1.95	0.18	93.88	900.00	AQ
	0.37	0.007	0.003	0	0.74	0.81	1.81	0.25	1.95	0.18	93.88	900.00	250.00
	0.37	0.007	0.003	0	0.74	0.81	1.81	0.25	1.95	0.18	93.88	900.00	325.00
	0.37	0.007	0.003	0	0.74	0.81	1.81	0.25	1.95	0.18	93.88	900.00	375.00
	0.37	0.007	0.003	0	0.74	0.81	1.81	0.25	1.95	0.18	93.88	900.00	400.00
AISI 4340+3Al	0.41	0.007	0.003	0	0.74	0.81	1.81	0.25	2.89	0.18	92.9	1100.0	AQ
	0.41	0.007	0.003	0	0.74	0.81	1.81	0.25	2.89	0.18	92.9	1100.0	300.00
	0.41	0.007	0.003	0	0.74	0.81	1.81	0.25	2.89	0.18	92.9	1100.0	350.00
	0.41	0.007	0.003	0	0.74	0.81	1.81	0.25	2.89	0.18	92.9	1100.0	400.00
	0.41	0.007	0.003	0	0.74	0.81	1.81	0.25	2.89	0.18	92.9	1100.0	450.00
AISI 4340+0.5Al+0.5 Si	0.4	0.007	0.003	0.6	0.74	0.81	1.81	0.25	0.51	0.18	94.63	900.00	AQ
	0.4	0.007	0.003	0.6	0.74	0.81	1.81	0.25	0.51	0.18	94.63	900.00	250.00

	0.4	0.007	0.003	0.6	0.74	0.81	1.81	0.25	0.51	0.18	94.63	900.00	300.00
	0.4	0.007	0.003	0.6	0.74	0.81	1.81	0.25	0.51	0.18	94.63	900.00	350.00
	0.4	0.007	0.003	0.6	0.74	0.81	1.81	0.25	0.51	0.18	94.63	900.0	400.0
AISI 4340+Al+ Si	0.39	0.007	0.003	1.1	0.74	0.81	1.81	0.25	1.00	0.18	93.66	900.0	AQ
	0.39	0.007	0.003	1.1	0.74	0.81	1.81	0.25	1.00	0.18	93.66	900.0	250.0
	0.39	0.007	0.003	1.1	0.74	0.81	1.81	0.25	1.00	0.18	93.66	900.0	300.00
	0.39	0.007	0.003	1.1	0.74	0.81	1.81	0.25	1.00	0.18	93.66	900.0	350.0
	0.39	0.007	0.003	1.1	0.74	0.81	1.81	0.25	1.00	0.18	93.66	900.0	400.0
AISI 4340+1.5Al+1.5 Si	0.39	0.007	0.003	1.6	0.74	0.81	1.81	0.25	1.51	0.18	92.66	950.0	AQ
	0.39	0.007	0.003	1.6	0.74	0.81	1.81	0.25	1.51	0.18	92.66	950.0	250.0
	0.39	0.007	0.003	1.6	0.74	0.81	1.81	0.25	1.51	0.18	92.66	950.0	300.0
	0.39	0.007	0.003	1.6	0.74	0.81	1.81	0.25	1.51	0.18	92.66	950.0	350.0
	0.39	0.007	0.003	1.6	0.74	0.81	1.81	0.25	1.51	0.18	92.66	950.0	400.0
	0.39	0.007	0.003	1.6	0.74	0.81	1.81	0.25	1.51	0.18	92.66	950.0	450.0
	0.39	0.007	0.003	1.6	0.74	0.81	1.81	0.25	1.51	0.18	92.66	950.0	500.0
	0.39	0.007	0.003	1.6	0.74	0.81	1.81	0.25	1.51	0.18	92.66	1000.	AQ
	0.39	0.007	0.003	1.6	0.74	0.81	1.81	0.25	1.51	0.18	92.66	1000.	300.0
	0.39	0.007	0.003	1.6	0.74	0.81	1.81	0.25	1.51	0.18	92.66	1000.	350.0
	0.39	0.007	0.003	1.6	0.74	0.81	1.81	0.25	1.51	0.18	92.66	1000.	400.0
	0.39	0.007	0.003	1.6	0.74	0.81	1.81	0.25	1.51	0.18	92.66	1000.	450.0
AISI 4340+2Al+2Si	0.39	0.007	0.003	2.1	0.74	0.81	1.81	0.25	1.97	0.18	91.74	1100.0	AQ
	0.39	0.007	0.003	2.1	0.74	0.81	1.81	0.25	1.97	0.18	91.74	1100.0	300.00
	0.39	0.007	0.003	2.1	0.74	0.81	1.81	0.25	1.97	0.18	91.74	1100.0	350.00
	0.39	0.007	0.003	2.1	0.74	0.81	1.81	0.25	1.97	0.18	91.74	1100.0	400.00
	0.39	0.007	0.003	2.1	0.74	0.81	1.81	0.25	1.97	0.18	91.74	1100.0	450.00
	0.39	0.007	0.003	2.1	0.74	0.81	1.81	0.25	1.97	0.18	91.74	1100.0	500.00
AISI 4340+Si	0.37	0.007	0.003	1.1	0.74	0.81	1.81	0.25	0	0.18	94.7	900.00	AQ

	0.37	0.007	0.003	1.1	0.74	0.81	1.81	0.25	0	0.18	94.7	900.00	250.00
	0.37	0.007	0.003	1.1	0.74	0.81	1.81	0.25	0	0.18	94.7	900.00	300.00
	0.37	0.007	0.003	1.1	0.74	0.81	1.81	0.25	0	0.18	94.7	900.00	350.00
	0.37	0.007	0.003	1.1	0.74	0.81	1.81	0.25	0	0.18	94.7	900.00	400.00
AISI 4340+2Si	0.37	0.007	0.003	2.1	0.74	0.81	1.81	0.25	0	0.18	93.72	900.00	AQ
	0.37	0.007	0.003	2.1	0.74	0.81	1.81	0.25	0	0.18	93.72	900.00	250.00
	0.37	0.007	0.003	2.1	0.74	0.81	1.81	0.25	0	0.18	93.72	900.00	300.00
	0.37	0.007	0.003	2.1	0.74	0.81	1.81	0.25	0	0.18	93.72	900.00	350.00
	0.37	0.007	0.003	2.1	0.74	0.81	1.81	0.25	0	0.18	93.72	900.00	400.00
AISI 4340+3Si	0.38	0.007	0.003	3.1	0.74	0.81	1.81	0.25	0	0.18	92.67	950.00	AQ
	0.38	0.007	0.003	3.1	0.74	0.81	1.81	0.25	0	0.18	92.67	950.00	250.00
	0.38	0.007	0.003	3.1	0.74	0.81	1.81	0.25	0	0.18	92.67	950.00	300.00
	0.38	0.007	0.003	3.1	0.74	0.81	1.81	0.25	0	0.18	92.67	950.00	350.00
	0.38	0.007	0.003	3.1	0.74	0.81	1.81	0.25	0	0.18	92.67	950.00	400.00
AISI 4330 +2Si	0.29	0.012	0.003	2.1	0.89	0.83	1.85	0.24	0.06	0	93.68	900.00	AQ
	0.29	0.012	0.003	2.1	0.89	0.83	1.85	0.24	0.06	0	93.68	900.00	250.00
	0.29	0.012	0.003	2.1	0.89	0.83	1.85	0.24	0.06	0	93.68	900.00	300.00
	0.29	0.012	0.003	2.1	0.89	0.83	1.85	0.24	0.06	0	93.68	900.00	350.00
	0.29	0.012	0.003	2.1	0.89	0.83	1.85	0.24	0.06	0	93.68	900.00	400.00
AISI 4140	0.39	0.010	0.021	0.2	0.73	1.06	0.13	0.176	0	0.13	97.14	900.00	AQ
	0.39	0.010	0.021	0.2	0.73	1.06	0.13	0.176	0	0.13	97.14	900.00	250.00
	0.39	0.010	0.021	0.2	0.73	1.06	0.13	0.176	0	0.13	97.14	900.00	300.00
	0.39	0.010	0.021	0.2	0.73	1.06	0.13	0.176	0	0.13	97.14	900.00	350.00
	0.39	0.010	0.021	0.2	0.73	1.06	0.13	0.176	0	0.13	97.14	900.00	400.00
34CrNiMo6	0.35	0.012	0.002	0.2	0.77	1.59	1.54	0.25	0	0.07	95.16	900.00	AQ
	0.35	0.012	0.002	0.2	0.77	1.59	1.54	0.25	0	0.07	95.16	900.00	250.00
	0.35	0.012	0.002	0.2	0.77	1.59	1.54	0.25	0	0.07	95.16	900.00	300.00

	0.35	0.012	0.002	0.2	0.77	1.59	1.54	0.25	0	0.07	95.16	900.00	350.00
	0.35	0.012	0.002	0.2	0.77	1.59	1.54	0.25	0	0.07	95.16	900.00	400.00
34CrNiMo6+0.02Al	0.35	0.005	0.001	0.2	0.75	1.58	1.55	0.23	0.02	0.06	95.19	900.00	AQ
	0.35	0.005	0.001	0.2	0.75	1.58	1.55	0.23	0.02	0.06	95.19	900.00	250.00
	0.35	0.005	0.001	0.2	0.75	1.58	1.55	0.23	0.02	0.06	95.19	900.00	300.00
	0.35	0.005	0.001	0.2	0.75	1.58	1.55	0.23	0.02	0.06	95.19	900.00	350.00
	0.35	0.005	0.001	0.2	0.75	1.58	1.55	0.23	0.02	0.06	95.19	900.00	400.00
30C-Cr-Mo	0.28	0.031	0.011	0.2	1	4.2	0	1.01	0.06	0	93.16	975.00	AQ
	0.28	0.031	0.011	0.2	1	4.2	0	1.01	0.06	0	93.16	975.00	205.00
	0.28	0.031	0.011	0.2	1	4.2	0	1.01	0.06	0	93.16	975.00	425.00
30CrMo+1Ni	0.28	0.038	0.011	0.2	0.91	4.5	1.07	0.97	0.05	0	91.97	930.00	AQ
	0.28	0.038	0.011	0.2	0.91	4.5	1.07	0.97	0.05	0	91.97	930.00	205.00
	0.28	0.038	0.011	0.2	0.91	4.5	1.07	0.97	0.05	0	91.97	930.00	445.00
30CrMo+2Ni	0.28	0.034	0.01	0.3	0.86	4.1	1.97	1.37	0.03	0	91.06	930.00	AQ
	0.28	0.034	0.01	0.3	0.86	4.1	1.97	1.37	0.03	0	91.06	930.00	205.00
	0.28	0.034	0.01	0.3	0.86	4.1	1.97	1.37	0.03	0	91.06	930.00	445.00
30CrMo +3.2 Ni	0.30	0.04	0.008	0.2	1.2	4.6	3.29	0.94	0.11	0	89.32	930.00	AQ
	0.30	0.04	0.008	0.2	1.2	4.6	3.29	0.94	0.11	0	89.32	930.00	205.00
	0.30	0.04	0.008	0.2	1.2	4.6	3.29	0.94	0.11	0	89.32	930.00	445.00

Table A2: Output data set (mechanical properties) of alloy steels

Name	YS (MPa)	UTS (MPa)	% Total Elongation	Fracture toughness	impact toughness (J)	% Retained austenite	Hardness (HRC)
AISI 4340	1420.00	2214.00	8.00	30.00	30.00	4.60	56.00
	1550.00	1825.00	7.80	65.00	31.00	1.20	51.50
	1510.00	1650.00	7.00	64.00	28.00	0.80	49.70
	1420.00	1580.00	9.00	61.00	26.00	0.80	48.00
	1237.00	1425.00	6.00	72.00	24.00	0.80	45.30
AISI 4340+Al	1405.56	1970.54	5.90	73.40	25.00	2.50	53.60
	1515.80	1777.62	5.30	85.16	24.80	3.80	51.00
	1446.90	1688.05	5.30	79.56	24.20	1.20	49.70
	1364.22	1591.59	5.30	81.00	23.00	0.20	48.00
	1267.76	1467.57	6.00	87.00	22.40	0.20	46.10

AISI 4340+2Al	1412.45	1722.50	5.60	60.44	24.75	1.20	54.00
	1529.58	1805.18	5.40	88.68	25.84	2.40	51.50
	1557.14	1798.29	5.50	82.41	22.98	0.80	51.25
	1564.03	1750.06	5.30	80.22	23.66	0.70	50.70
	1502.02	1674.27	4.80	81.50	22.98	0.20	50.00
AISI 4340+3Al	1474.64	1722.20	4.50	69.34	16.18	2.80	55.20
	1584.70	1818.96	5.90	89.23	14.96	2.60	53.50
	1591.59	1770.73	5.50	87.03	15.23	2.20	52.80
	1605.37	1791.40	5.00	92.19	15.10	2.20	52.20
	1508.89	1681.16	5.00	87.03	11.28	2.20	50.20
AISI	1570.92	2115.23	5.70	63.73	24.48	1.80	53.50
4340+0.5Al+0.5 Si	1605.37	1867.19	6.00	87.91	27.20	3.60	51.00
	1598.49	1846.52	5.80	87.91	30.46	1.04	50.25
	1567.03	1784.51	6.00	81.32	23.80	0.97	51.30
	1426.23	1626.04	6.80	89.01	18.08	0.97	50.75
AISI 4340+Al+ Si	1502.02	2094.56	6.00	47.25	25.00	0.50	55.50
	1605.37	1901.64	6.30	91.21	26.10	2.60	53.00
	1577.81	1853.41	5.90	89.01	22.00	2.90	52.50
	1591.59	1818.96	5.80	89.01	21.00	1.90	52.00
	1550.25	1722.50	5.60	90.10	19.00	1.10	51.00
AISI	1577.81	2191.02	9.80	45.82	24.50	2.60	56.50
4340+1.5Al+1.5 Si	1681.16	1977.43	11.60	80.55	25.70	2.20	54.00
	1688.05	1970.54	11.00	88.24	22.00	1.84	53.20
	1722.50	1984.32	11.30	79.89	21.00	1.70	53.00
	1708.72	1894.75	11.10	80.55	19.00	1.40	53.10
	1543.36	1736.28	9.00	81.50	18.00	1.20	50.75
	1426.23	1598.48	10.00	82.00	18.00	0.30	47.50
	1605.37	2039.44	11.00	46.48	17.13	2.60	53.30
	1632.93	1922.31	11.20	90.66	21.89	2.40	51.80
	1653.60	1874.08	12.00	81.54	31.68	2.04	51.40
	1605.37	1818.96	11.00	77.47	21.08	1.80	51.10
	1529.58	1729.39	9.80	59.34	14.42	1.40	49.30
AISI 4340+2Al+2Si	1584.70	2135.90	2.70	37.14	30.00	0.20	56.50
	1722.50	1998.10	4.40	89.34	32.00	1.40	54.00
	1736.28	1991.21	4.40	86.37	28.00	1.60	53.70
	1791.40	1984.32	4.50	81.54	27.40	1.80	54.40
	1715.61	1880.97	5.00	65.93	24.00	1.80	52.50
	1543.36	1708.72	5.00	75.00	21.50	0.70	50.00
AISI 4340+Si	1584.70	2073.89	6.20	78.57	30.60	0.80	53.40
	1619.15	1929.20	5.50	86.92	33.05	2.10	50.80
	1605.37	1867.19	5.40	77.25	29.40	2.40	45.30
	1557.14	1791.40	5.70	79.23	28.42	1.80	47.00
	1433.12	1612.26	5.70	66.15	23.26	0.90	46.00
AISI 4340+2Si	1763.84	2342.60	6.30	62.20	24.75	0.50	56.50
	1770.73	2115.23	5.90	82.19	27.06	1.60	53.30

	1694.94	2004.99	5.60	88.35	27.47	1.65	46.70
	1756.95	1991.21	5.20	88.24	31.00	1.57	47.20
	1694.94	1874.08	4.50	63.51	28.15	1.15	47.20
AISI 4340+3Si	1880.97	2411.50	5.80	43.95	19.04	0.40	53.00
	1860.30	2197.91	5.60	82.63	28.67	1.20	51.10
	1777.62	2101.45	5.40	89.67	28.67	1.25	48.00
	1818.96	2060.11	3.50	82.52	25.97	1.10	49.70
	1825.85	2018.77	4.80	86.15	24.88	0.75	48.00
AISI 4330 +2Si	957.71	1550.939	5.00	97.487	21.00	3.6	52.5
	985.27	1490.307	12.00	98.4	22.00	3.3	49.3
	1209.2	1482.039	11.00	81.478	20.00	2.4	46.7
	1208.00	1423.474	12.00	70.017	23.00	2	47.2
	1214.00	1420.718	15.00	73.74	25.00	2	46.2
AISI 4140	1100.00	1200.00	5.30	27.23	24.00	3.1	49.00
	1080.00	1195.12	5.10	36	28.00	2.4	48.00
	1074.30	1193.20	7.50	38	30.00	2.6	47.00
	1072.50	1192.40	8.10	40.5	35.00	4.3	47.00
	1074.60	1191.20	9.80	46	37.00	4.4	47.00
34CrNiMo6	960.00	1080.00	15.00	42	27.00	3.3	53.00
	958.00	1083.00	16.00	51.3	28.00	2.8	47.00
	954.00	1076.00	14.00	52.1	26.70	2.5	47.00
	956.00	1078.00	13.00	46	29.00	2.4	49.50
	961.00	1079.00	16.00	49	28.40	2.7	48.00
34CrNiMo6+0.02Al	1100.00	1180.00	18.00	44	28.00	3.1	48.00
	1098.00	1181.00	18.20	49	29.00	3.3	47.00
	1084.00	1179.00	17.00	52.3	29.60	2.2	49.00
	1092.00	1168.00	16.80	53	28.00	2.4	47.00
	1091.40	1175.00	19.10	54.5	28.70	2.1	46.00
30C-Cr-Mo	1450.00	1660.00	11.20	57.9	21.50	2.2	53.00
	1270.00	1340.00	11.50	59.2	19.80	2.27	51.00
	987.67	1167.00	12.50	57.3	22.10	2.24	49.00
30CrMo+1Ni	1500.00	1670.00	9.50	58.4	22.40	2.8	54.70
	1320.00	1343.00	9.70	60.1	21.60	2.98	51.70
	1032.00	1172.00	10.10	56.8	23.10	2.7	49.50
30CMo+2Ni	1506.00	1712.00	12.60	59.8	22.80	2.6	56.20
	1332.00	1380.00	12.70	60.9	21.70	2.7	53.10
	1041.00	1198.00	12.90	57.3	24.30	2.55	49.80
30Cr-Mo +3.2 Ni	1542.00	1758.00	9.60	55.6	21.90	2.4	57.40
	1341.00	1397.00	9.80	57.1	19.90	2.48	53.40
	1064.00	1206.00	10.20	55.2	21.20	2.31	50.10

Appendix B: Helical Gear Sizing Matlab Function

```
  %%%%% given parameters %%%%%%
T=75;           % input torque (Nm)
L=500;          % life (hrs)
N1=10,000;      % maximum speed (rpm) of pinion
Rt=0.32;        % wheel radius (m)
Vmax=37.5;      % top speed (m/s)
Ig= pi*N1*Rt/(30*Vmax);     % Total gear ratio
Z1= 22;        % number of teeth of pinion
Z2= 65;        % number of teeth of gear
i= Z2/Z1;       % first stage gear ratio
psi = deg2rad(psi_deg);           % helix angle(angle)
psi = deg2rad(14:2:30);           % angle
phi = deg2rad(22);                % pressure angle (angle)
phi_t = atan(tan(phi)/cos(psi)); % Transverse pressure angle (angle)
phi_r = acos((db1 + Db2)/2*c); % Operating Transverse pressure angle
(angle)
d= Z1/cos (psi);     % pitch diameter of pinion (mm)
D=Z2/ cos (psi);          % pitch diameter of gear (mm)
db1 = d*cos (phi_t);   % base diameter of pinion
Db2 = D*cos (phi_t);     % Base diameter of gear
mn = d*cos(psi)/Z1;       % normal module
mt = mn/cos(psi);        % transverse module
px= pi*mn/(sin(psi));      % axial pitch (mm)
pn= pi*mn*cos(phi);          % normal base pitch (mm)
pb= pi*db1/z1;                %transverse base pitch (mm)
pd=1/mn;                      % diameteral pitch pitch
Ft = 2*T/d;         % tangential force (N)
da1= d+2*mn;        % addendum diameter of gear (mm)
```

```
Da2 = D+2*mn;       % addendum diameter of pinion (mm)

C= (d+D)/2         % operating center distance (mm)

%% Correction Factors

Ko = 1.25;           % Application Factor for inconsistent loads

KB = 1;             % Rim Thickness Factor*

YZ = 1;             % Reliability Factor: 99.9% Reliablity Rating

KS = 1;             % Size Factor

YT = 1;             % Temperature Factor

ZR=1;               % surface condition fuctor

A=1;                 %  mesh accuracy

%% Material Property (case hardened Nitrided)
St_p =450;      % AGM bending strength for pinion (MPa)

Sc_p =1500;     % AGMA contact strength for pinion (MPa)

nu_p =0.3;          % poisnios ratio for pinion

E_p =206000;       %modulus of elasticity (MPa)

rho_den_p=7850;       % density for pinion  (kg/m^3)

BH_p= 650          % brill hardness for pinion

St_g =450;      % AGMA bending strength for gear (MPa)

Sc_g =1500;      % AGMA contact stregth for gear(MPa)

nu_g =0.3;       % poisnios ratio for gear

E_g =206000;      %modulus of elasticity (MPa)

rho_den_g=7850;    % density for gear  (kg/m^3)

BH_g= 650;           % brill hardness for gear

q=1;                % number of contacts assembly per revolution

%% Bending Life Factor YN
N_cycles = 60*L*N1*q;       % Number of Cycles - Pinion
N_cycles_g = N_cycles / i;
if N_cycles <= 10^3
YN = 3.5;
elseif N_cycles <= 1.2E6;
YN = 9.4518*(N_cycles^-0.148);
Else
```

```
YN = 1.3558*(N_cycles^-0.0178);
End
if N_cycles_g <= 10^3
YN_g = 3.5;
elseif N_cycles_g <= 1.2E6;
YN_g = 9.4518*(N_cycles_g^-0.148);
Else
YN_g = 1.3558*(N_cycles_g^-0.0178);
end
%% Surface Life Factor ZN
if N_cycles <=10^4      % Number of Cycles - Pinion
ZN = 2.466;
elseif N_cycles <=10^7
ZN = 2.466*(N_cycles^-0.056);
else
ZN = 1.4488*(N_cycles^-0.023);
end
if N_cycles_g <=10^4   % Number of Cycles -gear
ZN_g = 2.466;
elseif N_cycles_g <=10^7
ZN_g = 2.466*(N_cycles_g^-0.056);
else
ZN_g = 1.4488*(N_cycles_g^-0.023);

end

%% Hardness Ratio Factor ZW
BH_ratio = BH_p/BH_g;      % Brinell hardness ratio for Pinion and gear
if BH_ratio < 1.2
A_BH = 0;
elseif BH_ratio > 1.7
A_BH = 0.00698;
else
A_BH = 0.00898*BH_ratio - 0.00829;

end

ZW = 1 + A_BH*(i - 1); % Hardness Ratio Factor

%% Working Stresses

Sab_p = St_p*YN*/ (YT*YZ);% allowable bending stress for pinion (MPa)

Sab_g = St_g* YN_g/ (YT*YZ);   % allowable bending stress for gear (MPa)

Sac_p = Sc_p*ZW*ZN/ (YT*YZ);     % allowable contact stress for pinion
(MPa)

Sac_g = Sc_g*ZW_g*ZN_g/ (YT*YZ);   % allowable contact stress for gear
(MPa)

Sac = min (Sac_p, Sac_g);
```

```
%% AGMA Geometry Factor for Bending

if psi ~= 0
[J_s_p, J_s_g] = Geo_factor (psi_deg,'spur');

z1_low = J_s_p(1,2);

else z1_low = 21;

end
%% Initializing Arrays
b_array = linspace(14,28,15); % Face width array
teeth_p = H_ratio(mg, z1_low); % Pinion teeth for Hunting ratio
th = length(teeth_p);
Sb_p = zeros (th, 15);
Sb_g = zeros (th, 15);
Sc = zeros (th, 15);
z1 = zeros(th,1);
z2 = zeros(th,1);
khpm = 1.1;      % Pinion proportion modifier

khe=1.0;         % Mesh alignment correction factor = 1

khmc= 0.8;       % Lead Correction factor for properly modified

khmt=1.0;          % Transverse load distribution factor

% Mesh alignment empirical constants for precision enclosed gears

A_b=0.0675;         % empirical constants

B_b=0.0128;            % empirical constants

C_b=-0.0000926;       % empirical constants

Q_v = 8; % Gear Quality Rating

if psi ~= 0

psi_b = acos(pn/pb); % Base helix angle

psi_r = atan(atan(psi_b)/cos(phi_r)); % Operating helix angle

else
psi_b=0;
psi_r=0;
end

phi_nr = asin(cos(psi_b)*sin(phi_r)); % Operating normal pressure angle

C6 = C*sin(phi_r); % distances along line of action  mm

d=R_p*2;
D= R_g*2;
```

```
Ro_p = z1 (i)/Pd/2/cos (psi);        % Outside radius mm
Ro_g = z2 (i)/Pd/2/cos (psi);        % Outside radius mm

phi_o_p = acos(Rb_p/Ro_p);   % Tip pressure angles

phi_o_g = acos(Rb_g/Ro_g); % Tip pressure angles degrees

C1 = C6-sqrt(Ro_g^2-Rb_g^2); % SAP mm

C3 = C6/(ig); % Operating pitch point mm

C4 = C1 + pb;   % HPSTC mm

C5 = sqrt(Ro_p^2 - Rb_p^2); % EAP mm

C2 = C5 - pb;    % LPSTC mm

Z = C5 - C1; % Length of line of contact mm

mp = Z/pb; % Transverse contact ratio

if psi == 0
mF = 0;   % Axial contact ratio

else
px = pi/sin(psi)/Pd; % Axial pitch

mF = b/px; % Axial contact ratio

end
if mp > 2
disp('error in mp')
end
nr = mp - floor(mp); % Fractional part of transverse contact ratio

na = mF - floor(mF); % Fractional part of MF

Fe = b;

if psi == 0 && mp<2

Lmin = Fe; % Minimum length of lines of contact

elseif      psi      >      0      &&      na      <      =      (1-nr)
Lmin=(mp*Fe-na*nr*px)/cos(psi_b);
else
Lmin=(+mp*Fe-(1-na)*(1-nr)*px)/cos(psi_b);
end

Rm1 = 0.5*(min(Ro_p,Ro_g)+ (C - max(Ro_p,Ro_g))); % Mean radius of pinion

do_p = 2*C/(i+1); % Operating pitch diameter

% -----Geometry factors -----
```

```
if                                                                  psi==0;
J_p=J_spur(Pd,z1(i),z2(i),1,1);
J_g = J_spur(Pd, z1(i), z2(i), 1, 1);

else

J_p=interp2(J_s_p(1,:),J_s_p(:,1),J_s_p,z1(i),  z2(i));    % interpolate
from a table

J_g=interp2(J_s_g(1,:),J_s_g(:,1),J_s_g,  z1(i),  z2(i)); % interpolate
from a table

End

% ------- Dynamic factor (Kv) ---------

v=pi*d*N1/ (60000);   % pitch line velocity (rad/s)

B=0.25*(12-Q_v)^0.667;
A = 50 + 56*(1-B);

Kv = ((A+sqrt (200*v))/A) ^B; % Dynamic Factor

Cv = Kv; % Dynamic Factor

for j = 1: 12
b = b_array(j)*mn; % Face width ranges from 10mn to 20mn

% ---- Load distribution factor KH (b in mm) -----

if b <= 25

Khpf (1) = b/(10*d) - 0.025; % Pinion proportion factor

Khpf   (2)   =   b/(10*d)   -   0.025;   %   gear   proportion   factor
elseif                                                        b>25&&b<=432
Khpf      (1)      =      b/(10*d)      -      0.0375      +0.000492*b;
Khpf      (2)      =      b/(10*d)      -      0.0375      +0.000492*b;
else
Khpf    (1)    =    b/(10*d)    -    0.1109+0.000815*b-0.000000353*b^2;
Khpf (2) = b/(10*d) - 0.1109+0.000815*b-0.000000353*b^2;
end
khma = A_b + B_b*b + C_b*b^2; % Mesh alignment factor

KH = 1 + khmc*(khpf*khpm + khma*khe); % Face load distribution factor

Km = khmt*khmf;

Cm = max(Km);

%% ////// AGMA Bending Stress  and factor of safety Calculations //////

Sb_p(i,j)=Ft*(1/(b*J_p*mt))*Ko*KH*Ks*(KB_p)*Kv;
Sb_g(i,j) = Ft*(1/(b*mt*J_g)) *Ko*KH*Ks*(KB_g)*Kv;
```

```
SF_p=Sab_p/(Sb_p(i,j)); % bending stress factor of safety for pinion

SF_g=Sab_g/(Sb_g(i,j));  % bending stress factor of safety for pinion

%% ////// AGMA Contact Stress Calculations //////
ZE    =    sqrt(1/(pi*(((1-nu_p^2)/E_p)+((1-nu_g^2)/E_g))));    Elastic
coefficient for difference in p,g material

ifpsi==0;
rho_p=C2;
mnp=1;
elseifmF>1
rho_p=sqrt(Rm1^2-min(Rb_p,Rb_g)^2);
rho_p_2=sqrt((0.5*((dp_p/2+a_p)+(dp_p/2-a_g)))^2-(dp_p/2*cos(phi))^2);
mnp = b/Lmin;
end
% ----- Radius of curvature of the mesh geometry -----
rho_g = C6 - rho_p; % use '+ rho_p' for internal gear
I = cos(phi_r)/((1/rho_p + 1/rho_g)*do_p*mnp); % AGMA surface geometry
factor for pitting resistance; use - 1/rho_g
for internal gear
Sc(i,j) = ZE*sqrt(Ft*KO*Cv*Ks*Km*ZR/(b*I*do_p)); %Compressive stress
SH_p=Sac_p/(Sc(i,j)); % bending stress factor of safety for pinion

SH_g=Sab_g/(Sc(i,j));  % bending stress factor of safety for pinion

SH = min (SH_p, SH_g);
```

Appendix C: Matlab neural network training

```
% model parameters
clc;
close all;
clear all;
%%% load data
input = xlsread('input.xlsx');
output = xlsread('output.xlsx');
new_input = xlsread('new_input.xlsx');
input=input';
output=output';
new_input=new_input';
%%%% normalize data
[pn,ps] = mapstd(input);
[tn,ts] = mapstd(output);
[pnn,pss] = mapstd(new_input);
%%%%% network creation

net=newff(pn,tn,[65 32 7],{'tansig' 'tansig'
'purelin'},'trainlm');
net.divideParam.trainRatio = 0.7; % training set [%]
net.divideParam.valRatio   = 0.15; % validation set [%]
net.divideParam.testRatio  = 0.15; % test set [%]
%%% set training parameters
net.trainparam.show=25;
net.trainparam.epoches=1000;
net.trainparam.goal=1e-5;
net.trainParam.time=inf;
net.trainParam.min_grad=1e-6;
net.trainParam.max_fail=5;
%%% Train the network
[net,tr]=train(net,pn,tn);
%%%% Testing the network
yt=sim(net,pn);

%%% calculate training error

mset=meanSquaredError(tn',yt');

%%%% Validating the network

pnv=pn(:,(1:15));
tnv=tn(:,(1:15));
yv=sim(net,pnv);
```

```
%%% calculate training error

msev=meanSquaredError(tnv',yv');

%%%% predicting the output for new input data

yp=sim(net,pnn);

%%%% reverse the predicted output data

yp1 = mapstd('reverse',yp,ts);
%Plot the output data
out_yieldstrength_pre=yp1(1,:);
out_utt_pre=yp1(2,:);
out_totalelongation_pre=yp1(3,:);
out_fracturetoughness_pre=yp1(4,:);
out_impacttoughness_pre=yp1(5,:);
out_retainedaustenite=yp1(6,:);
out_surfacehardness=yp1(7,:);
figure(1);
plot(out_yieldstrength _pre,'b');
figure(2);
plot(out_uts_pre,'b');
figure(3);
plot(out_totalelongation_pre,'b');
figure(4);
plot(out_fracturetoughness_pre,'b');
figure(5);
plot(out_impacttoughness_pre,'b');
figure(6);
plot(out_retainedaustenite,'b');
figure(7);
plot(out_surfacehardness,'b');
```

Appendix D:

D: Components of temperature controlled Twin-disc Test rig

Concept design A

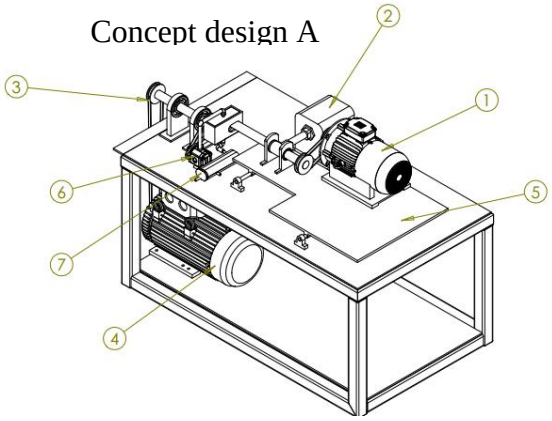

Where:
1 = AC motor,
2=Hydraulic system
3 = V-belt,
4 = AC motor,
5 = Slider,
6 = Oil pump &
7 = Heat exchanger

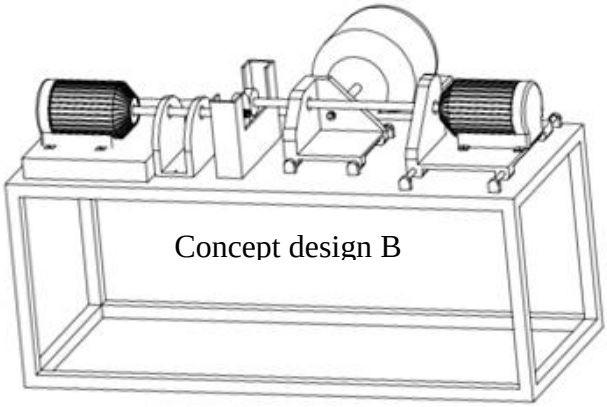

Concept design B

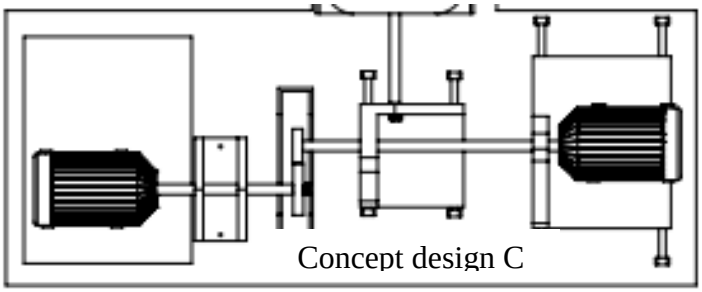

Concept design C

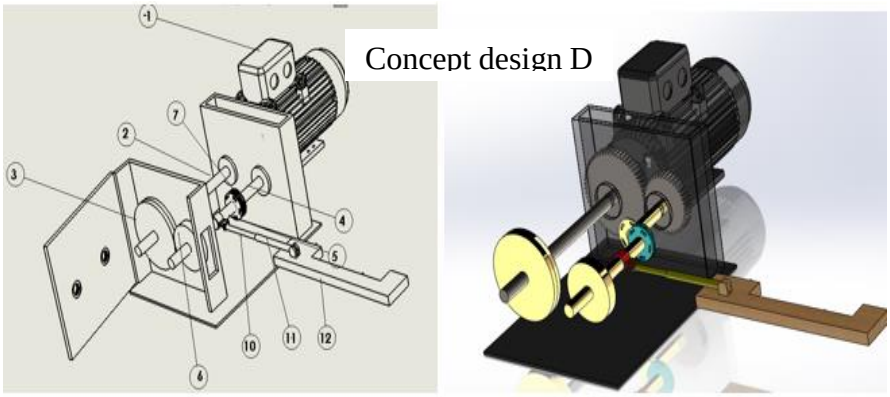

Where: 1.Motor
2. Low speed shaft
3. Low speed roller
4. Output shaft
5. High speed shaft
6. High speed roller
7. Clutch 8.Link
9. Pin 10.Piston
11. Cylinder
12. Table

Figure D-1: concept Design Configuration

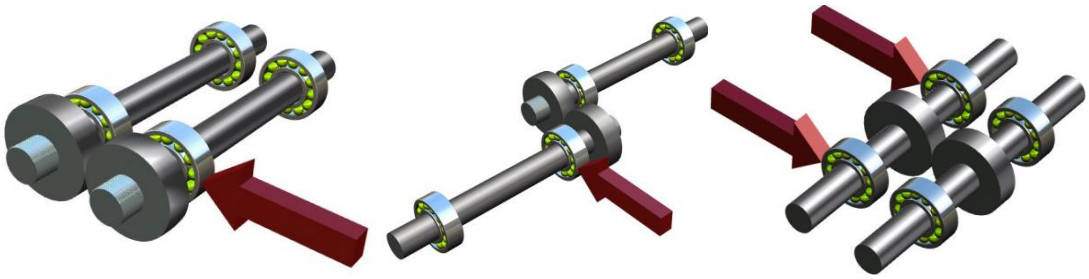

Figure D-2: load application concept configurations

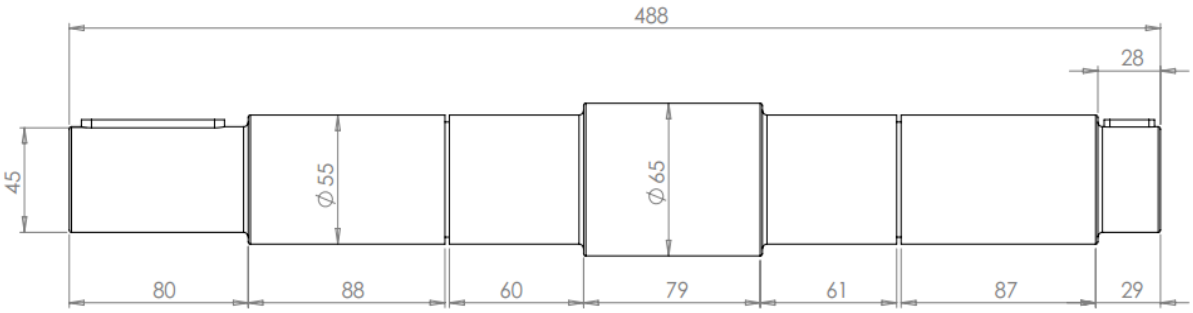

Figure D-3: Shaft Dimension for twin-disc test rig

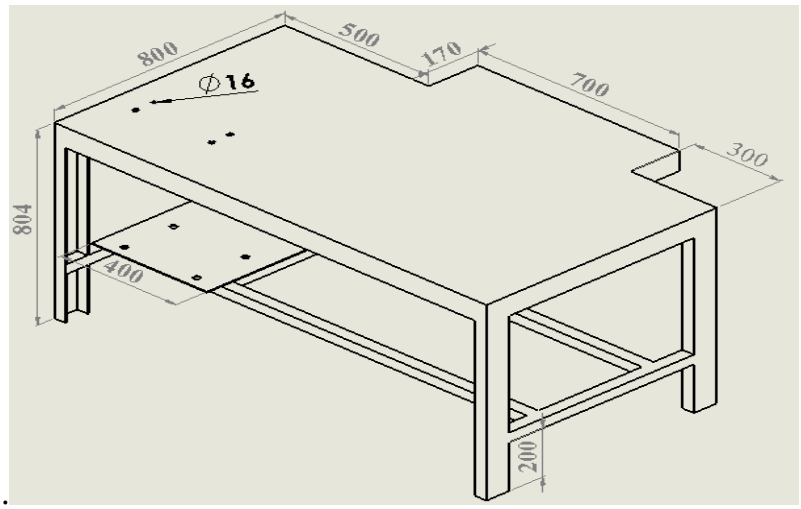

Figure D-4: Frame size

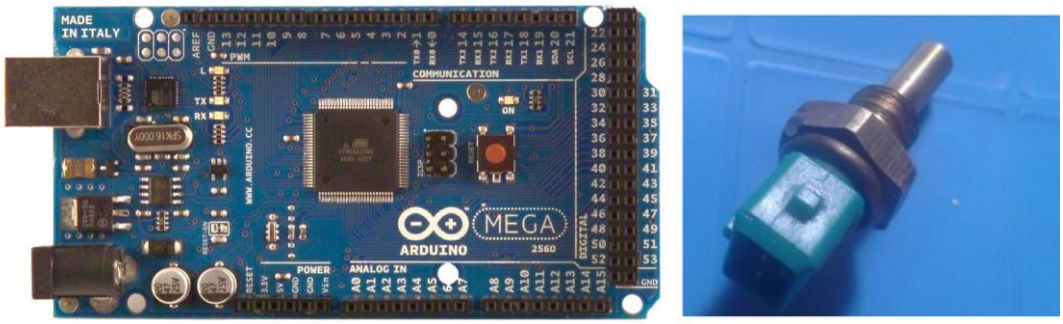

Figure D-5: Components for temperature lubricant control (a) Arduino (b) temperature sensor

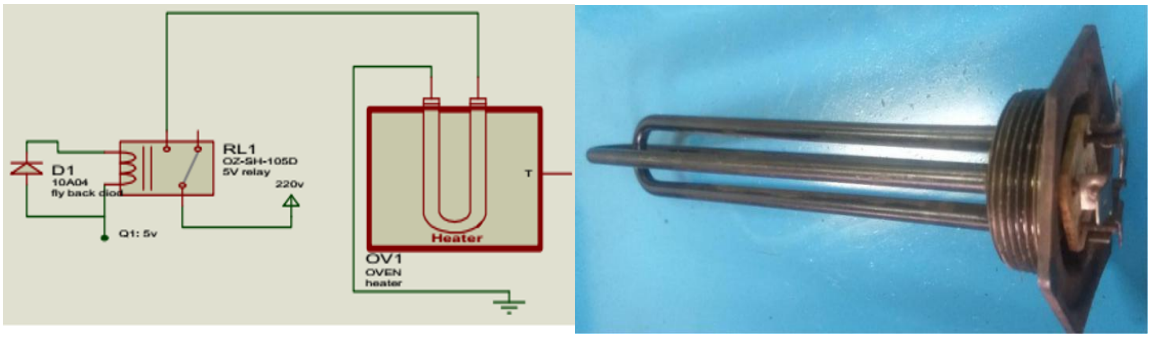

Figure D-6: Heating element of lubricants

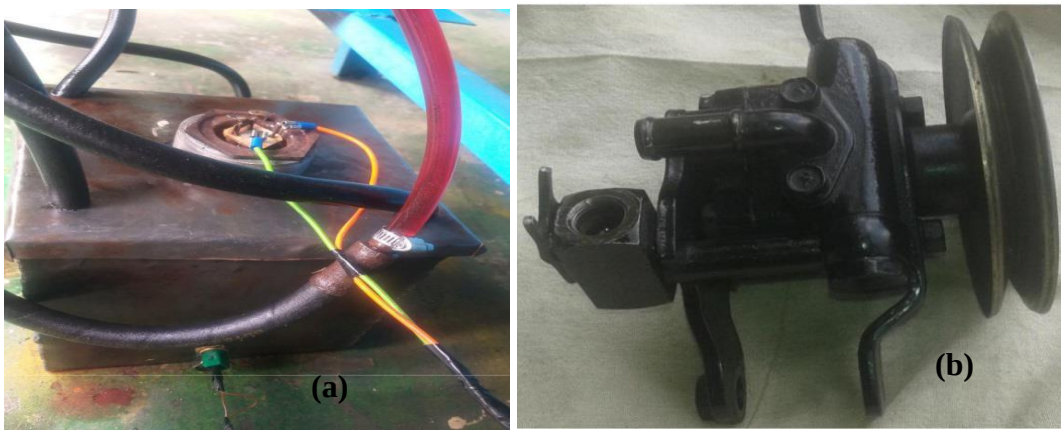

Figure D-7: (a): lubricant reservoir (b): oil pump

Figure D-8: Lubrication system assembly

Figure D-9: Assembled load application mechanism

Figure D-10: Final assembled of twin disc RCF test rig